

*The UNSATCHEM Software Package for Simulating the
One-Dimensional Variably Saturated Water Flow, Heat
Transport, Carbon Dioxide Production and Transport,
and Multicomponent Solute Transport with Major
Ion Equilibrium and Kinetic Chemistry*

Version 2 .0

Research Report No. 141

November, 1996

U. S. SALINITY LABORATORY
AGRICULTURAL RESEARCH SERVICE
U. S. DEPARTMENT OF AGRICULTURE
RIVERSIDE, CALIFORNIA

*The UNSATCHEM Software Package for Simulating the
One-Dimensional Variably Saturated Water Flow, Heat
Transport, Carbon Dioxide Production and Transport,
and Multicomponent Solute Transport with Major
Ion Equilibrium and Kinetic Chemistry*

Version 2.0

by

Jiří Šimůnek, Donald L. Suarez, and Miroslav Šejna

Research Report No. 141

November, 1996

U. S. SALINITY LABORATORY
AGRICULTURAL RESEARCH SERVICE
U. S. DEPARTMENT OF AGRICULTURE
RIVERSIDE, CALIFORNIA

DISCLAIMER

This report documents version 2.0 of UNSATCHEM, a software package for simulating one-dimensional water flow, heat transport, carbon dioxide transport and solute transport with major ion equilibrium and kinetic chemistry in variably saturated media. UNSATCHEM is a public domain code, and as such may be used and copied freely. The code has been verified against a number of test cases. However, no warranty is given that the program is completely error-free. If you do encounter problems with the code, find errors, or have suggestions for improvement, please contact one of the authors at

U. S. Salinity Laboratory
USDA, ARS
450 West Big Springs Road
Riverside, CA 92507

Tel. 909-369-4865 (J. Šimůnek)
Tel. 909-369-4816 (D. L. Suarez)
Fax. 909-342-4964
E-mail: jsimunek@ussl.ars.usda.gov
dsuarez@ussl.ars.usda.gov

ABSTRACT

Šimůnek, J., D. L. Suarez, and M. Šejna. 1996. The UNSATCHEM Software Package for Simulating One-Dimensional Variably Saturated Water Flow, Heat Transport, Carbon Dioxide Production and Transport, and Solute Transport with Major Ion Equilibrium and Kinetic Chemistry, Version 2.0. Research Report No. 141, U. S. Salinity Laboratory, USDA, ARS, Riverside, California.

This report documents version 2.0 of UNSATCHEM, a software package for simulating water, heat, carbon dioxide and solute movement in one-dimensional variably saturated media. The software consists of the UNSCHEM (version 2.0) computer program, and the UNSATCH interactive graphics-based user interface. The UNSCHEM program numerically solves the Richards' equation for variably-saturated water flow and convection-dispersion type equations for heat, carbon dioxide and solute transport. The flow equation incorporates a sink term to account for water uptake by plant roots. The heat transport equation considers transport due to conduction and convection with flowing water. Diffusion in both liquid and gas phases and convection in the liquid phase are considered as CO₂ transport mechanisms. The CO₂ production model is described. The major variables of the chemical system are Ca, Mg, Na, K, SO₄, Cl, NO₃, H₄SiO₄, alkalinity, and CO₂. The model accounts for equilibrium chemical reactions between these components such as complexation, cation exchange and precipitation-dissolution. For the precipitation-dissolution of calcite and dissolution of dolomite, either equilibrium or multicomponent kinetic expressions are used which include both forward and back reactions. Other dissolution-precipitation reactions considered include gypsum, hydromagnesite, nesquehonite, and sepiolite. Since the ionic strength of soil solutions can vary considerably with time and space and often reach high values, both modified Debye-Hückel and Pitzer expressions were incorporated into the model as options to calculate single ion activities.

The program may be used to analyze water and solute movement in unsaturated, partially saturated, or fully saturated porous media. The flow region may be composed of nonuniform soils. Flow and transport can occur in the vertical, horizontal, or a generally inclined, direction. The water flow part of the model can deal with prescribed head and flux boundaries. boundaries

controlled by atmospheric conditions, as well as free drainage boundary conditions. The governing flow and transport equations are solved numerically using finite differences and Galerkin-type linear finite element schemes, respectively.

This report serves as both a user manual and reference document. Detailed instructions are given for data input preparation. A graphics-based user interface, UNSATCH, for data preparation and graphical output display in the MS Windows environment is described in the second part of the manual.

TABLE OF CONTENTS

DISCLAIMER	iii
ABSTRACT	v
TABLE OF CONTENTS	vii
LIST OFFIGURES	xi
LISTOFTABLES	xiii
LISTOFVARIABLES	xv
GENERAL INTRODUCTION AND OVERVIEW OF UNSATCHEM	1
PART A - The UNSCHEM Code for Simulating the One-Dimensional Variably Saturated Water Flow, Heat Transport, Carbon Dioxide Production and Transport, and Multicomponent Solute Transport with Major Ion Equilibrium and Kinetic Chemistry J. Šimůnek and D. L. Suarez7
1. INTRODUCTION	9
2. VARIABLY SATURATED WATER FLOW	11
2.1. <i>Governing Flow Equation</i>	11
2.2. <i>Root Water Uptake</i>	11
2.3. <i>The Unsaturated Soil Hydraulic Properties</i>	16
2.4. <i>Initial and Boundary Conditions</i>	21
2.5. <i>Plant Yield Model</i>	23
3. MULTICOMPONENT SOLUTE TRANSPORT	25
3.1. <i>Governing Solute Transport Equations</i>	25
3.2. <i>Effective Dispersion Coefficient</i>	25
3.3. <i>Initial and Boundary Conditions</i>	26
4. HEAT TRANSPORT	27
4.1. <i>Governing Heat Transport Equations</i>	27
4.2. <i>Apparent Thermal Conductivity Coefficient</i>	28
4.3. <i>Initial and Boundary Conditions</i>	28
5. CARBON DIOXIDE TRANSPORT AND PRODUCTION	31

5.1.	<i>Governing CO, Transport Equations</i>	31
5.2.	<i>Effective Dispersion Coefficient</i>	34
5.3.	<i>Initial and Boundary Conditions</i>	36
5.4.	<i>Production of Carbon Dioxide</i>	37
5.5.	<i>Parameter Selection for the Production Model</i>	41
	5.5.1. <i>Optimum Production at 20°C</i>	42
	5.5.2. <i>Production Response to Temperature</i>	42
	5.5.3. <i>Production Response to Oxygen Concentration</i>	43
	5.5.4. <i>Production Response to Water Stress</i>	44
	5.5.5. <i>Production Response to Osmotic Stress</i>	44
6.	CARBONATE CHEMISTRY	45
6.1.	<i>Mass and Charge Balance Equations</i>	46
6.2.	<i>CO₂ - H₂O System</i>	47
6.3.	<i>Complexation Reactions</i>	48
6.4.	<i>Cation Exchange and Selectivity</i>	49
6.5.	<i>Precipitation-Dissolution Reactions</i>	49
6.6.	<i>Kinetic Model of Calcite Precipitation-Dissolution</i>	53
6.7.	<i>Kinetic Model of Dolomite Dissolution</i>	54
6.8.	<i>Silica Concentration in Soil Solution</i>	55
6.9.	<i>Activity Coefficients</i>	56
	6.9.1. <i>Extended Debye-Hückel Expression</i>	56
	6.9.2. <i>Pitzer Expressions</i>	58
6.10.	<i>Temperature Dependence</i>	61
6.11.	<i>Osmotic Coefficient</i>	63
6.12.	<i>Osmotic Pressure</i>	63
6.13.	<i>System Summary</i>	64
7.	NUMERICAL SOLUTION OF THE WATER FLOW EQUATION	65
7.1.	<i>Space and Time Discretization</i>	65
7.2.	<i>Treatment of Pressure Head Boundary Conditions</i>	67
7.3.	<i>Treatment of Flux Boundary Conditions</i>	67
7.4.	<i>Numerical Solution Strategy</i>	69
	7.4.1. <i>Iterative Process</i>	69
	7.4.2. <i>Time Control</i>	69
	7.4.3. <i>Atmospheric Boundary Conditions and Seepage Faces</i>	70
	7.4.4. <i>Water Balance Computations</i>	71
	7.4.5. <i>Computation of Nodal Fluxes</i>	72
	7.4.6. <i>Water Uptake by Plant Roots</i>	73
	7.4.7. <i>Evaluation of the Soil Hydraulic Properties</i>	73
8.	NUMERICAL SOLUTION OF THE TRANSPORT EQUATIONS	75
8.1.	<i>Space Discretization</i>	76
8.2.	<i>Time Discretization</i>	78

8.3. Numerical Solution Strategy	83
8.3.1. Solution Process	83
8.3.2. Upstream Weighted Formulation	84
8.3.3. Reverse Back-Step Particle Tracking	84
8.3.4. Solute Mass Balance Calculations	85
8.3.5. Carbon Dioxide Mass Balance Calculations	86
8.3.6. Oscillatory Behavior	87
9. SOLUTION OF THE CHEMICAL SYSTEM AND COUPLING	89
9.1. Solution of the Chemical System	89
9.2. Coupling the Chemical and Solute Transport Modules	90
10. PROBLEM DEFINITION	93
10.1. Construction of Finite Element Grid	93
10.2. Coding of Soil Types and Subregions	93
10.3. Coding of Boundary Conditions	94
10.4. Program Memory Requirements	99
11. EXAMPLE PROBLEMS	101
11.1. Example 1 - Column Infiltration	101
11.2. Example 2 - One Year Irrigation	106
11.3. Example 3 - 10 Day Irrigation Cycle	112
11.4. Example 4 - Missouri CO ₂ Experiment	117
12. INPUTDATA	123
13. OUTPUT DATA	145
14. PROGRAM ORGANIZATION	155
15. REFERENCES	161
PART B - Interactive Graphics-Based User Interface UNSATCH	171
J. Šimůnek, M. Šejna, M. Th. van Genuchten, and D. L. Suarez	
B. Brief Description of Selected Modules	174
B.1. Module UNSATCH	174
B.2. Module POSITION	183
B.3. Module PROFILE	183
B.3.1. Soil Profile Discretization	183
B.3.2. Specification of Soil Properties within the Soil Profile	184

LIST OF FIGURES

<u>Figure</u>		<u>Page</u>
Fig. 2.1..	Schematic of the potential water uptake distribution function, $b(z)$, in the soil root zone	13
Fig. 2.2.	Schematics of the soil water retention (a) and hydraulic conductivity (b) functions as given by equations (2.15) and (2.16), respectively	18
Fig. 11.1.	Water content profiles at various times for example 1	103
Fig. 11.2.	Tracer concentration profiles at various times for example 1	103
Fig. 11.3.	Calcium concentration profiles at various times for a) equilibrium and b) kinetic calcite precipitation-dissolution for example 1.	104
Fig. 11.4.	Alkalinity profiles at various times for a) equilibrium and b) kinetic calcite precipitation-dissolution for example 1.	104
Fig. 11.5.	Calcite profiles at various times for a) equilibrium and b) kinetic calcite precipitation-dissolution for example 1.	105
Fig. 11.6.	Water content profiles at various times for example 2	108
Fig. 11.7.	Tracer concentration profiles at various times for example 2	109
Fig. 11.8.	Calcium concentration profiles at various times for a) equilibrium and b) kinetic calcite precipitation-dissolution for example 2.	109
Fig. 11.9.	Alkalinity profiles at various times for equilibrium and kinetic calcite precipitation-dissolution for example 2.	110
Fig. 11.10.	CaCO_3 pIAP profiles at various times for equilibrium and kinetic calcite precipitation-dissolution for example 2.	110
Fig. 11.11.	Calcite concentration profiles at various times for a) equilibrium and b) kinetic calcite precipitation for example 2.	111
Fig. 11.12.	Gypsum concentration profiles at various times without (dashed line) and with (full line) iteration between the solute transport and chemical modules for example 2.	111

Fig. 11.13.	Water content profiles at various times for example 3	113
Fig. 11.14.	P_{CO_2} profiles at various times for example 3	114
Fig. 11.15.	Calcium concentration profiles at various times for equilibrium calcite precipitation with constant CO, and kinetic calcite precipitation with variable CO, concentrations for example 3.	114
Fig. 11.16.	Alkalinity profiles at various times for equilibrium calcite precipitation with constant CO, and kinetic calcite precipitation with variable CO, concentrations for example 3.	115
Fig. 11.17.	CaCO ₃ pIAP profiles at various times for a) constant and b) variable CO, concentrations for example 3.	11.5
Fig. 11.18.	pH profiles at various times for a) equilibrium calcite precipitation with constant CO, and b) kinetic calcite precipitation with variable CO, concentrations for example 3.	116
Fig. 11.19.	Measured [<i>Buyanovsky and Wagner, 1983</i>] and calculated water contents at a depth of 0.20 m for the Missouri wheat experiment, 1982 (example 4). 120	
Fig. 11.20.	Measured [<i>Buyanovsky and Wagner, 1983</i>] and calculated temperatures at a depth of 0.20 m for the Missouri wheat experiment, 1982 (example 4) . 120	
Fig. 11.21.	Measured [<i>Buyanovsky and Wagner, 1983</i>] and calculated CO, concentrations at a depth of 0.20 m for the Missouri wheat experiment, 1982 (example 4).	121
Fig. 11.22.	Measured [<i>Buyanovsky and Wagner, 1986</i>] and calculated daily and weekly CO, fluxes to the atmosphere for the Missouri wheat experiment, 1982 (example 4).	121
Fig. B.1.	Main window of the UNSATCH module, including the project manager.	175
Fig. B.2.	Main window of the PROFILE module; when used for soil profile discretization.	184
Fig. B.3.	Main window of the PROFILE module; when used for specification of soil properties.	186

LIST OF TABLES

<u>Table</u>	<u>Page</u>
Table 6.1. Chemical species considered by the model	45
Table 6.2. Temperature dependence of the kinetic constants for calcite precipitation-dissolution [Plummer <i>et al.</i> , 1978] and dolomite dissolution [Busenberg and Plummer, 1982]	55
Table 6.3. Ionic charge and adjustable parameters for calculation of extended Debye-Hückel activity coefficients	57
Table 6.4. Parameters for calculation of thermodynamic constants as a function of temperature	62
Table 6.5. Values for equilibrium and precipitation-dissolution reaction constants and AH, ” [Truesdell and Jones, 1974]	62
Table 8.1. Values of the diagonal entries d_i , and off-diagonal entries b , and e , of the matrix $[P_c]$ for linear finite elements.	79
Table 8.2. Values of the diagonal entries d_i , and off-diagonal entries b , and e , of the matrix $[P_c]$ for finite differences.	80
Table 8.3. Values of the diagonal entries d_i , and off-diagonal entries b , and e , of the matrix $[P_c]$ for linear finite elements with upstream weighting.	81
Table 10.1. Initial settings of $KodTop$ ($KodBot$), $rTop$ ($rBot$), and $h(n)$ for constant boundary conditions	94
Table 10.2. Initial settings of $KodTop$ ($KodBot$), $rTop$ ($rBot$), and $h(n)$ for variable boundary conditions	95
Table 10.3. Definition of the variables $KodTop$, $rTop$, and $h(n)$ when an atmospheric boundary condition is applied	96
Table 10.4. Definition of the variables $KodTop$ ($KodBot$), $rTop$ ($rBot$), and $h(n)$ when variable head or flux boundary conditions are applied	96
Table 10.5. Initial setting of $KodBot$, $rBot$, and $h(n)$ for seepage faces	98
Table 10.6. List of the array dimensions	100
Table 12.1. Block A - Basic information	125
Table 12.2. Block B - Material information	126
Table 12.3. Block C - Time information	128
Table 12.4. Block D - Root growth information	129

Table 12.5.	Block E - Root water uptake information	130
Table 12.6.	Block F - Heat transport information	131
Table 12.7.	Block G - Carbon dioxide transport and production information	132
Table 12.8.	Block H - Solute transport and chemical information	134
Table 12.9.	Block I - Nodal information	138
Table 12.10.	Block J - Atmospheric information	140
Table 12.11.	Input file 'COMP.DAT' [<i>Felmy,1990</i>]	141
Table 12.12.	Input file 'BINARYP.DAT' [<i>Felmy,1990</i>]	142
Table 12.13.	Input file 'TERNARYP.DAT' [<i>Felmy,1990</i>]	143
Table 12.14.	Input file 'LAMBDA.DAT' [<i>Felmy,1990</i>]	144
Table 13.1.	T_LEVEL.OUT - pressure heads and fluxes at the boundaries and in the root zone	147
Table 13.2.	CO2_INF.OUT - CO ₂ concentrations and CO ₂ fluxes at the boundaries and in the root zone	148
Table 13.3.	RUN_INF.OUT - time and iteration information	149
Table 13.4.	NOD_INF.OUT - profile information	150
Table 13.5.	BALANCE.OUT - mass balance variables	151
Table 13.6.	CONC.OUT - solute concentration information	152
Table 13.7.	SOLID.OUT - solid phase and surface species concentrations	153
Table 13.8.	EQUIL.OUT - chemical information	154
Table 14.1.	Input subroutines/files	156
Table 14.2.	Output subroutines/files	158
Table B.1.	Main modules of the UNSATCHEM software package	173
Table B.2.	Menu commands in the main module UNSATCH	176
Table B.3.	Description of all menu commands in the main module UNSATCH	177
Table B.4.	Graph options in the UNSATCHEM interface	179
Table B.5.	Information in the UNSATCH.DAT file	182
Table B.6.	Definition of terms in the PROFILE module	185

LIST OF VARIABLES

a	parameter in the exponential depth reduction function [L^{-1}]
a_i	activity of the i th ion [-]
A	amplitude of the temperature sine wave [K]
A	Debye-Hückel constant ($kg^{0.5}mol^{-0.5}$)
A_{qh}	empirical parameter in the deep drainage function [LT^{-1}]
Alk	alkalinity ($mol_c kg^{-1}$)
b	empirical constant in the water stress response function [-]
$b(z)$	normalized water uptake distribution function [L^{-1}]
b_1, b_2, b_3	parameters of the thermal conductivity function [$MLT^{-3}K^{-1}$] (e.g. $Wm^{-1}K^{-1}$)
B	Debye-Hückel constant ($kg^{0.5}cm^{-1}mol^{-0.5}$)
B_{ij}	Pitzer specific virial coefficient for double ion interaction
B_{qh}	empirical parameter in the deep drainage function [L^{-1}]
c	solution concentration [ML^{-3}]
\bar{c}	surface species concentration [MM^{-4}]
\hat{c}	solid phase concentration [MM^{-4}]
c'	finite element approximation of c [ML^{-3}]
c_g, c_w	CO, concentrations in the gas and liquid phase, respectively [L^3L^{-3}]
c_{ai}	initial CO, concentration in the gas phase [L^3L^{-3}]
c_{as}	CO, concentration in the soil gas at the soil surface [L^3L^{-3}]
c_{atm}	CO, concentration at the top of the stagnant boundary layer [L^3L^{-3}]
c_{a0}	boundary condition for CO, concentration in the gas phase [L^3L^{-3}]
c_i	initial solution concentration [ML^{-3}]
c_n	value of the concentration at node n [ML^{-3}]
c_T	total volumetric CO, concentration [L^3L^{-3}]
\bar{c}_T	cation exchange capacity ($mol_c kg^{-1}$)
c_o	prescribed concentration boundary condition [ML^{-3}]
C	soil water capacity [L^{-1}]

C_0	total salt concentration (mol ℓ^{-1})
C_a, C_n, C_o, C_w	volumetric heat capacities of the gas phase, solid phase, organic matter and liquid phase, respectively [$\text{ML}^{-1}\text{T}^{-2}\text{K}^{-1}$] (e.g. $\text{Jm}^{-3}\text{K}^{-1}$)
C_{ijk}	Pitzer specific virial coefficient for triple ion interaction
C_p	volumetric heat capacity of the porous medium [$\text{ML}^{-1}\text{T}^{-2}\text{K}^{-1}$] (e.g. $\text{Jm}^{-3}\text{K}^{-1}$)
CEC	cation exchange capacity (mol kg^{-1})
Cr_i^e	local Courant number [-]
d	thickness of stagnant boundary layer [L]
d^*	adjusted interlayer spacing [L]
D	effective dispersive coefficient [L^2T^{-1}]
D_a, D_w	effective soil matrix diffusion coefficients of CO_2 in the gas and liquid phase, respectively [L^2T^{-1}]
D_{as}, D_{ws}	diffusion coefficients of CO , in the gas and liquid phase, respectively [L^2T^{-1}]
D_E	effective dispersion coefficient in the soil matrix [L^2T^{-1}]
D_L	longitudinal dispersivity [L]
D_m	molecular diffusion coefficient in free water [L^2T^{-1}]
e	element number [-]
E	activation energy of the reaction [$\text{ML}^2\text{T}^{-2}\text{M}^{-1}$]
E_w	maximum (potential) rate of infiltration or evaporation under the prevailing atmospheric conditions [LT^{-1}]
EC	electric conductivity of the solution (dS m^{-1})
ESP	exchangeable sodium percentage
ESP*	adjusted exchangeable sodium percentage
ET_a, ET_p	actual and potential evapotranspiration, respectively [L]
ET_D	evapotranspiration deficit [L]
f_{mont}	weight fraction of montmorillonite in soil [-]
f_p, f_s	reduction functions for CO , production by plant roots and by soil microorganisms, respectively [-]
f_r	root growth coefficient [-]
g	dimensionless coefficient calculated from degree day model [-]
g	gravitational constant [L^2T^{-1}]

h	water pressure head [L]
h_a, h_b	pressure head interval within which the values of θ , K , and C are evaluated from the interpolation tables [L]
h_A, h_S	minimum and maximum pressure heads allowed at the soil surface. respectively [L]
h_i	water pressure head initial condition [L]
h_s	air-entry value [L]
h_ϕ	osmotic head [L]
$h_{\phi 50}$	osmotic head at which transpiration is reduced by 50% [L]
h_0	water pressure head boundary condition [L]
h_1, h_3	pressure head when CO ₂ production ceases [L]
h_2	pressure head when CO ₂ production is optimal [L]
h_{50}	empirical constant in the water stress response function [L]
I	ionic strength (mol kg ⁻¹)
IAP^C	ion activity product for calcite [-]
IAP^G	ion activity product for gypsum [-]
J_{ca}, J_{cw}	CO ₂ fluxes caused by convection in the gas and liquid phase, respectively [LT ⁻¹]
J_{da}, J_{dw}	CO ₂ fluxes caused by diffusion in the gas and liquid phase, respectively [LT ⁻¹]
k_{a1}	first dissociation constant of carbonic acid [-]
k_{a2}	second dissociation constant of carbonic acid [-]
k_x	multiplication factor
K	unsaturated hydraulic conductivity function [LT ⁻¹]
K_{CO_2}	Henry's Law constant [MT ² M ⁻¹ L ⁻²]
K_k	unsaturated hydraulic conductivity corresponding to θ_k [LT ⁻¹]
K_M, K_M^*	Michaelis' constants for O ₂ and CO ₂ concentrations, respectively [L ³ L ⁻³]
K_r	relative hydraulic conductivity [LT ⁻¹]
K_S	saturated hydraulic conductivity [LT ⁻¹]
K_{SP}^C	solubility product for calcite [-]
K_{SP}^G	solubility product for gypsum [-]
K_{SP}^H	solubility product for hydromagnesite [-]

K_{SP}^N	solubility product for nesquehonite [-]
K_{SP}^S	solubility product for freshly precipitated sepiolite [-]
K_W	dissociation constant for water [-]
$K_{1, \dots, K_{12}}$	equilibrium constants for complexation reactions [-]
$K_{13, \dots, K_{15}}$	selectivity constants for cation exchange reactions [-]
L	z-coordinate (depth of the soil profile) of the soil surface [L]
L_m	maximum rooting depth [L]
L_r	root depth [L]
L_0	initial value of the rooting depth at the beginning of the growth period [L]
m, n	parameters of the retention curve [-]
m_i	molality (mol kg ⁻¹)
m^0	unit molality (1 mol kg ⁻¹)
M	number of species in the solution mixture [-]
M_{CO}	total amount of CO, in the entire flow domain [L]
M_l	amount of solute in the liquid phase in the flow region at time t [ML ⁻¹]
M_p	amount of solute in the precipitated phase in the flow region at time t [ML ⁻¹]
M_s	amount of solute in the sorbed phase in the flow region at time t [ML ⁻¹]
M_s	molar weight (mol ⁻¹)
M_t	amount of solute in the flow region at time t [ML ⁻¹]
M_T	total amount of solute in the flow region at time t [ML ⁻¹]
M_t^e	amount of solute in element e at time t [ML ⁻¹]
M_0	amount of solute in the flow region at the beginning of the simulation [ML ⁻¹]
M_0^e	amount of solute in element e at the beginning of the simulation [ML ⁻²]
n	nodal number [-]
N	number of nodal points [-]
N_c	number of aqueous components [-]
O	rate of inflow/outflow to/from specified subregion [LT ⁻¹]
P	porosity [L ³ L ⁻³]
p_t	period of time necessary to complete one temperature cycle (1 day) [T]

P	production/sink term for CO, [$L^3L^{-3}T^{-1}$]
$Pe,$ "	local Peclet number [-]
P_{CO_2}	partial pressure of CO, [$ML^{-1}T^{-2}$] (atm)
P_T	actual CO, production rate [$L^3L^{-2}T^{-1}$]
P_ϕ	osmotic pressure of electrolyte solution [$ML^{-1}T^{-2}$] (Pa)
pH	negative logarithm of hydrogen activity [-]
$pIAP$	negative logarithm of the ion activity product [-]
4	oxygen uptake rate [$L^3L^{-3}T^{-1}$]
q_a, q_w	soil air and soil water fluxes, respectively [LT^{-1}]
q_E	CO, effective velocity [LT^{-1}]
q_{E0}	prescribed CO, effective boundary flux [LT^{-1}]
q_{max}	maximum oxygen uptake rate [$L^3L^{-3}T^{-1}$]
4_{w0}	water flux boundary condition [LT^{-1}]
	growth rate [T^{-1}]
r	scaling factor which represents the effect of solution composition (SAR, C_0 , pH) on the hydraulic conductivity [-]
r_1	scaling factor which represents the effect of solution composition (SAR, C_0) on the hydraulic conductivity [-]
r_2	scaling factor which represents the effect of solution pH on the hydraulic conductivity [-]
R	universal gas constant [$ML^2T^{-2}K^{-1}M^{-1}$]
R_f	retardation factor [-]
R^C	calcite dissolution-precipitation rate ($mmol\ cm^{-2}s^{-1}$)
R^D	dolomite dissolution rate ($mmol\ cm^{-2}s^{-1}$)
s	surface species concentration [-]
S	sink/source term, root water uptake [$L^3L^{-3}T^{-1}$]
S^*	CO, uptake rate associated with root water uptake [T^{-1}]
S_c	relative water saturation [-]
S_{ck}	degree of water saturation corresponding to θ_k [-]
S_p	potential root water uptake rate [$L^3L^{-3}T^{-1}$]

SAR	($\text{mmol}^{0.5} \ell^{-0.5}$)
t	t i m e [T]
t_p, t_m, t_h	time of planting, time at which maximum rooting depth is reached and time of harvesting, respectively [T]
T	temperature [K]
T_a, T_p	actual and potential transpiration rates, respectively [LT^{-1}]
T_{Bas}	heat units necessary for the plant to mature and roots to reach the maximum rooting depth [KT]
T_i	initial temperature condition [K]
T_0	boundary temperature condition [K]
\bar{T}	p_i
T_1	
T_2	T_3 interval up to temperature [K]
T_3	temperature above which increased temperature has a negative effect on growth [K]
V	
V^e	
V_s	($\text{cm}^3 \text{mol}^{-1}$)
W	
x	[-]
Y	
Y_M	$ET_a = ET_p$, n dry matter yield for the condition when
z	
α	[L^{-1}]
α_s, α_ϕ	[-]
α''	finite element method [-]
β_i	
β_0	$E, T, , ,$ [-]
γ_i	[-]
γ_i'''	Debye-Hückel of the i th solute ion [-]

γ_p, γ_s	actual CO ₂ production rate of plant roots and soil microorganisms, respectively [L ³ L ⁻³ T ⁻¹]
γ_{p0}, γ_{s0}	optimal CO ₂ production rate of plant roots and soil microorganisms (20°C), respectively [L ³ L ⁻² T ⁻¹]
Δt	time step [T]
Δz	size of the elements [L]
δ	reduction coefficient in the heat unit submodel [-]
δ_{mm}	Kronecker delta [-]
ϵ_a^c	absolute error in the solute mass balance [ML ⁻²]
ϵ_a^w	absolute error in the water mass balance [L]
ϵ_r^c	relative error in the solute mass balance [%]
ϵ_r^w	relative error in the water mass balance [%]
θ_a, θ_w	volumetric air and water content, respectively [L ³ L ⁻³]
θ_n, θ_o	volumetric fractions of solid phase and organic matter, respectively [L ³ L ⁻³]
θ_r, θ_s	residual and saturated volumetric water content, respectively [L ³ L ⁻³]
θ_p, θ_m	parameter of the retention curve [L ³ L ⁻³]
θ_k	parameter of the hydraulic conductivity function [L ³ L ⁻³]
λ	coefficient of the apparent thermal conductivity of the soil [MLT ⁻³ K ⁻¹] (e.g. W m ⁻¹ K ⁻¹)
λ_w	dispersivity in the water phase [L]
λ_0	thermal conductivity of the soil [MLT ⁻³ K ⁻¹] (e.g. W m ⁻¹ K ⁻¹)
ξ	local coordinate [-]
τ_a, τ_w	tortuosity factors in gas and liquid phase, respectively [LL ⁻¹]
ϕ	linear basis function [-]
ϕ	osmotic coefficient [-]
ϕ_n^u	upstream weighted basis functions [-]
Δt	time increment [T]
Δt_{min}	minimum permitted time increment [T]
Δt_{max}	maximum permitted time increment [T]

GENERAL INTRODUCTION AND OVERVIEW OF UNSATCHEM

Modelling the transport and chemical reactions of major solute species in and below the rootzone plays a critical role for proper irrigation, fertilization and surface and ground water management. Realistic modeling of the rootzone chemistry requires consideration of water flow, heat transport, plant water uptake, as well as prediction of the dynamic changes in CO_2 concentration with time and space. It must also account for solute movement and the chemical processes for the solutes of interest. Soil temperature, which can change annually from about -10 up to +50 °C, significantly affects the thermodynamic equilibrium constants and reaction rates and therefore influences even the selection of the method for prediction of the soil solution chemistry - from equilibrium models to models based on kinetic expressions. In addition, CO_2 concentrations can change several orders of magnitude from values which are at equilibrium with the CO_2 content in the atmosphere (0.035%) up to extreme values of about 20%. The solubility of many solid phases such as carbonates and oxihydroxides significantly changes within this range in CO_2 , primarily because changes in soil CO_2 produce changes in soil pH for all but acid soils.

The processes of evaporation and plant transpiration also exert a major influence on the solution composition and water and solute distribution in near surface environments. These processes concentrate the salts by decreasing the amount of water in the soil, and when combined with irrigation in arid regions, saline conditions can result. Ion activities for such chemical conditions should be calculated with expressions suitable for use in brines rather than the standard formulations for dilute solutions. The interaction of evapotranspiration, changing soil gas composition, ion exchange and soil-water reactions requires consideration of the possibility to precipitate or dissolve various minerals. Major ions (consisting mainly of Ca^{2+} , Mg^{2+} , Na^+ , K^+ , Cl^- , SO_4^{2-} , HCO_3^- , CO_3^{2-} , and NO_3^-) may accumulate in certain parts of the soil profile in such amounts that crop yield can be seriously reduced. Therefore any model attempting to successfully predict the solution chemistry of the major ions in the unsaturated zone should address all these processes and variables.

Traditionally the hydrological models for water flow and solute transport and the chemical models considering solution chemistry were developed separately. The solute transport models mostly considered only one solute and simplified chemical processes. The complex processes of

adsorption and cation exchange were usually accounted for by linear [Huyakorn et al., 1991] or nonlinear Freundlich isotherms [Yeh and Huff, 1985; Šimůnek and van Genuchten, 1993], where all reactions between solid and liquid phases were lumped into the distribution coefficient K_d [Liu and Narasimhan, 1989a] and possibly into the nonlinear exponent. Other processes such as precipitation, biodegradation, volatilization or radioactive decay were simulated by simple first- or zero-order rate constants. Several models were developed which simulate several solutes involved in sequential first-order decay reactions [Gureghian, 1981; Wagenet and Hutson, 1987; Šimůnek and van Genuchten, 1993].

Only in the last decade has there been significant effort to couple hydrological models for water flow and solute transport with chemical equilibrium models. Recent reviews on the development of the hydrogeochemical transport models of reactive multichemical components were given by Abriola [1987], Kirkner and Reeves [1988], Yeh and Tripathi [1989], Rubin [1990] and Mangold and Chin-Fu Tsang [1991]. Kirkner and Reeves [1988] presented an analysis of several methods for approximate solution of multicomponent transport with homogeneous and heterogeneous chemical reactions and discussed how the nature of the chemistry may affect the choice of the numerical formulation and solution algorithm. Yeh and Tripathi [1989] provided a critical review of many computational methods that have been presented in the hydrologic literature for solving multicomponent, equilibrium-controlled transport.

Most of the research has been, and still is, concentrated on the saturated zone where changes in water velocity, temperature and pH are relatively gradual and thus are less important than in the unsaturated zone. Therefore most of the developed models were based on one-dimensional steady-state saturated water flow with fixed water velocity, temperature and pH [Valocchi et al., 1981; Jennings et al., 1982; Walsh et al., 1984; Cederberg et al., 1985; Kirkner et al., 1985; Förster, 1986; Bryant et al., 1986; Förster and Gerke, 1988; Kirkner and Reeves, 1988; among others]. Only recently several models were published that can be applied to problems that include multicomponent solute transport in variably saturated water flow [Liu and Narasimhan, 1989a; Yeh and Tripathi, 1991; Šimůnek and Suarez, 1994]. For example, Narasimhan et al. [1986] and Liu and Narasimhan [1989a] developed the model DYNAMIX that was coupled with an integral finite difference program for fluid flow in variably saturated porous

media. *Yeh and Tripathi [1991]* presented the development and demonstration of a two-dimensional finite element hydrogeochemical transport model, HYDROGEOCHEM, for simulating transport of reactive multispecies chemicals.

Modeling of major ion chemistry in the soil profile requires the coupling of a chemical model to a transient variably saturated water flow model which allows the simulation of processes such as root water uptake. *Robbins et al. [1980a,b]* developed chemical precipitation-dissolution and cation exchange subroutines using equilibrium chemistry and coupled them with a one-dimensional water movement-salt transport-plant growth model. They tested their model by comparing its results with experimental data obtained from a lysimeter study. Further evaluation of their model was done by *Dudley et al. [1981]* for field conditions under cropped and uncropped conditions. They reported that the model gave adequate simulation of salinity but not individual ion concentrations. *Russo [1986]* combined the salinity model of *Robbins et al. [1980a]* with the transport model of *Bresler [1973]* to theoretically investigate the leaching of gypsiferous-sodic soil under different soil conditions and water qualities. Robbins' equilibrium chemistry model was also the basis for the numerical code LEACHM of *Wagenet and Hutson [1987]*. One simplification in these models is that they call the equilibrium chemistry model only once at each time step without iterating between transport and chemical modules. In many cases this simplification produces noticeable numerical error, as was shown by *Yeh and Tripathi [1991]*. The second simplification is that these models consider only equilibrium reactions, while published data in natural systems have indicated that kinetic reactions often control solution composition. For example, studies of major ion compositions in and below the rootzone of calcareous arid zone soils have indicated that calcite equilibrium is not a reasonable assumption for predicting water composition [*Suarez, 1977b; Suarez and Rhoades, 1982*] and that a kinetic expression yields values closer to the field measurements [*Suarez, 1985*]. Existing models also assume either a fixed pH or a fixed CO₂, which are questionable assumptions for soils, which usually exhibit fluctuation of both of these variables [*Suarez and Šimůnek, 1997*]. The UNSATCHEM model also differs from other water flow - solute transport models in that it considers the effects of chemical composition on hydraulic conductivity [*Suarez and Šimůnek, 1997*].

The main purpose of this report is to document the UNSATCHEM software package for

simulating one-dimensional variably-saturated water flow, heat movement, carbon dioxide production and transport, and the multicomponent transport of major ions. UNSATCHEM consists of the UNSCHEM (version 2.0) computer program, and the UNSATCH (version 1.0) interactive graphics-based user interface. UNSCHEM numerically solves the Richards' equation for saturated-unsaturated water flow and convection-dispersion type equations for carbon dioxide, heat and solute transport. The water flow equation incorporates a sink term to account for water uptake by plant roots. The heat transport equation considers movement by conduction as well as convection with flowing water. The diffusion in both liquid and gas phases and convection in the liquid phase are considered as CO₂ transport mechanisms. CO₂ production model is described. The major variables of the chemical system are Ca, Mg, Na, K, SO₄, Cl, NO₃, H₄SiO₄, alkalinity, and CO₂. The model accounts for equilibrium chemical reactions between these components such as complexation, cation exchange and precipitation-dissolution. For the precipitation-dissolution of calcite and dissolution of dolomite, either equilibrium or multicomponent kinetic expressions are used which include both forward and back reactions. Other dissolution-precipitation reactions considered include gypsum, hydromagnesite, nesquehonite, and sepiolite. Since the ionic strength of soil solutions can vary considerably with time and space and often reach high values, both modified Debye-Hückel and Pitzer expressions were incorporated into the model to calculate single ion activities.

The UNSATCHEM package may be used to analyze water and solute movement in unsaturated, partially saturated, or fully saturated porous media. The flow region itself may be composed of nonuniform soils. Flow and transport can occur in the vertical, horizontal, or in a generally inclined direction. The water flow part of the model considers prescribed head and flux boundaries, as well as boundaries controlled by atmospheric conditions or free drainage. First and third-type boundary conditions can be implemented in both the solute and heat transport parts of the model.

The governing flow and transport equations are solved numerically using standard Galerkin-type linear finite element schemes, or modification thereof. The program is a modified one-dimensional version of the UNSATCHEM-2D code simulating water, CO₂, heat and multicomponent solute movement in two-dimensional variably saturated media [*Šimůnek and Suarez, 1993b, 1994*], and an extension of the one-dimensional variably saturated flow and solute

transport code **HYDRUS-1D** of Šimůnek *et al.* [1997], and carbon dioxide transport code SOILCO2 [Šimůnek and Suarez, 1993c], which in turn were based in part on the variably saturated flow codes S WMS_1D and S WMI of Šimůnek [1991] and Vogel [1990], respectively. Several sections in this report were adopted from the **HYDRUS-1D** [Šimůnek *et al.*, 1997] and **SOILCO2** [Šimůnek and Suarez, 1993c] manuals. The source code was developed and tested on a P.5 using the Microsoft's Fortran PowerStation compiler. Several extensions of the MS Fortran beyond the ANSI standard were used to enable communication with graphic based user-friendly interface.

One major problem which often prevents the widespread use of otherwise well-documented numerical computer codes is the extensive work generally required for input data preparation, finite element grid design, and graphical presentation of the output results. To avoid or simplify the preparation and management of complex input data files for flow problems, and to graphically display the final simulation results, we developed the **UNSATCH** interactive graphics-based user-friendly interface for the MS Windows 3.1, Windows 95, and Windows NT environment. The UNSATCH interface is directly connected to UNSCHEM. The software package is distributed on two 3½ inch floppy diskettes containing all necessary files needed to run the interface and the input and output files of four examples discussed in this report.

A general overview of the UNSATCH graphics-based interface is described in Part B of this manual. In addition to the detailed descriptions in this section, extensive on-line help files are available with each module of the user interface.

PART A

*The UNSCHEM Code for Simulating the One-Dimensional
Variably Saturated Water Flow, Heat Transport, Carbon
Dioxide Production and Transport, and Multicomponent
Solute Transport with Major Ion Equilibrium and Kinetic
Chemistry*

Version 2.0

by

J. Šimůnek and D. L. Suarez

1. INTRODUCTION

This part gives a detailed description of the UNSCHEM computer code which numerically solves the Richards' equation for variably-saturated water flow and convection-dispersion type equations for carbon dioxide, heat and solute transport. The flow equation incorporates a sink term to account for water uptake by plant roots. The heat transport equation considers transport due to conduction and convection with flowing water. The diffusion in both liquid and gas phases and convection in the liquid phase are considered as CO₂ transport mechanisms. CO₂ production model is described. The major variables of the chemical system are Ca, Mg, Na, K, SO₄, Cl, NO₃, H₄SiO₄, alkalinity, and CO₂. The model accounts for equilibrium chemical reactions between these components such as complexation, cation exchange and precipitation-dissolution. For the precipitation-dissolution of calcite and dissolution of dolomite, either equilibrium or multicomponent kinetic expressions are used which include both forward and back reactions. Other dissolution-precipitation reactions considered include gypsum, hydromagnesite, nesquehonite, and sepiolite. The model includes the option to use either an extended Debye-Hückel model to calculate individual ion activities or Pitzer expressions (adapted from *Felmy* [1990]) for calculation of activities at high ionic strength. The program may be used to analyze water and solute movement in unsaturated, partially saturated, or fully saturated porous media. The flow region may be composed of nonuniform soils. Flow and transport can occur in the one-dimensional either vertical, horizontal, or a generally inclined direction. The water flow part of the model can deal with prescribed head and flux boundaries, boundaries controlled by atmospheric conditions, as well as free drainage boundary conditions. The governing flow and transport equations are solved numerically using finite differences and Galerkin-type linear finite element schemes, respectively.

Part B gives a general overview of the UNSATCH graphics-based interface.

2. VARIABLY SATURATED WATER FLOW

2.1. Governing Flow Equation

One-dimensional water movement in a partially saturated rigid porous medium is described by a modified form of the Richards' equation under the assumptions that the air phase plays an insignificant role in the liquid flow process and that water flow due to a thermal gradient can be neglected [Richards, 1952]:

$$\frac{\partial \theta_w}{\partial t} = \frac{\partial}{\partial z} \left[K \left(\frac{\partial h}{\partial z} + \cos \alpha \right) \right] - S \quad (2.1)$$

where h is the water pressure head [L] (terms expressed within [] represent dimensions of the variable), θ_w is the volumetric water content [L^3L^{-3}], K is the unsaturated hydraulic conductivity function [LT^{-1}], t is time [T], z is the spatial coordinate [L] (positive upward), α is the angle between the flow direction and the vertical axis (i.e., $\alpha = 0^\circ$ for vertical flow, 90° for horizontal flow, and $0^\circ < \alpha < 90^\circ$ for inclined flow), and S is the sink/source term [$L^3L^{-3}T^{-1}$], which encompasses water uptake by plant roots. The assumptions and limitations of this prevalent approach have been discussed in detail by others [e.g. Nielsen *et al.*, 1986].

2.2. Root Water Uptake

The sink term, S , is defined as the volume of water removed from a unit volume of soil per unit time due to plant water uptake. A detailed review of different expressions for the root water uptake can be found in Molz [1981]. We based the root water uptake model on the expression first proposed by Feddes *et al.* [1978], modified to include osmotic stress [van Genuchten, 1987]

$$S(h, h_\phi) = \alpha_s(h) \alpha_\phi(h_\phi) S_p \quad (2.2)$$

where S_p is the potential water uptake rate [$L^3L^{-3}T^{-1}$] in the root zone, $\alpha_\phi(h_\phi)$ is the osmotic stress response function [-], h_ϕ is the osmotic head [L], and where the water stress response function,

$\alpha_s(h)$, is a prescribed dimensionless function of the soil water pressure head ($0 \leq \alpha_s \leq 1$) [van Genuchten, 1987]

$$\alpha_s(h) = \frac{1}{1 + \left(\frac{h}{h_{50}}\right)^b} \quad (2.3)$$

where h_{50} [L] and b [-] are empirical constants. The parameter h_{50} represents the pressure head at which the water extraction rate is reduced by 50 %. Note that this formulation of the water stress response function, $\alpha_s(h)$, in contrast to the expression of Feddes *et al.* [1978], does not consider the transpiration reduction near saturation. The osmotic stress response function, $\alpha_\phi(h_\phi)$, is expressed in a similar way as $\alpha_s(h)$ in (2.3), replacing the pressure heads with the osmotic heads.

The potential water uptake rate in the root zone is expressed as the product of the potential transpiration rate, T_p [LT^{-1}], and the normalized water uptake distribution function, $b(z)$ [L^{-1}], which describes the spatial variation of the potential water uptake rate, S_p , over the root zone.

$$S_p = b(z)T_p \quad (3.4)$$

This function describes the spatial variation of the potential extraction term, S_p , over the root zone (Fig. 2.1), and is obtained by normalizing any arbitrarily measured or prescribed root distribution function, $b'(z)$, as follows

$$b(z) = \frac{b'(z)}{\int_{L_r} b'(z) dz} \quad (2.5)$$

where L_r is the region occupied by the root zone. Normalizing the uptake distribution ensures that $b(z)$ integrates to unity over the flow domain, i.e.,

$$\int_{L_r} b(z) dz = 1 \quad (2.6)$$

There are many ways to express the function $b(z)$; constant with depth, linear [Feddes *et al.*,

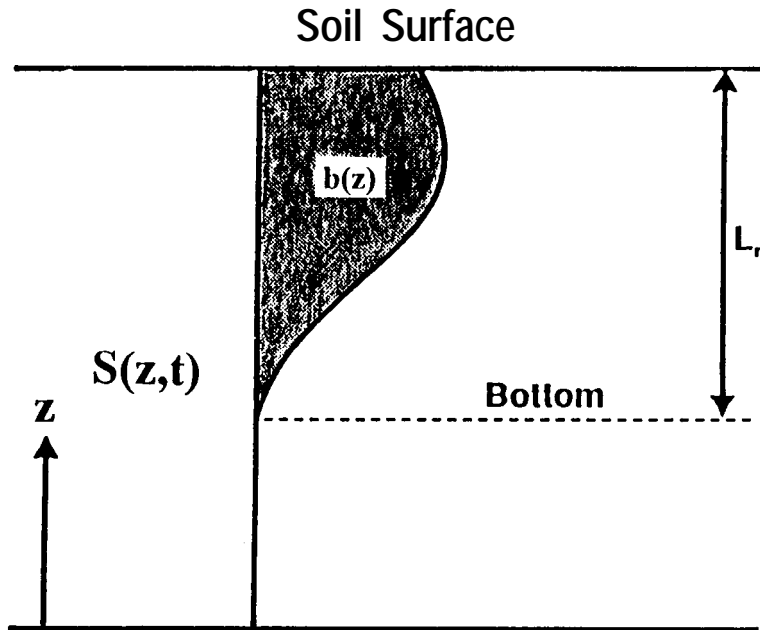


Fig. 2.1. Schematic of the potential water uptake distribution function, $b(z)$, in the soil root zone.

1978], exponential with a maximum at the soil surface [Rum, 1974]:

$$b(z) = a e^{-a(L-z)} \quad (2.7)$$

where L is the z -coordinate of the soil surface [L] and a is an empirical constant [L^{-1}]. *van Genuchten* [1987] suggested the following depth-dependent root distribution function $\beta(z)$:

$$\begin{aligned} b(z) &= \frac{5}{3L_r} & L - 0.2L_r \leq z \leq L \\ b(z) &= \frac{25}{12L_r} \left(1 - \frac{L-z}{L_r}\right) & L - L_r < z < L - 0.2L_r \\ b(z) &= 0 & z \leq L - L_r \end{aligned} \quad (2.8)$$

where L_r is the root depth [L]. The actual transpiration rate, T_a , is obtained by integrating the root water uptake rate over the root zone as follows

$$T_a = \int_{L_r}^L S(h, h_\phi, z) dz = T_p \int_{L_r}^L \alpha_s(h) \alpha_\phi(h_\phi) \beta(z) dz \quad (2.9)$$

The root depth, L_r , can be either constant or variable during the simulation. For annual vegetation a growth model is required to simulate the change in rooting depth with time. In this model we consider the root depth to be the product of the maximum rooting depth, L_m [L], and the root growth coefficient, $f_r(t)$ [-]:

$$L_r(t) = L_m f_r(t) \quad (2.10)$$

To calculate the root growth coefficient, $f_r(t)$, we combined the Verhulst-Pearl logistic growth function with the growth degree day (*GDD*) or heat unit concept [*Gilmore and Rogers, 1958*]. The logistic growth function is usually used to describe the biological growth at constant temperature, whereas the heat unit model is utilized for determining the time between planting and maturity of the plant. The heat unit model cannot be used directly to predict biomass during the growth stage since it would predict a linear growth with time at constant temperature. By combining the heat unit concept with the logistic growth function, we incorporate both time and temperature dependence on growth.

For the growth degree day function we used a modified version of the relation developed by *Logan and Boyland* [1983], who assumed that this function is fully defined by the temperature, T [K], which can be expressed by a sine function to approximate the behavior of temperature during the day, and by the three temperature limits, T_b , T_2 , and T_3 [K]. When the actual temperature is below the base value T_b , plants register little or no net growth. The plant growth is at a maximum level at temperature T_2 , which remains unchanged for some interval up to a maximum temperature T_3 , above which increased temperature has an adverse effect on growth. From this consideration, we use the following dimensionless growth function [*Šimůnek and Suarez, 1993*]:

$$g(t) = \frac{1}{T_{Bas}} \left[\int_0^{t \leq t_p; t \geq t_h} \delta (T - T_1) dt - \int_0^1 \delta (T - T_2) dt - \int_0^{t \leq t_p; t \geq t_h} \delta (T - T_3) dt \right] \quad t \in (t_p, t_m) \quad (2.11)$$

where T_{Bas} are the heat units [KT] necessary for the plant to mature and the roots to reach the maximum rooting depth, t_p, t_m , and t_h represent time of planting, time at which the maximum rooting depth is reached and time of harvesting, respectively; and parameter $\delta[-]$ introduces into the heat unit concept the reduction in optimal growth due to the water and osmotic stress. The expression inside the parenthesis of equation (2.11) reaches value T_{Bas} at time t_m when roots reach the maximum rooting depth. The individual integrals in (2.11) are evaluated only when the particular arguments are positive. The parameter $\delta[-]$ is defined as the ratio of the actual to potential transpiration rates:

$$\delta = \frac{T_a}{T_p} \quad (2.12)$$

Biomass or root development during the growth stage can also be expressed by the Verhulst-Pearl logistic growth function

$$f_r(t) = \frac{L_0}{L'' + (L_m - L_0) e^{-rt}} \quad (2.13)$$

where L_0 is the initial value of the rooting depth at the beginning of the growth period [L] and r is the growth rate [T^{-1}].

Both growth functions (2.11) and (2.13) can be used directly to model root growth. However, to avoid the drawbacks of both concepts, as discussed above, we combine equations (2.11) and (2.13) by substituting the growth function calculated from the heat unit concept (2.11) for the time factor in the logistic growth function (2.13):

$$t = t_m g(t) \quad (2.14)$$

where t_m is the time when GDD reaches the required value for the specific plant species (T_{Bas}). This value is not known a priori; only the product rt_m must be known and that can be selected, for example, so that $f_r(t)$ equals 0.99 for $g(t)=1$.

2.3. The Unsaturated Soil Hydraulic Properties

The unsaturated soil hydraulic properties in the UNSCHEM code are described by a set of closed-form equations resembling those of *van Genuchten* [1980] who used the statistical pore-size distribution model of *Mualem*[1976] to obtain a predictive equation for the unsaturated hydraulic conductivity function. The original van Genuchten equations were modified to add extra flexibility in the description of the hydraulic properties near saturation [Štřir *et al.*, 1985; Vogel and Císlerová, 1988]. The soil water retention, $O(h)$, and hydraulic conductivity, $K(h)$, functions in UNSCHEM are given by:

$$\theta_w(h) = \begin{cases} \theta_p + \frac{\theta_m - \theta_p}{(1 + |\alpha h|^n)^m} & h < h_s \\ \theta_s & h \geq h_s \end{cases} \quad (2.15)$$

and

$$K(h) = \begin{cases} K_s K_r(h) & h \leq h_k \\ K_k + \frac{(h - h_k)(K_s - K_k)}{h_s - h_k} & h_k < h < h_s \\ K_s & h \geq h_s \end{cases} \quad (2.16)$$

respectively, where

$$K_r = \frac{K_k}{K_s} \left[\frac{S_e}{S_{ek}} \right]^{1/2} \left[\frac{F(\theta_r) - F(\theta_w)}{F(\theta_r) - F(\theta_k)} \right]^2 \quad (2.17)$$

$$F(\theta_w) = \left[1 - \left(\frac{\theta_w - \theta_p}{\theta_m - \theta_p} \right)^{1/m} \right]^m \quad (2.18)$$

$$m = 1 - 1/n, \quad n > 1 \quad (2.19)$$

$$S_e = \frac{\theta_w - \theta_r}{\theta_s - \theta_r} \quad (2.20)$$

$$S_{ek} = \frac{\theta_k - \theta_r}{\theta_s - \theta_r} \quad (2.21)$$

in which θ_r and θ_s denote the residual and saturated water contents [L^3L^{-3}], respectively, and K_s is the saturated hydraulic conductivity [LT^{-1}]. To increase the flexibility of the analytical expressions, and to allow for a non-zero air-entry value, h_s [L], the parameters θ_r and θ_s in the retention function were replaced by the fictitious (extrapolated) parameters $\theta_p \leq \theta_r$ and $\theta_m \geq \theta_s$ as shown in Fig. 2.2. This approach maintains the physical meaning of θ_r and θ_s as measurable quantities. Equation (2.17) assumes that the predicted hydraulic conductivity function is matched to a measured value of the hydraulic conductivity, $K_k = K(\theta_k)$, at some water content, θ_k , less than or equal to the saturated water content, i.e., $\theta_k \leq \theta_s$ and $K_k \leq K_s$ [Vogel and Císlerová, 1988; Luckner et al., 1989].

Inspection of (2.15) through (2.21) shows that the hydraulic characteristics contain 9 unknown parameters: θ_r , θ_s , θ_p , θ_m , α , n , K_s , K_k , and θ_k . When $\theta_p = \theta_r$, $\theta_m = \theta_k = \theta_s$ and $K_k = K_s$, the soil hydraulic functions reduce to the original expressions of van Genuchten [1980]:

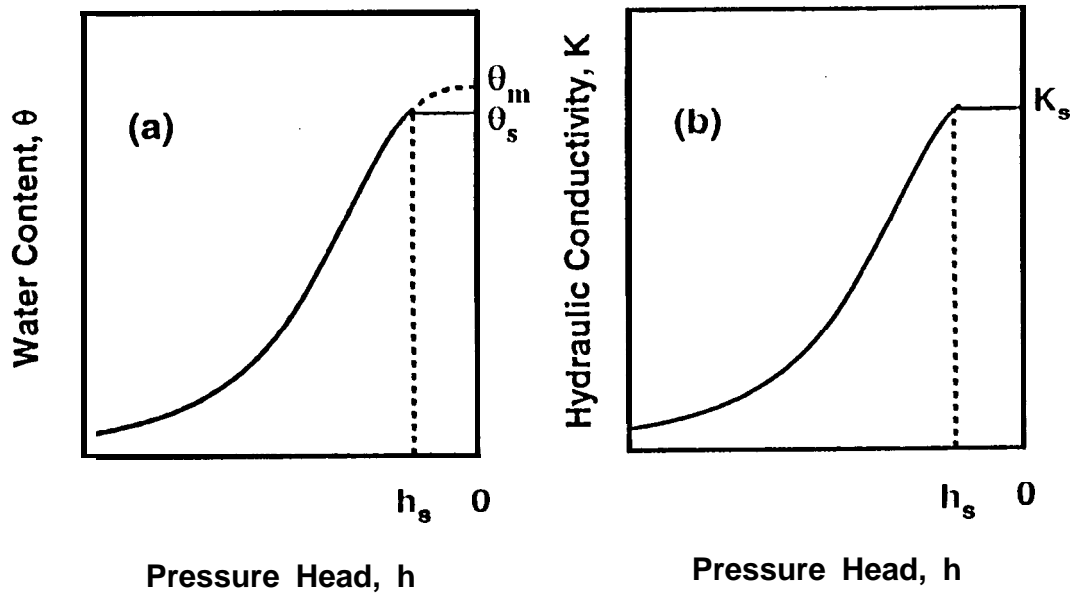


Fig. 2.2. Schematics of the soil water retention (a) and hydraulic conductivity (b) functions as given by equations (2.15) and (2.16), respectively.

$$\theta_w(h) = \begin{cases} \theta_r + \frac{\theta_s - \theta_r}{[1 + |\alpha h|^n]^m} & h < 0 \\ \theta_s & h \geq 0 \end{cases} \quad (2.22)$$

$$K(h) = \begin{cases} K_s K_r(h) & h < 0 \\ K_s & h \geq 0 \end{cases} \quad (2.23)$$

where

$$K_r = S_e^{1/2} [1 - (1 - S_e^{1/m})^m]^2 \quad (2.24)$$

Accumulation of monovalent cations, such as sodium and potassium, may lead to clay dispersion, swelling, flocculation and overall poor soil physicochemical properties. These processes have an adverse effect on the water transmission properties including hydraulic conductivity, infiltration rates and soil retention as the results of swelling and clay dispersion.

These negative effects are usually explained based on the diffuse double layer theory. A consequence of the more diffuse double layer in the presence of monovalent ions as compared to divalent ions is the greater repulsion force or swelling pressure between neighbouring clay platelets. These negative effects become more pronounced with decreasing salt concentration and valence of the adsorbed ions [Shainberg and Levy, 1992]. In addition, Suarez *et al.* [1984] determined that elevated levels of pH also had an adverse effect on the saturated hydraulic conductivity in experiments in which the pH effects were compared at the same exchangeable Na and salinity levels.

The effect of solution chemistry on the hydraulic conductivity is implemented in UNSCHEM as follows

$$K(h, pH, SAR, C_0) = r(pH, SAR, C_0) K(h) \quad (2.25)$$

where SAR is the sodium adsorption ratio, C_0 is the total salt concentration of the ambient solution in $\text{mmol}_c \ell^{-1}$, and r is a scaling factor which represents the effect of the solution composition on the final hydraulic conductivity [-], and which is related to pH , SAR and salinity. The hydraulic conductivity without the scaling factor r can be assumed to be the optimal value under favorable chemical conditions with optimal pH , SAR and salinity. Although the magnitude of these effects appears to be soil specific this process is too important to ignore. We include reduction functions calculated for some illitic soils of California based on the experimental work of McNeal [1968] and Suarez *et al.* [1981]. We divided the overall scaling factor r into two parts

$$r(pH, SAR, C_0) = r_1(SAR, C_0) r_2(pH) \quad (2.26)$$

where the first part, $r_1[-]$, reflects the effect of the exchangeable sodium percentage and dilution of the solution on hydraulic conductivity, while the second part, $r_2[-]$, represents the effect of the soil solution pH . The first term is based on a simple clay-swelling model, which treats mixed-ions clays as simple mixture of homoionic sodium and calcium clay. The clay swelling is then related to decreases in soil hydraulic conductivity [McNeal, 1974]. The r_1 term was defined by McNeal [1968] as

$$r_1 = 1 - \frac{cx^n}{1 + cx^n} \quad (2.27)$$

where c and n are empirical parameters, and x is a swelling factor. The interlayer swelling of soil montmorillonite, x , is defined in the following way

$$x = f_{mont} 3.6 \cdot 10^{-4} \text{ESP}^* d^* \quad (2.28)$$

where f_{mont} is a weight fraction of montmorillonite in the soil, d^* is adjusted interlayer spacing [L] and ESP^* is adjusted exchangeable sodium percentage. For most soils, we can use the assumption that $f_{mont} = 0.1$ [McNeal,1968]. Adjusted exchangeable sodium percentage is calculated as

$$\text{ESP}^* = \max[0, \text{ESP} - (1.24 + 11.63 \log C_0)] \quad (2.29)$$

where C_0 is total salt concentration of the ambient solution in $\text{mmol}_c \ell^{-1}$ and ESP is defined as

$$\text{ESP} = \frac{\bar{N}_{\text{Na}}}{\text{CEC}} \cdot 100 \quad (2.30)$$

where CEC is a soil cation exchange capacity ($\text{mmol}_c \text{kg}^{-1}$) and \bar{N}_{Na} is exchangeable sodium concentration ($\text{mmol}_c \text{kg}^{-1}$). The adjusted interlayer spacing, d^* , is given as follows

$$\begin{aligned} d^* &= 0 && \text{for } C_0 > 300 \text{ mmol}_c \ell^{-1} \\ d^* &= 356.4 C_0^{-1/2} + 1.2 && \text{for } C_0 < 300 \text{ mmol}_c \ell^{-1} \end{aligned} \quad (2.31)$$

McNeal [1968] reported that the values of the empirical factor n in equation (2.27) depend primarily on the soil ESP and that as a first approximation acceptable n values are

$$\begin{aligned} n &= 1 && \text{for } \text{ESP} < 25 \\ n &= 2 && \text{for } 25 \leq \text{ESP} \leq 50 \\ n &= 3 && \text{for } \text{ESP} > 50 \end{aligned} \quad (2.32)$$

Only the values of empirical factor c vary from one soil to the next. In UNSCHEM we use values reported by McNeal[1968]

$$\begin{aligned} c &= 35 && \text{for } \text{ESP} < 25 \\ c &= 932 && \text{for } 25 \leq \text{ESP} \leq 50 \\ c &= 25000 && \text{for } \text{ESP} > 50 \end{aligned} \quad (2.33)$$

The reduction factor, r_2 , for the effect of pH on hydraulic conductivity was calculated from the experimental data of *Suarez et al.* [1984] after first correcting for the adverse effects of low salinity and high exchangeable sodium using the r_1 values.

$$\begin{aligned}
 r_2 &= 1 && \text{for } \text{pH} < 6.83 \\
 r_2 &= 3.46 - 0.36\text{pH} && \text{for } 6.83 \leq \text{pH} \leq 9.3 \\
 r_2 &= 0.1 && \text{for } \text{pH} > 9.3
 \end{aligned}
 \tag{2.34}$$

Note, that although the models for the reduction of the soil hydraulic conductivity due to effects of solution composition were derived from the data on the saturated hydraulic conductivity, we use the same reduction factors for the entire range of the pressure heads. The assumption that the r values for saturated conditions can be applied to the entire range of pressure heads has not yet been adequately evaluated.

2.4. Initial and Boundary Conditions

The initial condition for the soil water pressure head is given by

$$h(z, t) = h_i(z) \quad t = t_0 \tag{2.35}$$

where h_i [L] is a prescribed function of z , and t_0 is the time at the start of the simulation.

One of the following boundary conditions must be specified at the soil surface ($z=L$) or at the bottom of the soil profile ($z=0$):

$$\begin{aligned}
 h(z, t) &= h_0(t) && \text{at } z = 0 \text{ or } z = L \\
 -K \left(\frac{\partial h}{\partial z} + \cos \alpha \right) &= q_{w0}(t) && \text{at } z = 0 \text{ or } z = L \\
 \frac{\partial h}{\partial z} &= 0 && \text{at } z = 0
 \end{aligned}
 \tag{2.36}$$

where h_0 [L] and q_{w0} [L T^{-1}] are the prescribed pressure head and soil water flux at the boundary, respectively.

In addition to the system-independent boundary conditions given by (2.36), we consider two system-dependent boundary conditions which cannot be defined a priori. One of these boundary conditions involves the soil-air interface which is exposed to atmospheric conditions. The potential fluid flux across this interface is controlled exclusively by external conditions. However, the actual flux depends also on the prevailing (transient) soil moisture conditions (among other factors). The soil surface boundary condition may change from prescribed flux to prescribed head type condition (and vice-versa). The numerical solution of (2.1) is obtained by limiting the absolute value of the flux by the following two conditions [Neuman *et al.*, 1974]:

$$\left| -K\left(\frac{\partial h}{\partial z} + \cos\alpha\right) \right| \leq E_w \quad \text{at } z = L \quad (2.37)$$

and

$$h_A \leq h \leq h_S \quad \text{at } z = L \quad (2.38)$$

where E_w is the maximum potential rate of infiltration or evaporation under the current atmospheric conditions [LT^{-1}], h is the pressure head at the soil surface, and h_A and h_S are, respectively, minimum and maximum pressure heads allowed under the prevailing soil conditions [L]. The value for h_A is determined from the equilibrium conditions between soil water and atmospheric water vapor, whereas h_S is usually set equal to zero and, if positive, it represents a small layer of water ponded at the soil surface. which can form during heavy rains before initiation of runoff. UNSCHEM assumes when using this boundary condition that any excess water on the soil surface above the value h_S is immediately removed. When one of the endpoints of (2.37) is reached, a prescribed head boundary condition will be used to calculate the actual surface flux. Methods of calculating E_w and h_A on the basis of atmospheric data have been discussed by Feddes *et al.* [1974].

Another option in UNSCHEM is to permit water to build up on the surface. If surface ponding is expected to develop, a “surface reservoir” boundary condition of the type [Mls,1982]

$$-K\left(\frac{\partial h}{\partial z} + \cos\alpha\right) = q_{w0}(t) - \frac{dh}{dt} \quad \text{at } z = L \quad (2.39)$$

may be applied. The flux q_{w0} in this equation is the net infiltration rate, i.e., the difference between precipitation and evaporation. Equation (2.39) shows that the height $h(L,t)$ of the surface water layer increases due to precipitation, and reduces because of infiltration and evaporation.

A third type of system-dependent boundary condition considered in UNSCHEM which can be applied at the bottom of the soil profile is a seepage face through which water leaves the saturated part of the flow domain. This type of boundary condition assumes that a zero-flux boundary condition applies as long as the local pressure head at the bottom of the soil profile ($z = 0$) is negative. However, a zero pressure head will be used as soon as the bottom of the profile becomes saturated. This type of boundary condition often applies to finite lysimeters which are allowed to drain under gravity.

Another system-dependent lower boundary condition may be imposed in cases where a functional relationship between the position of the water table and drainage from the soil profile can be established. One possible relationship of this type is discussed in Section 10.3.

2.5. Plant Yield Model

Calculation of plant yield is based on the assumption that crop production is directly related to actual-evapotranspiration, ET , [L], or evapotranspiration deficit, ET_d , [L] [Hanks and Hill, 1980]. This concept was introduced by Stewart and co-workers [Stewart and Hagan, 1973; Stewart et al., 1974; Stewart et al., 1975] whose basic equation for dry matter production is

$$\frac{Y}{Y_M} = 1 - \beta_0 ET_d = 1 - \beta_0 \left(1 - \frac{ET_a}{ET_p}\right) \quad (2.40)$$

where Y is actual dry matter yield [M], Y_M is maximum dry matter yield for the conditions when $ET_a = ET_p$ [M], ET_a is actual evapotranspiration [L], ET_p is potential seasonal evapotranspiration [L], and β_0 is the slope of the relative yield (Y/Y_M) versus the ET_d relation [-]. Stewart et al. [1977] have shown that the value of β_0 is relatively constant and varies only from about 1. to 1.3. In our model the default value of β_0 is 1.0.

3. MULTICOMPONENT SOLUTE TRANSPORT

3.1. Governing Solute Transport Equations

The partial differential equation governing one-dimensional advective-dispersive chemical transport under transient water flow conditions in partially saturated porous medium is taken as

$$\frac{\partial \theta_w c_k}{\partial t} + \rho \frac{\partial \bar{c}_k}{\partial t} + \rho \frac{\partial \hat{c}_k}{\partial t} \cong \frac{\partial}{\partial z} [\theta_w D \frac{\partial c_k}{\partial z} - q_w c_k] \quad k=1,2,\dots,N_c \quad (3.1)$$

where c_k is the total dissolved concentration of the aqueous species k [ML⁻³], \bar{c}_k is the total surface species concentration of the aqueous component k [MM⁻¹], \hat{c}_k is the total solid phase concentration of aqueous component k [MM⁻¹], ρ is the bulk density of the medium [ML⁻³], D is the dispersion coefficient [L²T⁻¹], q_w is the volumetric flux [LT⁻¹] and N_c is the number of primary aqueous species. The second and third terms on the left side of eq. (3.1) are zero for species that do not undergo ion exchange or precipitation/dissolution. The volumetric flux q_w is calculated with Darcy's Law

$$q_w = -K \left(\frac{\partial h}{\partial z} + \cos \alpha \right) \quad (3.2)$$

3.2. Effective Dispersion Coefficient

The effective dispersion coefficient, D , in (3.1) is given by

$$\theta_w D = D_L |q_w| + \theta_w D_m \tau_w \quad (3.3)$$

where $D_{L,m}$ is the ionic or molecular diffusion coefficient in free water [L²T⁻¹], τ_w is a tortuosity factor in the dissolved phase [-], $|q_w|$ is the absolute value of the Darcian fluid flux density [L T⁻¹], and $D_{L,m}$ is the longitudinal dispersivity [L]. The dispersion coefficient represents the combined effect of molecular diffusion and mechanical dispersion.

The tortuosity factor is evaluated in UNSCIEM as a function of the water content using

the relationship of *Millington and Quirk [1961]*:

$$\tau_w = \frac{\theta_w^{7/3}}{\theta_s^2} \quad (3.4)$$

3.3. Initial and Boundary Conditions

The solution of (3.1) requires knowledge of the initial concentration within the flow region, i.e.,

$$c(z, 0) = c_i(z) \quad t = 0 \quad (3.5)$$

where c_i is a prescribed function of z [ML³]. The index k is dropped to simplify the notation.

Two types of boundary conditions (Dirichlet and Cauchy type conditions) can be specified on both the upper and lower soil profile boundaries. First-type (or Dirichlet type) boundary conditions prescribe the concentration:

$$c(z, t) = c_0(z, t) \quad \text{at } z = 0 \text{ or } z = L \quad (3.6)$$

whereas third-type (Cauchy type) boundary conditions may be used to prescribe the concentration flux as follows:

$$-\theta_w D \frac{\partial c}{\partial z} + q_w c = q_w c_0 \quad \text{at } z = 0 \text{ or } z = L \quad (3.7)$$

in which c_0 is the concentration of the fluid [ML⁻³]. In some cases, for example when a boundary is impermeable ($q_w=0$) or when water flow is directed out of the region, (3.7) reduces to a second-type (Neumann type) boundary condition of the form:

$$\frac{\partial c}{\partial z} = 0 \quad \text{at } z = 0 \quad (3.8)$$

4. HEAT TRANSPORT

4.1. Governing Heat Transport Equations

Neglecting the effect of water vapor diffusion on transport, one-dimensional heat transport can be described by a convective-dispersive equation in a conservative form as

$$\frac{\partial C_p(\theta_w)T}{\partial t} = \frac{\partial}{\partial z} [\lambda(\theta_w) \frac{\partial T}{\partial z}] - C_w \frac{\partial q_w T}{\partial z} - C_w S T \quad (4.1)$$

or in a more often used advective form [*Sophocleous*, 1979]:

$$C_p(\theta_w) \frac{\partial T}{\partial t} = \frac{\partial}{\partial z} [\lambda(\theta_w) \frac{\partial T}{\partial z}] - C_w q_w \frac{\partial T}{\partial z} \quad (4.2)$$

where $\lambda(\theta_w)$ is the coefficient of the apparent thermal conductivity of the soil [$\text{WL}^{-1}\text{K}^{-1}$] and $C_p(\theta_w)$ and C_w are the volumetric heat capacities [$\text{JL}^{-3}\text{K}^{-1}$] of the porous medium and the liquid phase, respectively. Volumetric heat capacity is defined as the product of the bulk density and gravimetric heat capacity. The first term on the right-hand side of (4.1) represents the heat flow due to conduction, the second term the heat transported by the flowing water and the third term the energy uptake by plant roots associated with root water uptake. The equation (4.2) is derived from (4.1) by substituting the continuity equation which describes isothermal Darcian flow of water in a variably saturated porous medium

$$\frac{\partial \theta_w}{\partial t} = - \frac{\partial q_w}{\partial z} - S \quad (4.3)$$

We do not consider the transfer of latent heat by vapor movement. The volumetric heat capacity can be expressed as [*de Vries*, 1963]

$$C_p(\theta_w) = C_n \theta_n + C_o \theta_o + C_w \theta_w + C_a \theta_a \approx (1.92 \theta_n + 2.51 \theta_o + 4.18 \theta_w) 10^6 \quad (\text{Jm}^{-3} \text{ } ^\circ\text{C}^{-1}) \quad (4.4)$$

where θ is the volumetric fraction [L^3L^{-3}] and subscripts n, o, a, w represent mineral solid phase, organic matter (solid phase), gas phase and liquid phase, respectively.

4.2. Apparent Thermal Conductivity Coefficient

The coefficient of the apparent thermal conductivity $\lambda(\theta_w)$ combines the thermal conductivity $\lambda_0(\theta_w)$ of the porous medium (solid plus water) in the absence of flow and the macrodispersivity, which is a linear function of the velocity [de Marsily, 1986]

$$\lambda(\theta_w) = \lambda_0(\theta_w) + \beta_l C_w |q_w| \quad (4.5)$$

where β_l is thermal dispersivity [L]. The volumetric heat capacity of the liquid phase is included in the definition of the thermal conductivity in order to have the dimensions of the thermal dispersivity in units of length. Thermal conductivity is described by Chung and Horton [1987] with the equation

$$\lambda_0(\theta_w) = b_1 + b_2 \theta_w + b_3 \theta_w^{0.5} \quad (4.6)$$

where b_1 , b_2 , and b_3 are empirical parameters [$WL^{-1}K^{-1}$].

4.3. Initial and Boundary Conditions

The solution of (4.1) requires knowledge of the initial temperature within the flow region, i.e.,

$$T(z, t) = T_i(z) \quad t = 0 \quad (4.7)$$

where T_i is a prescribed function of z .

Two types of boundary conditions (Dirichlet and Cauchy type conditions) can be specified at the boundary. First-type (or Dirichlet type) boundary conditions prescribe the temperature:

$$T(z, t) = T_0(t) \quad \text{a t } z = 0 \quad \text{o r } z = L \quad (4.8)$$

whereas third-type (Cauchy type) boundary conditions may be used to prescribe the heat flux as follows:

$$-\lambda \frac{\partial T}{\partial z} + T C_w q_w = T_0 C_w q_w \quad \text{at } z = 0 \text{ or } z = L \quad (4.9)$$

in which T_0 is either the temperature of the incoming fluid or the temperature at the boundary. In some cases, for example for an impermeable boundary ($q_w=0$) or when water flow is directed out of the region, (4.9) reduces to a second-type (Neumann type) boundary condition of the form:

$$\frac{\partial T}{\partial z} = 0 \quad \text{at } z = 0 \quad (4.10)$$

The atmospheric boundary condition for soil temperature is determined by a sine function as follows [Kirkham and Powers, 1972]:

$$T_0 = \bar{T} + A \sin\left(\frac{2\pi t}{p_t} - \frac{7\pi}{12}\right) \quad (4.11)$$

where p_t is a period of time [T] necessary to complete one cycle of the sine wave (taken to be 1 day), \bar{T} is the average temperature at the soil surface [K] during the period p_t , and A is the amplitude of the sine wave [K]. The second part of the sine term is included to allow for a maximum in the daily temperature at 1 p.m.

5. CARBON DIOXIDE TRANSPORT AND PRODUCTION

5.1. Governing CO₂ Transport Equations

Gas transport in the unsaturated zone is a complex physical process that includes three general transport mechanisms [Massmann and Farrier, 1992]: Knudsen diffusion, multicomponent molecular diffusion and viscous flow. Thorstenson and Pollock [1989] presented the equations that describe these transport mechanisms in a multicomponent gas mixture, as well as the Stefan-Maxwell approximation of these equations, where Knudsen diffusion and viscous flow are neglected. The original equations, as well as the Stefan-Maxwell approximation, are fully coupled and generally highly nonlinear. However, Massmann and Farrier [1992] showed that gas fluxes in the unsaturated zone can be simulated using the single-component transport equation if the gas permeability of the porous media is greater than about 10^{-10} cm². For these conditions the effects of Knudsen diffusion can be neglected. They also showed that overestimation of the gas fluxes using the single component advection diffusion equation becomes quite large for permeabilities of the order of 10^{-12} to 10^{-13} cm². Since permeabilities smaller than 10^{-12} cm² occur only for very fine grained materials or for soils close to saturation, use of the transport equation based on Fick's law to represent diffusive flux seems to be justified and adequate. Also, Freijer and Leffelaar [1996] showed that CO₂ concentrations and fluxes can be described by Fick's law to within 5% accuracy. A detailed development of the carbon dioxide transport model and justification of assumptions were given in Šimůnek and Suarez [1993].

We assume that the CO₂ transport in the unsaturated zone can occur in both the liquid and gas phases. Furthermore, we consider that the CO₂ concentration in the soil is governed by two transport mechanisms [Patwardhan et al., 1988], convective transport and diffusive transport in both gas and aqueous phases, and by CO₂ production and/or removal. Thus one-dimensional CO₂ transport is described by the following mass balance equation:

$$\frac{\partial c_t}{\partial t} = -\frac{\partial}{\partial z} (J_{da} + J_{lw} + J_{ca} + J_{cw}) - Sc_w + P \quad (5.1)$$

where J_{da} describes the CO₂ flux caused by diffusion in the gas phase [LT⁻¹], J_{lw} the CO₂ flux

caused by dispersion in the dissolved phase [LT^{-1}], J_{ca} the CO, flux caused by convection in the gas phase [LT^{-1}], and J_{cw} the CO, flux caused by convection in the dissolved phase [LT^{-1}]. The term c_T is the total volumetric concentration of CO, [L^3L^{-3}] and P is the CO, production/sink term [$\text{L}^3\text{L}^{-3}\text{T}^{-1}$]. The term S_{c_w} , represents the dissolved CO, removed from the soil by root water uptake. This assumes that when plants take up water the dissolved CO_2 is also removed from the soil-water system. The individual terms in (5.1) can be defined [*Patwardhan et al., 1988*] as

$$\begin{aligned} J_{da} &= -\theta_a D_a \frac{\partial c_a}{\partial z} \\ J_{dw} &= -\theta_w D_w \frac{\partial c_w}{\partial z} \\ J_{ca} &= -q_a c_a \\ J_{cw} &= -q_w c_w \end{aligned} \quad (5.2)$$

where c_w and c_a , are the volumetric concentrations of CO, in the dissolved phase and gas phase [L^3L^{-3}], respectively, D_a is the effective soil matrix diffusion coefficient of CO, in the gas phase [L^2T^{-1}], D_w is the effective soil matrix dispersion coefficient of CO_2 in the dissolved phase [L^2T^{-1}], q_a is the soil air flux [LT^{-1}], q_w is the soil water flux [LT^{-1}] and θ_a is the volumetric air content [L^3L^{-3}].

The total CO, concentration, c_T [L^3L^{-3}], is defined as the sum of CO, in the gas and dissolved phases

$$c_T = c_a \theta_a + c_w \theta_w \quad (5.3)$$

. After substituting (5.2) and (5.3) into (5.1) we obtain

$$\frac{\partial (c_a \theta_a + c_w \theta_w)}{\partial t} = \frac{\partial}{\partial z} \theta_a D_a \frac{\partial c_a}{\partial z} + \frac{\partial}{\partial z} \theta_w D_w \frac{\partial c_w}{\partial z} - \frac{\partial}{\partial z} q_a c_a - \frac{\partial}{\partial z} q_w c_w - S_{c_w} + P \quad (5.4)$$

The total aqueous phase CO_2 , c_w , is defined as the sum of $\text{CO}_2(\text{aq})$ and H_2CO_3 , and is related to the CO, concentration in the gas phase by [*Stumm and Morgan, 1981*]

$$c_w = K_{CO_2} R T c_a \quad (5.5)$$

where K_{CO_2} is the Henry's Law constant [$MT^2M^{-1}L^{-2}$], R is the universal gas constant ($8.314 \text{ kg m}^2 \text{ s}^{-2} \text{ K}^{-1} \text{ mol}^{-1}$) [$ML^2T^{-2}K^{-1}M^{-1}$] and T is the absolute temperature [K]. The value of K_{CO_2} as a function of temperature is taken from *Harned and Davis* [1943]. We do not consider the interaction of dissolved CO_2 with the solid phase at this time. The quantity of CO_2 added or removed by mineral dissolution/precipitation reactions is relatively small compared to the production and flux values in rootzone environment. This assumption will not be suitable for saturated water flow or at large depths.

Substituting equation (5.5) into (5.4) gives

$$\frac{\partial R_f c_a}{\partial t} = \frac{\partial}{\partial z} D_E \frac{\partial c_a}{\partial z} - \frac{\partial}{\partial z} q_E c_a - S^* c_a + P \quad (5.6)$$

where R_f is the CO_2 retardation factor [-], D_E is the effective dispersion coefficient for the CO_2 in the soil matrix [L^2T^{-1}], q_E is the effective velocity of CO_2 , [LT^{-1}], S^* is the CO_2 uptake rate [T^{-1}] associated with root water uptake and θ_a is the volumetric air content [L^3L^{-3}]. These parameters are defined as

$$\begin{aligned} R_f &= \theta_a + K_{CO_2} R T \theta_w \\ D_E &= \theta_a D_a + K_{CO_2} R T \theta_w D_w \\ q_E &= q_a + K_{CO_2} R T q_w \\ \theta_a &= p - \theta_w \\ S^* &= S K_{CO_2} R T \end{aligned} \quad (5.7)$$

Equation (5.6) is a nonlinear partial differential equation where, except for c_a and q_a , all parameters are either known or are obtained from solution of the water flow equation. The nonlinearity of (5.6) is caused by the term P which is dependent on CO_2 concentration, c_a . Since we do not consider coupled water and air movement, the flux of air, q_a , is unknown and thus it is necessary to make some additional assumptions. One possibility is to assume that the advection of CO_2 , in response to the total pressure gradient is not important compared to CO_2

diffusion, and therefore to assume a stagnant gas phase and consider only diffusion transport with the gas phase ($q_a=0$). Another possibility is to consider that because of the much lower viscosity of air in comparison to water, significant gas flow can be caused by a relatively small pressure gradient. Thus, only rarely will the gas phase not be at atmospheric pressure throughout the unsaturated zone. Therefore, under most conditions, the compressibility of the air can be neglected. Then, with the assumption that the air flux is zero at the lower soil boundary and that the water volume changes in the soil profile caused by the water flow must be immediately matched by the corresponding changes in the gas volume, we obtain the following equation [Šimůnek and Suarez, 1993]:

$$q_a(z) = q_w(0) - q_w(z) + \int_{l-l_r}^z S(z) dz \quad (5.8)$$

This latter assumption seems to be reasonable, since when water leaves the soil system due to evaporation and root water uptake, air enters the soil at the surface and, vice versa, when water enters the soil during precipitation and irrigation events, soil air is escaping. Only in the case of saturation (typically at the soil surface) does the condition arise that air can not escape and is compressed under the wetting front.

5.2. Effective Dispersion Coefficient

We define the dispersion coefficients, D_w , and the diffusion coefficient, D_a , as

$$D_w = D_{ws} \tau_w + \lambda_w \left| \frac{q_w}{\theta_w} \right| = D_{ws} \frac{\theta_w^{7/3}}{p^2} + \lambda_w \left| \frac{q_w}{\theta_w} \right| \quad (5.9)$$

$$D_a = D_{as} \tau_a = D_{as} \frac{\theta_a^{7/3}}{p^2}$$

where D_w , and D_{ws} are the diffusion coefficients [L^2T^{-1}] of CO, in the gas and dissolved phase, respectively, τ_a and τ_w are the tortuosity factors [LL^{-1}] in both phases, respectively. p is porosity

[L³L⁻³] assumed to be equal to the saturated water content θ_s , and λ_w is the dispersivity in the water phase [L]. The tortuosity factors τ_a and τ_w include not only the tortuosity of the flow paths but also the amount of air and liquid space available for diffusion, respectively. The tortuosity factors in both phases are defined in a manner similar to that used by *Millington and Quirk* [1961]. The first term in (5.9) represents the diffusion component and the second term the hydrodynamic component of the dispersion coefficient. We did not consider the mechanical dispersion in the gas phase since diffusion is the dominant process of CO₂ transport in this phase unless the air velocity is very high. The diffusion coefficients D_{as} and D_{ws} , as functions of temperature, are taken from *Glinski and Stepniewski* [1985].

The existing non-empirical models for CO₂ transport are mostly based on the assumption that the principal transport mechanism for CO₂ is molecular diffusion [*van Bavel*, 1951; *de Jong and Schappert*, 1972; *Solomon and Cerling*, 1987] and do not consider other transport mechanisms nor the influence of water and air flow. *Suarez and Šimůnek* [1993] have shown that water flow can have a significant effect on the soil CO₂ concentration profiles by redistributing CO₂ in the direction of flow. Thus downward flow of a water containing high concentrations of dissolved CO₂ increases the CO₂ concentrations of the gas phase in the lower horizons and upward flow of a water depleted of CO₂ decreases the concentration of CO₂ in the lower horizons. Diffusion in the liquid phase is usually neglected because the diffusion coefficient of CO₂ in the gas phase, D_{as} , is about ten thousand times higher than the diffusion coefficient in the liquid phase, D_{ws} . Therefore the diffusion in the gas phase is dominant within almost the entire range of water contents observed under natural conditions. However, it can be shown that near saturation, due to the combined effect of tortuosity in both phases, the contribution of liquid phase diffusion to the effective diffusion coefficient in the soil matrix, D_{fs} , is higher than the contribution by gas phase diffusion. Both contributions are equal when the volumetric air content, θ_a , is about 6% of the total porosity, as can be calculated from the following expression derived from (5.7), (5.9) and (5.10) for stagnant soil water [*Šimůnek and Suarez*, 1993]

$$\frac{\theta_a}{p} = \left[\left(\frac{D_{as}}{K_{CO_2} R T D_{ws}} \right)^{3/10} + 1 \right]^{-1} \quad (5.11)$$

A similar expression can be derived for the minimum value of the effective diffusion coefficient. D_E , only the exponent 3/10 must be replaced by 3/7. This minimum is reached when only about 2% of the total porosity is occupied by air. At this point the effective diffusion coefficient. D_E , is about five orders of magnitude smaller than the maximum possible effective diffusion coefficient for completely dry soil.

5.3. Initial and Boundary Conditions

The initial condition for the CO, concentration in the gas phase is given by

$$c_a(z, t) = c_{ai}(z) \quad t = 0 \quad (5.12)$$

where $c_{ai}(z)$ is a prescribed function of z [L^3L^{-3}].

The first-type or the third-type boundary conditions may be specified at the surface (or at the bottom) of the soil profile

$$c_a(z, t) = c_{a0}(t) \quad \text{at } z = 0 \text{ or } z = L \quad (5.13)$$

$$-D_E \frac{\partial c_a}{\partial z} + q_E c_a = q_{E0} c_{a0} \quad \text{at } z = 0 \text{ or } z = L \quad (5.14)$$

where q_{E0} is a prescribed CO, effective total flux [LT^{-1}] and c_{a0} is the concentration [L^3L^{-3}] associated with this flux or prescribed at the boundary.

At the soil surface, c_{a0} represents the equilibrium concentration of CO, in the atmosphere (0.035%). In this case the first-type boundary condition (5.13) allows the maximum CO, flux into the atmosphere. It is difficult to apply the third-type boundary condition (5.14), since the parameter q_E includes both the soil air and soil water fluxes, which are not known a priori and are obtained from solution of the water flow equation. Another option is to neglect the convective fluxes and to assume that there is a stagnant boundary layer of thickness d [L] at the soil surface through which the transport of a gas occurs by vapor diffusion only [*Jury et al.*, 1983,1990; *Sleep and Sykes*. 1989], which leads to the following equation

$$D_E \frac{\partial c_a}{\partial z} + q_E c_a = \frac{\alpha_s}{\tau} (c_{as} - c_{atm}) \quad \text{at } z = L \quad (5.15)$$

where c_{as} is the concentration in the soil gas at the soil surface [L^3L^{-3}] and c_{atm} is the concentration at the top of the stagnant boundary layer [L^3L^{-3}]. *Jury et al.* [1983] referred to D_{as}/d as the boundary transfer coefficient [LT^{-1}] and discussed ways of estimating this coefficient.

At the bottom of the soil profile either a continuous concentration profile is assumed

$$\frac{\partial c_a}{\partial z}(z, t) = 0 \quad \text{at } z = 0 \quad (5.16)$$

or the third-type boundary condition (5.14) may be used, in which case the convective fluxes q_{a0} and q_a are equal to zero as discussed above. Boundary condition (5.16) implies that the dispersive flux is equal to zero and that the flux through the boundary is only due to convection. A discussion of the applicability of different types of boundary conditions is given by, among others, *Baehr* [1987] and *Patwardhan et al.* [1988].

5.4. Production of Carbon Dioxide

The mechanism of production/consumption of CO₂ is a complex process that includes not only biological processes, such as the production of CO₂ by soil microbes and plant roots, but also chemical reactions with mineral and organic components, respiration of soil microfauna, etc. Since processes other than the biological ones are generally of relatively minor importance for CO₂ production in the soil, we do not include them into our present production submodel. The production of CO₂ is influenced by many environmental factors, the most important ones being water content and temperature. The changes in CO₂ concentration and corresponding changes in oxygen concentration in the soil atmosphere may affect the CO₂ production rate. Other important factors affecting the CO₂ production are, for example, soil depth, salinity, nutrient status of the soil, and agricultural practices, such as plowing or application of fertilizers, etc. Overviews of the rather large literature on the processes influencing CO₂ production are provided by *Singh and Gupta* [1977] and *Glinski and Stepniewski* [1985].

We assume that the individual CO₂ production processes are additive (5.17) and that it is possible to superpose individual mechanisms which reduce production from the optimal value (5.18) [Šimůnek and Suarez, 1993]. The production of CO₂ is then considered as the sum of the production by the soil microorganisms, γ_s [L³L⁻³T⁻¹], and the production by plant roots, γ_p [L³L⁻³T⁻¹]:

$$S = \gamma_s + \gamma_p \quad (5.17)$$

$$\gamma_s = \gamma_{s0} \prod_i f_{si} \quad \gamma_p = \gamma_{p0} \prod_i f_{pi} \quad (5.18)$$

$$\prod f_i = f(z) f(h) f(T) f(c_a) f(h_\phi) f(t) \quad (5.19)$$

where the subscript s refers to soil microorganisms and the subscript p refers to plant roots, $f(z)$ is the reduction coefficient dependent on depth [L⁻¹], $f(T)$ is the reduction coefficient dependent on temperature [-], $f(h)$ on the pressure head (the soil water content) [-], $f(c_a)$ on the CO₂ concentration [-], $f(h_\phi)$ on the osmotic head [-], and $f(t)$ on time [-]. The parameters γ_{s0} and γ_{p0} represent the optimal CO₂ production by the soil microorganisms or plant roots for the entire soil profile at 20°C under optimal water, solute and CO₂ concentration conditions [L³L⁻²T⁻¹], respectively [Šimůnek and Suarez, 1993]. An expression similar to (5.19) was used by Hansen and Aslyng [1984] to represent nitrogen mineralization. The definition of particular reduction coefficients was given by Šimůnek and Suarez [1993].

The CO₂ production decreases sharply with depth as a result of a decrease in root mass and readily decomposable organic matter. Glinski and Stepniewski [1985] stated that over 90% of soil respiration activity is concentrated in the humus horizon of the soil. There are many possible expressions to relate the dependence of the production term $f_s(z)$ on soil depth. One example is an expression similar to the normalized distribution function $\beta(z)$ given by van Genuchten [1987] for the root water uptake. Another possibility is to use, again, the exponential distribution with depth [Runts, 1974]

$$f_s(z) = a e^{-a(l-z)} \quad (5.20)$$

where a is an empirical constant [L^{-1}]. The exponential function is multiplied by a constant a in order to insure that the integral from the soil surface to infinite depth of the function $f_s(z)$ is equal to unity. However, since the depth of the soil profile or the root depth is finite, the distribution function $f_s(z)$ must always be normalized. We assume that at any time t the dependence of the CO₂ production by plant roots corresponds to the distribution function $\beta(z)$ used for the water uptake by plant roots (see Section 2.2).

The dependence of CO₂ production on water content was studied by many researchers [Miller and Johnson, 1964; Ekpete and Cornfield, 1965; Rixon, 1968; Williams et al., 1972; Bridge and Rixon, 1976; among others]. With respect to the water requirement of microbes, there is a reduction in the respiration rate at low as well as at high water contents. Low accessibility of soil water causes a reduction in CO₂ production at high pressure heads [Ekpete and Cornfield, 1965; Wilson and Griffin, 1975]. The observed reduction of the respiration rate at low pressure heads is explained by the unavailability of oxygen because of the high water content and, therefore, its low diffusion rate through the soil. On the basis of the foregoing discussion and in view of the experimental data of Williams et al. [1972] and Rixon [1968], the CO₂ reduction coefficient $f_s(h)$ as a function of the soil water content for soil microorganisms is expressed as

$$\begin{aligned} f_s(h) &= 1 & h \in (h_2, +\infty) \\ f_s(h) &= \frac{\log |h| - \log |h_3|}{\log |h_2| - \log |h_3|} & h \in (h_3, h_2) \\ f_s(h) &= 0 & h \in (-\infty, h_3) \end{aligned} \quad (5.21)$$

where h_2 is the pressure head when CO₂ production is optimal [L] and h_3 is the pressure head when production ceases [L]. Note that the pressure head reduction function is assumed to be one close to saturation for water pressure heads higher than h , [L]. Rather than treat the oxygen stress with a pressure head relation it seems preferable to consider a separate response function $f(c_a)$. The dependence of the reduction term $f_p(h)$ on soil pressure head is represented by

expressions similar to the reduction function $a_{r,h}$ described by (2.3).

The influence of temperature on chemical processes is described by the Arrhenius equation [Stumm and Morgan, 1981]

$$\ln q = -\frac{E}{RT} + a \quad (5.22)$$

where T is absolute temperature [K], E the activation energy of the reaction [$\text{ML}^2\text{T}^{-2}\text{M}^{-1}$] and q is the reaction rate constant. In our application q represents the rate of CO_2 production. This equation together with the Van't Hoff equation was successfully used by many authors to represent the influence of temperature on soil and root CO_2 production [Carey and Berry, 1978; Howard and Howard, 1979; Ross and Cairns, 1978]. Assuming that $f(T)=1$ for the temperature $T_{20}=293.15$ K (20°C), then the temperature reduction coefficient can be expressed as

$$f(T) = \exp \left[\frac{E(T - T_{20})}{RTT_{20}} \right] \quad (5.23)$$

The use of the term “reduction” coefficient with $f(T)$ may seem inappropriate since this coefficient is greater than 1 for temperatures above 20°C . We use the term to characterize the change in production with-temperature, with values greater than 1 above 20°C and less than 1 below 20°C .

The dependence of CO_2 production on its own concentration (actually O_2 deficiency) can be expressed with the Michaelis-Menton equation [Glinski and Stepniewski, 1985]

$$q = \frac{q_{\max}}{1 + \frac{K_M}{c_{\text{O}_2}}} \quad (5.24)$$

where K_M is the Michaelis' constant [L^3L^{-3}], i.e., the oxygen concentration c_{O_2} , at which the oxygen uptake is equal to $1/2 q_{\max}$, and where q is oxygen uptake rate and q_{\max} is the maximum oxygen uptake rate [$\text{L}^3\text{L}^{-3}\text{T}^{-1}$]. Assuming that the respiratory quotient is equal to unity, then the Michaelis' constant for the CO_2 concentration. $K_M^* = 0.21 - K_M$, and $c_a = 0.21 - c_{\text{O}_2}$, then the reduction coefficient is given by

$$f(c_a) = \frac{c_{O_2}}{c_{O_2} + K_M} = \frac{0.21 - c_a}{0.42 - c_a - K_M^*} \quad (5.25)$$

The disadvantage of this expression is that if $c_a=0$ the value for $f(c_a)$ is not equal to one. Therefore, the values of the optimal production γ_{p0} and γ_{s0} must be adjusted accordingly.

The coefficient $f(t)$ introduces a time dependence into the production term. This coefficient should describe the diurnal and seasonal dynamics of soil and plant respiration. We assume that the diurnal dynamics for both soil and plant respiration is sufficiently reflected by the temperature dependent coefficient $f(T)$ and that the seasonal dynamics of soil production of CO₂ is sufficiently described by other reduction coefficients. Therefore, we use this coefficient only for the description of the changes in CO₂ production caused by the different growth stage of plants. For example, we use the same approach for annual vegetation as we used for root growth. The coefficient $f(t)$ can be described in the same way as coefficient $g(t)$ when the *GDD* concept is used (2.1 1), possibly with different constants.

Finally, the actual CO₂ production rate, P_T [L³L⁻²T⁻¹], is obtained by integrating the CO₂ production throughout the whole soil profile as follows

$$P_T = \int_0^L P dz = \gamma_{s0} f_s(t) \int_0^L f_s(z) f_s(h) f_s(T) f_s(c_a) f_s(h_\phi) dz + \gamma_{p0} f_p(t) \int_0^L f_p(z) f_p(h) f_p(T) f_p(c_a) f_p(h_\phi) dz \quad (5.26)$$

5.5. Parameter Selection for the Production Model

The following discussion on the selection of the values for optimal CO₂ production, as well as coefficients for particular reduction functions was given in *Suarez and Šimůnek [1993]*. The values of different reduction coefficients as suggested below, are used as default values in the graphics-based user interface UNSATCH (see Part B).

5.5.1. Optimum Production at 20 °C

For summer months, *Lundegard* [1927] calculated an average soil respiration of $0.005 \text{ m}^3\text{m}^{-2}\text{day}^{-1}$ for oats and 0.0034 for cabbage. *Monteith et al.* [1964] reported CO_2 fluxes in England of around $0.003 \text{ m}^3\text{m}^{-2}\text{day}^{-1}$ for bare soil, and approximately $0.005 \text{ m}^3\text{m}^{-2}\text{day}^{-1}$ for soils with different crops and with a soil temperature in the 10 to 15 °C range. *Buyanovsky et al.* [1986] reported the CO_2 flux from the surface of soil cultivated to wheat to be from about $0.0025 \text{ m}^3\text{m}^{-2}\text{day}^{-1}$ in April to maximum values in July of 0.0095 , 0.007 , and $0.006 \text{ m}^3\text{m}^{-2}\text{day}^{-1}$ for three years with wheat, with the maximum flux occurring at soil temperatures in excess of 20°C. Data presented by *de Jong and Schappert* [1972] suggest that the average respiration in the summer is about $0.013 \text{ m}^3\text{m}^{-2}\text{day}^{-1}$, however, temperature data were not reported. Values greater than $0.01 \text{ m}^3\text{m}^{-2}\text{day}^{-1}$ are also possible under conditions where microbial decomposition and root respiration occur in a high porosity litter layer on the surface, such as in tropical soils without biomass harvesting. We assume that the optimal production for the whole soil profile at 20°C, $\gamma_0 = \gamma_{s0} + \gamma_{p0}$, is in the range from 0.006 to $0.009 \text{ m}^3\text{m}^{-2}\text{day}^{-1}$, thus, the variation in CO_2 concentration as a result of this parameter is much less than a factor of 2 for any depth, as shown in *Suarez and Šimůnek* [1993]. Optimal production for any given ecosystem may be even less variable if we consider other factors such as soil nutrient status and plant type. We assume that under optimal conditions root respiration is responsible for 40 % of the total soil respiration. This value is consistent with *Holt et al.* [1990], who measured a value of 39%, and *Kucera and Kirkham* [1971], who estimated a value of 37% from their data. In our simulations we chose an intermediate value of $0.007 \text{ m}^3\text{m}^{-2}\text{day}^{-1}$ for the optimal production, where $\gamma_{s0} = 0.0042 \text{ m}^3\text{m}^{-2}\text{day}^{-1}$ and $\gamma_{p0} = 0.0028 \text{ m}^3\text{m}^{-2}\text{day}^{-1}$ (see Section 11).

5.5.2. Production Response to Temperature

The production coefficient response to temperature is based on the Arrhenius equation (5.23). *Carey and Berry* [1978] reported a constant activation energy of 49.4 kJ mol^{-1} for the respiration of corn roots between 10 and 35 °C (116 kJ mol^{-1} between 5 and 10 °C) and 53.6 kJ mol^{-1} for barley roots for temperatures between 5 and 35 °C. From these data we consider that

the activation energy for root respiration can be well characterized by the value of 50 kJ mol⁻¹.

A fairly wide range in activation values has been reported for soil microbial respiration. The coefficient Q_{10} has often been used to represent the relative increase in respiration intensity per 10 °C increase in temperature. A majority of the respiration studies report Q_{10} values between 1.5 and 3.0 although Anderson [1973], for example, reported Q_{10} values greater than 3 for a forest soil. We consider that measured values are often affected by limiting factors other than temperature. *Witkamp* [1969] calculated a value of 2.5 in the temperature range of 10 to 20 °C for leaf litter bags, in the leaf litter layer the Q_{10} value was slightly greater than 3.0, whereas for the whole soil the value was 1.5. In a study of tree and shrub leaf litter decomposition, *Howard and Howard* [1979] calculated mean Q_{10} values ranging from 2.29 to 2.56 for various species. From the data of *Ross and Cairns* [1978] we calculated a mean Q_{10} value of 2.3, based on laboratory measurements from 9 grassland soils. They report that the Q_{10} value decreased with increasing temperature, which is consistent with the use of the Arrhenius concept.

One of the few data sets where the water content was reported is that of *Kucera and Kirkham* [1971] who reported CO₂ flux data as a function of temperature for different water contents. Eliminating data where saturation or water deficiency existed at the soil surface, we calculate a Q_{10} value of 2.5. For a mesophytic forest stand dominated by poplar, *Edwards and Sollins* [1973] reported soil water content, temperature and CO₂ evolution. In the temperature range of 10 to 20 °C, we calculated a Q_{10} value of 1.8 for data at a relatively constant water content. Based on all measurements where water content was reported to be roughly constant, we selected a Q_{10} value of 2.1, which corresponds to an activation energy of 55.5 kJ mol⁻¹ for the temperature interval of 20-30 °C.

5.5.3. Production Response to Oxygen Concentration

The production response to the CO₂ concentration is based on the Michaelis-Menton equation (5.25). Soil respiration rates decrease to half of their maximum value when the CO₂ concentration decreases below 0.02 m³m⁻³ in the soil air [*Glinski and Stepniowski*, 1985]. Since we assume that the sum of the CO₂ and O₂ concentrations is constant and equal to 21% of the soil atmosphere, we use a CO₂ Michaelis' constant for soil respiration, K_{M, CO_2}^* equal to 0.19 m³m⁻³.

The critical oxygen concentration, below which respiration is reduced, is much higher for plant roots than for microorganisms. *Luxmoore et al.* [1970] reported the O_2 Michaelis' constant for excised maize roots to be within 0.07 to $0.12 \text{ m}^3\text{m}^{-3}$, but *Armstrong and Gaynard* [1976] considered that for intact roots this constant can be much lower. In view of this consideration we selected a value at the lower end of the interval reported by *Luxmoore et al.* [1970], giving a calculated CO_2 Michaelis' constant for plant respiration of $K_{M}^*=0.14 \text{ m}^3\text{m}^{-3}$.

5.5.4. Production Response to Water Stress

We assume that the depth and water content reduction of CO_2 production by plant roots is the same as the corresponding reduction of potential transpiration.

The soil CO_2 production response function to water stress is represented by (5.21). On the basis of the experimental data presented by *Williams et al.* [1972], we selected the pressure head $h_2 = -1.0 \text{ m}$ for the optimal soil respiration and the pressure head h_3 , when production ceases, is assigned the value -10^5 m .

5.5.5. Production Response to Salinity Stress

The production response function to salinity stress for both the soil and root CO_2 production is described using the S-shaped function (2.3) of *van Genuchten* [1987]. The h_ϕ values for specific crops can be obtained from the compilation of *Mass* [1990], by calculating the osmotic pressure at 50% relative yield.

6. CARBONATE CHEMISTRY

When using the ion-association model (and Debye-Hückel activity coefficient calculations) we assume that the chemical system for predicting major ion solute chemistry of the unsaturated zone includes 37 chemical species. We divided these species into six groups as listed in Table 6.1. Seven primary dissolved species (calcium, magnesium, sodium, potassium, sulfate, chloride, and nitrate), 10 complex aqueous species, six possible solid phases (calcite, gypsum, nesquehonite, hydromagnesite, sepiolite and dolomite), four surface species, seven species which form the CO₂-H₂O system, and three silica species are considered. The species from the last two groups could be generally included in other groups (i.e., CO₃²⁻, H₂SiO₄²⁻, and H⁺ could be included in the first group). Their consideration into separate groups is mainly due to the different treatment compared to that of the other species. For example, complex species of these groups are considered also at high ionic strength when using the Pitzer equations to calculate activity coefficients while the species of the second group are in that case dropped from the system, as discussed later. One of the solid phases (dolomite) is not included into the equilibrium

Table 6.1. Chemical species considered by the model.

1	Aqueous components	7	Ca ²⁺ , Mg ²⁺ , Na ⁺ , K ⁺ , SO ₄ ²⁻ , Cl ⁻ , NO ₃ ⁻
2	Complexed species	10	CaCO ₃ ⁰ , CaHCO ₃ ⁺ , CaSO ₄ ⁰ , MgCO ₃ ⁰ , MgHCO ₃ ⁺ , MgSO ₄ ⁰ , NaCO ₃ ⁻ , NaHCO ₃ ⁰ , NaSO ₄ ⁻ , KSO ₄ ⁻
3	Precipitated species	6	CaCO ₃ , CaSO ₄ · 2H ₂ O, MgCO ₃ · 3H ₂ O, Mg ₅ (CO ₃) ₄ (OH) ₂ · 4H ₂ O, Mg ₂ Si ₃ O _{7.5} (OH) · 3H ₂ O, CaMg(CO ₃) ₂
4	Sorbed species	4	$\bar{\text{Ca}}$, $\bar{\text{Mg}}$, $\bar{\text{Na}}$, $\bar{\text{K}}$
5	CO ₂ -H ₂ O species	7	P _{CO2} , H ₂ CO ₃ [*] , CO ₂ ^g , HCO ₃ ⁻ , H ⁺ , OH ⁻ , H ₂ O
6	Silica species	3	H ₄ SiO ₄ , H ₃ SiO ₄ ⁻ , H ₂ SiO ₄ ²⁻

system and its dissolution is always treated kinetically. Also, exclusion of calcite from the equilibrium system is optional as its precipitation-dissolution can be treated as a kinetic process. As a result, we need either 36 or 3.5 independent equations to solve this system. In the following sections we present this set of equations and in Section 9.1 we discuss the method of its solution.

6.1. Mass and Charge Balance Equations

Seven mass balance equations for the primary species in the first group and one for the silica species in the six group of Table 6.1 are defined

$$\begin{aligned}
 \text{Ca}_T &= [\text{Ca}^{2+}] + [\text{CaSO}_4^0] + [\text{CaCO}_3^0] + [\text{CaHCO}_3^+] \\
 \text{Mg}_T &= [\text{Mg}^{2+}] + [\text{MgSO}_4^0] + [\text{MgCO}_3^0] + [\text{MgHCO}_3^+] \\
 \text{Na}_T &= [\text{Na}^+] + [\text{NaSO}_4^-] + [\text{NaCO}_3^-] + [\text{NaHCO}_3^0] \\
 \text{K}_T &= [\text{K}^+] + [\text{KSO}_4^-] \\
 \text{SO}_{4,T} &= [\text{SO}_4^{2-}] + [\text{CaSO}_4^0] + [\text{MgSO}_4^0] + [\text{NaSO}_4^-] + [\text{KSO}_4^-] \\
 \text{Cl}_T &= [\text{Cl}^-] \\
 \text{NO}_{3,T} &= [\text{NO}_3^-] \\
 \text{SiO}_{4,T} &= [\text{H}_4\text{SiO}_4] + [\text{H}_3\text{SiO}_4^-] + [\text{H}_2\text{SiO}_4^{2-}]
 \end{aligned} \tag{6.1}$$

where variables with subscript T represent the total analytical concentration in solution of that particular species and where brackets refer to molalities (mol kg^{-1}). Two mass balance equations for the total analytical concentration of carbonate and bicarbonate are defined

$$\begin{aligned}
 \text{CO}_{3,T} &= [\text{CO}_3^{2-}] + [\text{CaCO}_3^0] + [\text{MgCO}_3^0] + [\text{NaCO}_3^-] \\
 \text{HCO}_{3,T} &= [\text{HCO}_3^-] + [\text{CaHCO}_3^+] + [\text{MgHCO}_3^+] + [\text{NaHCO}_3^0]
 \end{aligned} \tag{6.3}$$

which are used to calculate inorganic alkalinity, Alk ($\text{mol}_c\text{kg}^{-1}$):

$$Alk = 2 CO_{,T} + HCO_{,T} + [OH^-] - [H^+] \quad (6.4)$$

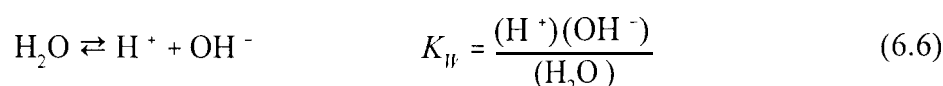
Most chemical and multicomponent transport models use the total inorganic carbon as a conservative property [e.g., *Westal et al.*, 1986; *Liu and Narasimhan*, 1989b; *Yeh and Tripathi*, 1991]. However, this approach can be used only for closed systems. In a soil environment with fluctuating CO₂ concentrations this approach is inappropriate and use of alkalinity as a conservative property is preferable.

In addition to the mass balance equations, the overall charge balance equation for the solution is given as

$$2 [Ca^{2+}] + 2 [Mg^{2+}] + [Na^+] + [K^+] + [CaHCO_3^+] + [MgHCO_3^+] + [H^+] - 2 [CO_3^{2-}] - [HCO_3^-] - 2 [SO_4^{2-}] - [Cl^-] - [NO_3^-] - [OH^-] - [NaCO_3^-] - [NaSO_4^-] - [KSO_4^-] = 0 \quad (6.5)$$

6.2. CO₂-H₂O System

The activities of the species present in solution at equilibrium are related by the mass-action equations. The dissociation of water is written as follows



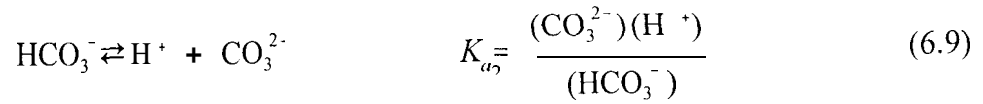
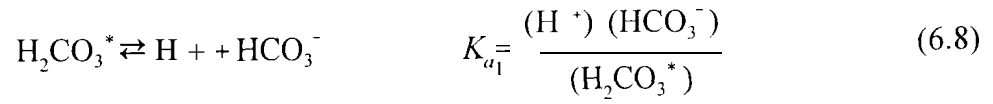
where K_w is the dissociation constant for water [-]. The parentheses denote ion activity, the calculation of which will be discussed later.

The solubility of CO₂(g) in water is described by Henry's Law



where the activity of CO_{2(g)} is expressed in terms of the partial pressure P_{CO_2} (atm), K_{CO_2} is Henry's law constant and H₂CO₃^{*} represents both aqueous CO₂ and H₂CO₃.

Protolysis reactions of dissolved CO₂ are written as



where K_{a1} and K_{a2} are the first and the second dissociation constants of carbonic acid [-], respectively.

6.3. Complexation Reactions

Each complexation reaction for the species in the second group of Table 6.1 and for silica species can be represented by the law of mass action:

$$K_1 = \frac{(\text{Ca}^{2+})(\text{SO}_4^{2-})}{(\text{CaSO}_4^0)} \quad K_2 = \frac{(\text{Ca}^{2+})(\text{CO}_3^{2-})}{(\text{CaCO}_3^0)} \quad K_3 = \frac{(\text{Ca}^{2+})(\text{HCO}_3^-)}{(\text{CaHCO}_3^+)} \quad (6.10)$$

$$K_4 = \frac{(\text{Mg}^{2+})(\text{SO}_4^{2-})}{(\text{MgSO}_4^0)} \quad K_5 = \frac{(\text{Mg}^{2+})(\text{CO}_3^{2-})}{(\text{MgCO}_3^0)} \quad K_6 = \frac{(\text{Mg}^{2+})(\text{HCO}_3^-)}{(\text{MgHCO}_3^+)} \quad (6.11)$$

$$K_7 = \frac{(\text{Na}^+)(\text{SO}_4^{2-})}{(\text{NaSO}_4^-)} \quad K_8 = \frac{(\text{Na}^+)(\text{CO}_3^{2-})}{(\text{NaCO}_3^-)} \quad K_9 = \frac{(\text{Na}^+)(\text{HCO}_3^-)}{(\text{NaHCO}_3^0)} \quad (6.12)$$

$$K_{10} = \frac{(\text{K}^+)(\text{SO}_4^{2-})}{(\text{KSO}_4^-)} \quad (6.13)$$

$$K_{11} = \frac{(\text{H}^+)(\text{H}_3\text{SiO}_4^-)}{(\text{H}_4\text{SiO}_4)} \quad K_{12} = \frac{(\text{H}^+)^2(\text{H}_2\text{SiO}_4^{2-})}{(\text{H}_4\text{SiO}_4)} \quad (6.14)$$

where K_i are the equilibrium constants of the i th complexed species [-].

6.4. Cation Exchange and Selectivity

Partition between the solid phase and the solution is described by the Gapon equation [White and Zelazny, 1986]

$$K_{ij} = \frac{\bar{c}_i^{y^+} (c_j^{x^+})^{1/x}}{\bar{c}_j^{x^+} (c_i^{y^+})^{1/y}} \quad (6.15)$$

where y and x are the valence of species i and j , respectively, and K_{ij} is the Gapon selectivity coefficient [-]. The adsorption concentration is expressed in ($\text{mol}_c \text{kg}^{-1}$ soil). It is assumed, that the cation exchange capacity \bar{c}_T ($\text{mol}_c \text{kg}^{-1}$ soil) is constant and independent of pH .

$$\bar{c}_T = \Sigma \bar{c}_i \quad (6.16)$$

In the case of exchange of four cations ($\bar{\text{Ca}}, \bar{\text{Mg}}, \bar{\text{Na}}$ and $\bar{\text{K}}$) we obtain the following system of equations.

$$\bar{c}_T = \bar{\text{Ca}}^{2+} + \bar{\text{Mg}}^{2+} + \bar{\text{Na}}^+ + \bar{\text{K}}^+ \quad (6.17)$$

$$K_{13} = \frac{\bar{\text{Mg}}^{2+} (\text{Ca}^{2+})^{1/2}}{\bar{\text{Ca}}^{2+} (\text{Mg}^{2+})^{1/2}}$$

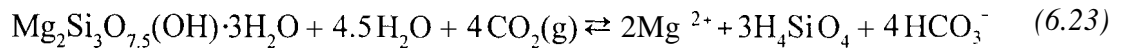
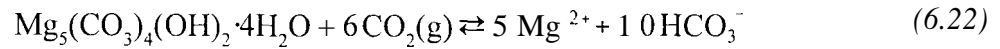
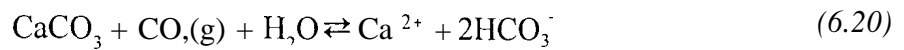
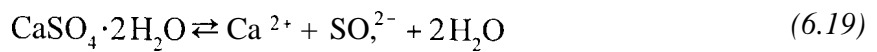
$$K_{14} = \frac{\bar{\text{Ca}}^{2+} (\text{Na}^+)}{\bar{\text{Na}}^+ (\text{Ca}^{2+})^{1/2}} \quad (6.18)$$

$$K_{15} = \frac{\bar{\text{Ca}}^{2+} (\text{K}^+)}{\bar{\text{K}}^+ (\text{Ca}^{2+})^{1/2}}$$

6.5. Precipitation-Dissolution Reactions

We consider four solid phases in our model which if specified or approached from

over-saturation must be in equilibrium with solution: gypsum, nesquehonite, hydromagnesite and sepiolite. Precipitation-dissolution of calcite can be optionally treated with either the equilibrium condition or by rate equations. In the latter case the equation corresponding to calcite equilibrium presented in this section is omitted from the equilibrium system and the rate of calcite precipitation-dissolution is calculated from the rate equation as described later. Dissolution of dolomite, which will also be discussed later, is always considered as a kinetic process and never included into an equilibrium system, since ordered dolomite almost never precipitates under earth surface conditions. Discussion for the selection and consideration of these solids is given in *Suarez and Šimůnek [1997]*. The precipitation or dissolution of gypsum, calcite (if considered in equilibrium system), nesquehonite, hydromagnesite and sepiolite in the presence of CO₂ can be described by



with the corresponding solubility products K_{sp} [-]

$$K_{sp}^G = (\text{Ca}^{2+})(\text{SO}_4^{2-})(\text{H}_2\text{O})^2 \quad (6.24)$$

$$K_{sp}^C = (\text{Ca}^{2+})(\text{CO}_3^{2-}) \quad (6.25)$$

$$K_{sp}^N = (\text{Mg}^{2+})(\text{CO}_3^{2-})(\text{H}_2\text{O})^3 \quad (6.26)$$

$$K_{SP}^H = (\text{Mg}^{2+})^5 (\text{CO}_3^{2-})^4 (\text{OH}^-)^2 (\text{H}_2\text{O})^4 \quad (6.27)$$

$$K_{SP}^S = \frac{(\text{Mg}^{2+})^2 (\text{H}_4\text{SiO}_4)^3 (\text{OH}^-)^4}{(\text{H}_2\text{O})^{4.5}} \quad (6.28)$$

where indexes G, C, N, H, and S refer to gypsum, calcite, nesquehonite, hydromagnesite and sepiolite, respectively.

Substituting of (6.6) through (6.9) into (6.25) through (6.28) we get the solubility products for the carbonate solids expressed in terms of bicarbonate, which is almost always the major carbonate ion under conditions ($6 < \text{pH} < 10.5$) for which this model is envisioned:

$$(\text{Ca}^{2+})(\text{HCO}_3^-)^2 = K_{SP}^C \frac{K_{\text{CO}_2} K_{a_1} P_{\text{CO}_2} (\text{H}_2\text{O})}{K_{a_2}} \quad (6.29)$$

$$(\text{Mg}^{2+})(\text{HCO}_3^-)^2 = K_{SP}^N \frac{K_{\text{CO}_2} K_{a_1} P_{\text{CO}_2}}{K_{a_2} (\text{H}_2\text{O})^2} \quad (6.30)$$

$$(\text{Mg}^{2+})^5 (\text{HCO}_3^-)^{10} = K_{SP}^H \frac{K_{\text{CO}_2}^6 K_{a_1}^6 P_{\text{CO}_2}^6}{K_{a_2}^4 K_w^2} \quad (6.31)$$

$$(\text{Mg}^{2+})^2 (\text{HCO}_3^-)^4 = K_{SP}^S \frac{K_{\text{CO}_2}^4 K_{a_1}^4 P_{\text{CO}_2}^4 (\text{H}_2\text{O})^{4.5}}{K_w^4 (\text{H}_4\text{SiO}_4)^3} \quad (6.32)$$

Expressing the solubility products in this way decreases significantly the number of iterations necessary to numerically reach the equilibrium conditions, in comparison to the case when using equations (6.25) through (6.28).

The concentrations of Ca^{2+} and SO_4^{2-} in equilibrium with gypsum can be obtained by solving the quadratic algebraic equation corresponding to (6.24) as follows. The ion activity product for (Ca^{2+}) and (SO_4^{2-}), ZAP'' , in solution is given by

$$[\text{Ca}^{2+}][\text{SO}_4^{2-}] = \frac{IAP^G}{\gamma_{\text{Ca}^{2+}} \gamma_{\text{SO}_4^{2-}} (\text{H}_2\text{O})^2} \quad (6.33)$$

where γ 's are activity coefficients [-] and brackets represent molalities. To obtain equilibrium, i.e. when the IAP^G is equal to the solubility product K_{sp}^G , a quantity of gypsum x must be added or removed from the solution

$$[\text{Ca}^{2+} + x][\text{SO}_4^{2-} + x] = \frac{K_{sp}^G}{\gamma_{\text{Ca}^{2+}} \gamma_{\text{SO}_4^{2-}} (\text{H}_2\text{O})^2} \quad (6.34)$$

By solving (6.34) we get the quadratic equation

$$x^2 + Ax + B = 0 \quad (6.35)$$

where

$$A = [\text{Ca}^{2+}] + [\text{SO}_4^{2-}]$$

$$B = \frac{IAP^G - K_{sp}^G}{\gamma_{\text{Ca}^{2+}} \gamma_{\text{SO}_4^{2-}} (\text{H}_2\text{O})^2} \quad (6.36)$$

from which we obtain the new Ca^{2+} and SO_4^{2-} concentrations.

The concentrations of Ca^{2+} , Mg^{2+} , and HCO_3^- in equilibrium with the carbonate solids is reached by solving the cubic algebraic equations corresponding to (6.29) through (6.32) as described in *Suarez and Šimůnek* [1997] and as demonstrated here for calcite. The ion activity product for calcite, IAP^C , in solution is given by

$$[\text{Ca}^{2+}][\text{HCO}_3^-]^2 = \frac{IAP^C \cdot K_{\text{CO}_2} \cdot K_{a1} \cdot P_{\text{CO}_2} (\text{H}_2\text{O})}{\gamma_{\text{Ca}^{2+}} \gamma_{\text{HCO}_3^-}^2 \cdot K_{a2}} = \frac{IAP^C}{\gamma_{\text{Ca}^{2+}} \gamma_{\text{HCO}_3^-}^2} K_r \quad (6.37)$$

To obtain equilibrium, i.e. when the ZAP^C is equal to the solubility product K_{sp}^C , a quantity of calcite x must be added or removed from the solution

$$[\text{Ca}^{2+} + x][\text{HCO}_3^- + 2x]^2 = \frac{K_{SP}^C K_T}{\gamma_{\text{Ca}^{2+}} \gamma_{\text{HCO}_3^-}^2} \quad (6.38)$$

By solving (6.38) we get the resulting cubic equation

$$Ax^3 + Bx^2 + Cx + D = 0 \quad (6.39)$$

where

$$\begin{aligned} A &= 4 \\ B &= 4[\text{Ca}^{2+}] + 4[\text{HCO}_3^-] \\ C &= 4[\text{HCO}_3^-][\text{Ca}^{2+}] + [\text{HCO}_3^-]^2 \\ D &= \frac{(\text{ZAP}^C - K_{SP}^C) K_T}{\gamma_{\text{Ca}^{2+}} \gamma_{\text{HCO}_3^-}^2} \end{aligned} \quad (6.40)$$

6.6. Kinetic Model of Calcite Precipitation-Dissolution

The reaction rates of calcite precipitation-dissolution in the absence of inhibitors such as “foreign ions” and dissolved organic matter, R^C ($\text{mmol cm}^{-2}\text{s}^{-1}$), were calculated with the rate equation of *Plummer et al.* [1978]

$$R^C = k_1(\text{H}_2\text{O}) + k_2(\text{H}_2\text{CO}_3^*) + k_3(\text{H}_2\text{O}) - k_4 \frac{K_{a2}}{K_{SP}^C} (\text{Ca}^{2+})(\text{HCO}_3^-) \quad (6.41)$$

where

$$k_4 = k_1 + \frac{1}{(\text{H}_2\text{O})} [k_2(\text{H}_2\text{CO}_3^*) + k_3(\text{H}_2\text{O})] \quad (6.42)$$

and where $k_1, k_2,$ and k_3 are temperature dependent first order rate constants representing the forward reactions ($\text{mmol cm}^{-2}\text{s}^{-1}$) and k_4 is a function dependent on both temperature and CO₂,

concentration representing the back reactions ($\text{mmol cm}^{-2}\text{s}^{-1}$). The dissolution-precipitation rate R^c is expressed in mmol of calcite per cm^2 of surface area per second. The term $(H,')$ is the H^+ activity at the calcite surface. It is assumed to be (H') at calcite saturation where activities of H_2CO_3^* and H_2O at the calcite surface are equal to their bulk fluid values [Plummer *et al.*, 1978; Suarez, 1985]. The temperature dependence of the constants k, k_2, k_3 is expressed as

$$\log k = a_1 + \frac{a_2}{T} \quad (6.43)$$

where values of the empirical constants a , and a_2 are given by Plummer *et al.* [1978] and in Table 6.2. For the condition where $pH > 8$ and $p\text{CO}_2 < 1000$ Pa, an alternative expression for the precipitation rate is used which is considered more accurate for those conditions [Inskeep and Bloom, 1985]

$$R^c = -11.82 [(Ca^{2+})(CO_3^{2-}) - K_{sp}'] \quad (6.44)$$

with an apparent Arrhenius activation energy of 48.1 kJ mol^{-1} for the precipitation rate constant [Inskeep and Bloom, 1985].

The precipitation or dissolution rate of calcite is reduced by the presence of various inhibitors. Suarez and Šimůnek [1997] developed the following function for the reduction of the precipitation-dissolution rates due to surface poisoning by dissolved organic carbon, based on the experimental data of Inskeep and Bloom [1986]

$$r = \exp(-b_1x - b_2x^2 - b_3x^{0.5}) \quad (6.45)$$

where r is the reduction constant [-], x is the dissolved organic carbon ($\mu\text{mol l}^{-1}$) and $b_1, b_2,$ and b_3 are regression coefficients (0.005 104, 0.000426, 0.069111, respectively).

6.7. Kinetic Model of Dolomite Dissolution

The reaction rates of dolomite dissolution, R^D ($\text{mmol cm}^{-2}\text{s}^{-1}$), were calculated with the rate equation of Busenberg and Plummer [1982]

Table 6.2. Temperature dependence of the kinetic constants for calcite precipitation-dissolution [Plummer *et al.*, 1978] and dolomite dissolution [Busenberg and Plummer, 1982].

	a_1	a_2
Calcite		
k_1	0.198	-444.
k_2	2.84	-2177.
k_3 ($T < 298.15$)	-5.86	-317
k_3 ($T > 298.15$)	-1.1	-1737.
Dolomite'		
k_1	2.12	-1880.
k_2	-0.07	-1800.
k_3	0.53	-2700.
k_4^{**}	3.16	-2300.
k_4	7.34	-3700.

+ for sedimentary dolomite

** for $\text{FeCO}_3 < 0.007$

$$R^D = k_1 (\text{H}^+)^{0.5} + k_2 (\text{H}_2\text{CO}_3^*)^{0.5} + k_3 (\text{H}_2\text{O})^{0.5} - k_4 (\text{HCO}_3^-) \quad (6.46)$$

where the temperature dependent first order rate constants k_1, k_2, k_3 ($\text{mmol cm}^{-2}\text{s}^{-1}$), representing the forward reactions, and k_4 ($\text{mmol cm}^{-2}\text{s}^{-1}$), representing the back reaction, are expressed by (6.43) with empirical constants a_1 and a_2 given by Busenberg and Plummer [1982], and again in Table 6.2. The dissolution rate R^D is again expressed in mmol of dolomite per cm^2 of surface area per second. These rate constants are used for ion activity products $IAP^D < 10^{-19}$. At values below 10^{-19} the rate is exceedingly small and assumed as zero [Busenberg and Plummer, 1982] in the absence of additional data.

6.8. Silica Concentration in Soil Solution

Relatively little information exists on the Si concentration in soil water. Use of equilibrium calculations of silica solubility from the stable mineral (quartz) results in the unrealistic prediction that solution concentrations are independent of pH up to pH 8 and then the solubility increases due to the dissociation of silicic acid. In soil (and other near-earth surface

environments) Si concentrations are not fixed by quartz solubility but rather by dissolution (and possibly precipitation) of aluminosilicates including poorly crystallized phases and Si adsorption-desorption onto oxides and aluminosilicates. As a result of these reactions Si concentrations in soil solution follow a U shaped curve with pH , similar to Al oxide solubility with a Si minimum around pH 7.5 [Suarez,1977a]. Suarez [1977a] developed a simple relation between silica content in the soil solution and the soil pH :

$$SiO_{4T} = d_1 + d_2 pH + d_3 pH^2 \quad (6.47)$$

where empirical constants d_1 , d_2 , and d_3 are equal to 6340, 1430, and 81.9, respectively, and SiO_{4T} is the sum of all silica species expressed in $mol\ l^{-1}$. We utilize this expression and the dissociation expressions for K_{11} and K_{12} (eq. (6.14)) only to obtain estimates of H_4SiO_4 from total SiO_4 . As a result we do not express sepiolite reactions in terms of $H_3SiO_4^-$ and $H_2SiO_4^{2-}$ and do not include these species in the charge balance expressions. Only the species H_4SiO_4 is used by the program.

6.9. Activity Coefficients

6.9.1. Extended Debye-Hückel Expression

The activity coefficients are formally defined as [Stokes, 1979]:

$$a_i = \gamma_i \frac{m_i}{m^0} \quad (6.48)$$

where a_i is the activity [-], m , is the molality ($mol\ kg^{-1}$), m^0 is the unit molality (i.e., $1\ mol\ kg^{-1}$) and γ_i is the activity coefficient of the i th ion [-]. For the calculation of the activity coefficient in the dilute to moderately saline solution range the extended version of the Debye-Hückel equation can be used [Truesdell and Jones, 1974]

$$\ln \gamma = - \frac{Az^2\sqrt{I}}{1 + Ba\sqrt{I}} + bI \quad (6.49)$$

where A ($\text{kg}^{0.5}\text{mol}^{-0.5}$) and B ($\text{kg}^{0.5}\text{cm}^{-1}\text{mol}^{-0.5}$) are constants depending only on the dielectric constant, density, and temperature. z is the ionic charge in protonic units, a (cm) and b (kg mol^{-1}) are two adjustable parameters, and I is the ionic strength (mol kg^{-1}):

$$I = 0.5 \sum_{i=1}^M z_i^2 c_i \quad (6.50)$$

where A_4 is the number of species in the solution mixture. The adjustable parameters a and b for individual species are given by *Truesdell and Jones* [1974] and *Suarez and Šimůnek* [1997] (Table 6.3). The activities of neutral species are calculated as

$$\ln \gamma = a' I \quad (6.51)$$

where a' is an empirical parameter. The values of this parameter for neutral species are listed in *Suarez and Šimůnek* [1997] and in Table 6.3.

Table 6.3. Ionic charge and adjustable parameters for calculation of extended Debye-Hückel activity coefficients.

Species	z_i	a^\dagger	b^\dagger	a'
Ca^{2+}	2	5.0	0.165	
Mg^{2+}	2	5.5	0.20	
Na^+	1	4.0	0.075	
K^+	1	3.5	0.015	
SO_4^{2-}	2	5.0	-0.04	
CO_3^{2-}	2	5.4	0.	
HCO_3^-	1	5.4	0.	
CaHCO_3^+	1	6.0	0.	
MgHCO_3^+	1	4.0	0.	
H^+	1	9.0	0.	
OH^-	1	3.5	0.	
H_3SiO_4^-	1	5.4	0.	
$\text{H}_2\text{SiO}_4^{2-}$	2	4.0	0.	
CaCO_3^0	0			-0.5
CaSO_4^0	0			-0.45:
MgCO_3^0	0			-0.63‡
MgSO_4^0	0			-0.5
H_4SiO_4	0			-0.5

[†]*Truesdell and Jones* [1974]

[‡]*Reardon and Langmuir* [1976]

If the extended Debye-Hückel theory is used to calculate activity coefficients then activity of water is calculated in the same way as in the program WATEQ [Truesdell und Jones, 1974] by the approximate relation

$$(H_2O) = 1 - 0.017 \sum_{i=1}^M m_i \quad (6.52)$$

6.9.2. Pitzer Expressions

At high ionic strength activity coefficients are no longer universal functions of ionic strength, but are dependent on the relative concentration of the various ions present in solution [Felmy and Weare, 1986]. The activity coefficients can then be expressed in a virial-type expansion of the form [Pitzer, 1979]

$$\ln \gamma_i = \ln \gamma_i^{DH} + \sum_j B_{ij}(I) m_j + \sum_j \sum_k C_{ijk} m_j m_k + \dots \quad (6.53)$$

where γ_i^{DH} is a modified Debye-Hückel activity coefficient which is a universal function of ionic strength, B_{ij} and C_{ijk} are specific coefficients for each interaction. The coefficients in (6.53) have the following form for cations, anions and neutral species [Felmy and Weare, 1986]

$$\begin{aligned}
\ln \gamma_M &= z_M^2 F + \sum_{a=1}^{N_a} m_a (2B_{Ma} + ZC_{Ma}) + \sum_{c=1}^{N_c} m_c (2\Phi_{Mc} + \sum_{a=1}^{N_a} m_a \psi_{Mca}) + \\
&+ \sum_{a=1}^{N_a-1} \sum_{a'=a+1}^{N_a} m_a m_{a'} \psi_{aa'M} + |z_M| \sum_{c=1}^{N_c} \sum_{a=1}^{N_a} m_c m_a C_{ca} + \sum_{n=1}^{N_n} m_n (2\lambda_{nM}) + \sum_{n=1}^{N_n} \sum_{a=1}^{N_a} m_n m_a \xi_{naM} \\
\ln \gamma_X &= z_X^2 F + \sum_{c=1}^{N_c} m_c (2B_{Xc} + ZC_{Xc}) + \sum_{a=1}^{N_a} m_a (2\Phi_{Xa} + \sum_{c=1}^{N_c} m_c \psi_{Xca}) + \\
&+ \sum_{c=1}^{N_c-1} \sum_{c'=c+1}^{N_c} m_c m_{c'} \psi_{cc'X} + |z_X| \sum_{c=1}^{N_c} \sum_{a=1}^{N_a} m_c m_a C_{ca} + \sum_{n=1}^{N_n} m_n (2\lambda_{nX}) + \sum_{n=1}^{N_n} \sum_{c=1}^{N_c} m_n m_c \xi_{ncX} \\
\ln \gamma_N &= \sum_{c=1}^{N_c} m_c (2\lambda_{Nc}) + \sum_{a=1}^{N_a} m_a (2\lambda_{Na}) + \sum_{c=1}^{N_c} \sum_{a=1}^{N_a} m_c m_a \xi_{Nca}
\end{aligned} \tag{6.54}$$

where subscripts M, X, N and c, a, n refer to cations, anions and neutral species, respectively, and where

$$\begin{aligned}
F &= -A^\phi \left[\frac{I^{1/2}}{1 + bI^{1/2}} + \frac{2}{b} \ln(1 + bI^{1/2}) \right] + \\
&+ \sum_{c=1}^{N_c} \sum_{a=1}^{N_a} m_c m_a B'_{ca} + \sum_{c=1}^{N_c-1} \sum_{c'=c+1}^{N_c} m_c m_{c'} \Phi'_{cc'} + \sum_{a=1}^{N_a-1} \sum_{a'=a+1}^{N_a} m_a m_{a'} \Phi'_{aa'} \\
C_{MX} &= \frac{C_{MX}^\phi}{2 |Z_M Z_X|^{1/2}} \\
Z &= \sum |z_i| m_i
\end{aligned} \tag{6.55}$$

and where A^ϕ is one third of the Debye-Hückel limiting slope and equal to 0.39 at 25°C. The second virial coefficients B , are given by the following ionic strength dependence [Pitzer,1973]

$$\begin{aligned}
B_{MX}^{\phi} &= \beta_{MX}^{(0)} + \beta_{MX}^{(1)} \exp(-\alpha_1 \sqrt{I}) + \beta_{MX}^{(2)} \exp(-\alpha_2 \sqrt{I}) \\
B_{MX} &= \beta_{MX}^{(0)} + \beta_{MX}^{(1)} g(\alpha_1 \sqrt{I}) + \beta_{MX}^{(2)} g(\alpha_2 \sqrt{I}) \\
B'_{MX} &= \beta_{MX}^{(1)} \frac{g'(\alpha_1 \sqrt{I})}{I} + \beta_{MX}^{(2)} \frac{g'(\alpha_2 \sqrt{I})}{I}
\end{aligned} \tag{6.56}$$

The functions g and g' are defined by

$$\begin{aligned}
g(x) &= 2 \frac{(1 - (1+x)e^{-x})}{x^2} \\
g'(x) &= -2 \frac{(1 - (1+x + \frac{x^2}{2})e^{-x})}{x^2}
\end{aligned} \tag{6.57}$$

with $x = \alpha_1 I^{0.5}$ or $= \alpha_2 I^{0.5}$. When either cation A4 or anion X is univalent $\alpha_1 = 2$. For 2-2 or higher valence pairs $\alpha_1 = 1.4$. For all electrolytes $\alpha_2 = 12, b = 1.2$. The dimensions of α_1 and α_2 are $\text{kg}^{0.5} \text{mol}^{-0.5}$. The second virial coefficients, Φ , which depend upon ionic strength, are in the form [Pitzer, 1973].

$$\begin{aligned}
\Phi_{ij}^{\phi} &= \theta_{ij} + \theta_{ij}^{E_i}(I) + I \theta_{ij}^{E'_i}(I) \\
\Phi_{ij} &= \theta_{ij} + \theta_{ij}^{E_i}(I) \\
\Phi'_{ij} &= \theta_{ij}^{E'_i}(I)
\end{aligned} \tag{6.58}$$

The functions $\theta_{ij}^{E_i}(I)$ and $\theta_{ij}^{E'_i}(I)$ are functions only of ionic strength and the electrolyte pair type.

The second and third virial coefficients, A_{ij} , and ξ_{nij} , representing the interactions between ions and neutral species are assumed constant. The third virial coefficients, C_{MX}^{ϕ} and ψ_{ijk} are also assumed to be independent of ionic strength. The subroutines for calculation of the Pitzer activity coefficients were adopted from the code GMIN [Felmy, 1990].

This model is considered accurate even for solutions with very high ionic strength (up to **20** mol kg⁻¹) and can be used down to infinite dilution. Explicit definition of complex species

(e.g. NaSO_4^- , NaHCO_3^0) for this type of model is generally not required [Harvie et al., 1984]. However, ion complex species which exhibit strong attractive interactions (e.g. HCO_3^-) must still be taken into account. Therefore when the virial-type expressions are used to calculate ion activities, the complex species from the second group in Table 6.1 are not included into the equilibrium chemical system and equations (6.10) through (6.13) are not used. The complexed species in group five and six are considered even when using the Pitzer expressions. Note that when the ion complex species from the second group in Table 6.1 are not considered, then the apparent ionic strength I increases significantly, since the complexes have lower charge than the original components.

If the Pitzer theory is used, then the activity of water is obtained from the expression [Felrny and Weare, 1986]

$$\ln(\text{H}_2\text{O}) = -\frac{W}{1000} \left[\sum_{i=1}^M m_i \right] \phi \quad (6.59)$$

where W is the molecular weight of water and ϕ is the osmotic coefficient (see Felrny and Weare [1986] for the definition and method of calculation and Section 6.11).

6.10. Temperature Dependence

Most of the thermodynamic equilibrium constants are dependent on the temperature and pressure of the system. The temperature dependence of the thermodynamic equilibrium constants is often expressed as a power function of the absolute temperature

$$\log K = a_1 + \frac{a_2}{T} + a_3 T + a_4 \log T + \frac{a_5}{T^2} \quad (6.60)$$

where T is the absolute temperature [K], and a_1 through a_5 are empirical constants. The pressure dependence can be neglected for near earth surface conditions (such as soils). The empirical constants for the temperature dependent thermodynamic constants used in the calculations are listed in Suarez and Šimůnek [19973] and in Table 6.4. The temperature dependence of the equilibrium constants for which the constants of equation (6.60) do not exist is expressed with

the enthalpy of reaction and the Van't Hoff expression [Truesdell and Jones, 1974] (Table 6.5).

Table 6.4. Parameters for calculation of thermodynamic constants as a function of temperature.

Constant	a_1	a_2	a_3	a_4	a_5	Reference	
$\log K_{CO}$	108.3865	-6919.53	0.01985076	-40.45154	669395.	Plummer and Busenberg [1982]	
$\log K_{a1} H_2CO_3$	-356.3094	21834.37	-0.0609	1964	126.8339	-1684915.	Plummer and Busenberg [1982]
$\log K_{a2} H_2CO_3$	-107.8871	5151.79	-0.03252849	38.92561	-563713.9		Plummer and Busenberg [1982]
$\log K CaCO_3^0$	1228.732	-35512.75	0.299444	-485.818	0.		Plummer and Busenberg [1982]
$\log K CaSO_4^0$	-1.24	0.	-0.0036	0.	0.		Bell and George [1953]
$\log K CaHCO_3^+$	-1209.120	34765.05	-0.3	1294	478.782	0.	Plummer and Busenberg [1982]
$\log K MgCO_3^0$	21.39	-3265.	-0.04467	0.	0.		Reardon and Langmuir [1974]
$\log K MgSO_4^0$	0.95	0.	-0.011	0.	0.		Jacobson [1973]
$\log K MgHCO_3^+$	76.344	-11132.0	-0.1338	0.	0.		Reardon [1974]
$\log A$	-1.15083	93.642	0.001830	0.	0.		Robinson and Stokes [1965]
$\log B$	-0.76645	30.7702	0.0006058	0.	0.		Robinson and Stokes [1965]
$\log K_w$	6.0875	4470.99	0.01705	0.	0.		Stumm and Morgan [1981]
$\log K_{Calcite}$	-171.9065	2839.319	-0.077993	71.595	0.		Plummer and Busenberg [1982]

Table 6.5. Values for equilibrium and precipitation-dissolution reaction constants and ΔH_r^0 [Truesdell and Jones, 1974].

Complex	K	ΔH_r^0 , (289.15°K) [J mol ⁻¹]
NaCO ₃ ⁻	0.053958	-37337.1
NaSO ₄ ⁻	0.1995	-4692.8
NaHCO ₃ ⁰	0.5623	
KSO ₄	0.14125	-9427.5
H ₃ SiO ₄ ⁻	1.17490e-10	37436.65
H ₂ SiO ₄ ²⁻	2.40436e-22	124501.7
Gypsum	2.51189e-5	1131.3
Hydromagnesite	1.72982e-37	-106928.8
Nesquehonite	2.39332e-6	-28366.1
Sepiolite	3.13762e-38	

6.11. Osmotic Coefficient

We use the semiempirical equation of *Pitzer* [1973] and co-workers to calculate the osmotic coefficient ϕ :

$$\begin{aligned} \sum_i m_i(\phi - 1) = & 2 \left(-\frac{A^\phi I^{3/2}}{1 + 1.2 I^{1/2}} + \sum_{c=1}^{N_c} \sum_{a=1}^{N_a} m_c m_a (B_{ca}^\phi + Z C_{ca}) + \right. \\ & + \sum_{c=1}^{N_c-1} \sum_{c'=c+1}^{N_c} m_c m_{c'} (\Phi_{cc'}^\phi + \sum_{a=1}^{N_a} m_a \psi_{cc'a}) + \sum_{a=1}^{N_a-1} \sum_{a'=a+1}^{N_a} m_a m_{a'} (\Phi_{aa'}^\phi + \sum_{c=1}^{N_c} m_c \psi_{aa'c}) + \quad (6.61) \\ & \left. + \sum_{n=1}^{N_n} \sum_{a=1}^{N_a} m_n m_a \lambda_{na} + \sum_{n=1}^{N_n} \sum_{c=1}^{N_c} m_n m_c \lambda_{nc} \right) \end{aligned}$$

The variables used in (6.61) were previously defined in Section 6.9.2.

6.12. Osmotic Pressure Head

The osmotic pressure of electrolyte solutions, P_ϕ (Pa), is related to the osmotic coefficient ϕ and molality as follows [Stokes, 1979]

$$P_\phi = RT \frac{M_s}{V_s} \frac{\nu m \phi}{m^0} \quad (6.62)$$

where V_s is the partial molar volume of the solvent ($\text{cm}^3 \text{mol}^{-1}$), m^0 is unit molality (1 mol kg^{-1}), and M_s is molar weight (mol^{-1}). The osmotic pressure head, h_ϕ [L], is related to the osmotic pressure by

$$h_\phi = \frac{P_\phi}{\rho g} \quad (6.63)$$

where ρ is the density of water [ML^{-3}] and g is the gravitational constant [$\text{L}^2 \text{T}^{-1}$].

6.13. System Summary

As discussed in section 6 we need either 36 or 35 independent equations to solve the equilibrium system depending on whether calcite precipitation-dissolution is considered as a fast (instantaneous equilibrium) or slow (rate-controlled) process. Seven primary aqueous species of the first group of Table 6.1 are replaced by the mass balance equations (6.1). The analytical concentrations of the first six species are obtained from the solution of the solute transport equation and the analytical concentration of the last component is obtained from the charge balance equation (6.5). The complex species of the second group are replaced by ten equations (6.10) through (6.13). As discussed in section 6.9.2, this group is not used for solutions of high ionic strength when virial-type expressions are used to calculate the ion activities. Mineral phases from the third group are replaced by equation (6.24) and (6.29) through (6.32), and surface species from the fourth group by four equations (6.17) and (6.18). The CO_2 partial pressure is obtained from the carbon dioxide transport submodel and the activity of water is calculated by equation (6.52) or (6.59), depending on the method used to calculate activity coefficients. The last five species from the sixth group are replaced by equations (6.6) through (6.9) and the defining equation for alkalinity (6.4), which is also obtained from the solution of the transport equation. Mass. balance for the silica species (6.2) and two equations (6.14) replace the silica species from the six group. The total amount of silica species in the soil solution is given by (6.47). The whole system of equations is now mathematically closed.

7. NUMERICAL SOLUTION OF THE WATER FLOW EQUATION

7.1. Space and Time Discretization

The soil profile is first discretized into $N-1$ adjoining elements, with the ends of the elements located at the nodal points, and N being the number of nodes. The same spatial discretization is used for water flow, solute transport and heat movement. UNSCHEM assumes that the vertical coordinate z is directed positive upward.

A mass-lumped linear finite elements scheme was used for discretization of the mixed form of the Richards' equation (2.1). Since the mass-lumped scheme results in an equivalent and somewhat standard finite difference scheme, we omit the detailed finite element development and give immediately the invoked final finite difference scheme [Šimůnek *et al.*, 1997]:

$$\frac{\theta_i^{j+1,k+1} - \theta_i^j}{\Delta t} = \frac{1}{\Delta Z} \left[K_{i+1/2}^{j+1,k} \frac{h_{i+1}^{j+1,k+1} - h_i^{j+1,k+1}}{\Delta Z} - K_{i-1/2}^{j+1,k} \frac{h_i^{j+1,k+1} - h_{i-1}^{j+1,k+1}}{\Delta Z} \right] - \frac{K_{i+1/2}^{j+1,k} - K_{i-1/2}^{j+1,k}}{\Delta Z} - S_i^j \quad (7.1)$$

where

$$\begin{aligned} \Delta t &= t^{j+1} - t^j \\ \Delta Z &= \frac{z_{i+1} - z_{i-1}}{2} \quad \Delta Z_i = z_{i+1} - z_i \quad \Delta Z_{i-1} = z_i - z_{i-1} \\ K_{i+1/2}^{j+1,k} &= \frac{K_{i+1}^{j+1,k} + K_i^{j+1,k}}{2} \quad K_{i-1/2}^{j+1,k} = \frac{K_i^{j+1,k} + K_{i-1}^{j+1,k}}{2} \end{aligned} \quad (7.2)$$

in which subscripts $i-1$, i , and $i+1$ indicate the position in the finite difference mesh; superscripts k and $k+1$ denote the previous and current iteration levels, respectively; and superscripts j and $j+1$ represent the previous and current time levels, respectively. Equation (7.1) is based on a fully implicit discretization of the time derivative, and will be solved with a Picard iterative solution scheme. Notice also that the sink term, S , is evaluated at the previous time level. The mass-

conservative method proposed by *Celia et al.* [1990], in which $\theta^{j+1,k+1}$ is expanded in a truncated Taylor series with respect to h about the expansion point $h^{j+1,k}$, is used in the time difference scheme of (7.1) (note that subscript w is dropped in discretized equations):

$$\frac{\theta_i^{j+1,k+1} - \theta_i^j}{\Delta t} = C_i^{j+1,k} \frac{h_i^{j+1,k+1} - h_i^{j+1,k}}{\Delta t} + \frac{\theta_i^{j+1,k} - \theta_i^j}{\Delta t} \quad (7.3)$$

where C represents the nodal value of the soil water capacity [L⁻¹]:

$$C_i^{j+1,k} = \left. \frac{d\theta_w}{dh} \right|^{j+1,k} \quad (7.4)$$

This method has been shown to provide excellent results in terms of minimizing the mass balance error. Notice that the second term on the right hand side of (7.3) is known prior to the current iteration. The first term on the right hand side of (7.3) should vanish at the end of the iteration process if the numerical solution converges. The derivation leads to the following matrix equation with matrix $[P_w]$ and vectors $\{h\}$ and $\{F_w\}$

$$[P_w]^{j+1,k} \{h\}^{j+1,k+1} = \{F_w\} \quad (7.5)$$

where the symmetrical tridiagonal matrix $[P_w]$ in (7.5) has the form:

$$[P_w] = \begin{pmatrix} d_1 & e_1 & 0 & & & 0 \\ e_1 & d_2 & e_2 & 0 & & 0 \\ 0 & e_2 & d_3 & e_3 & 0 & 0 \\ & & & & & \\ & & & & & \\ 0 & & 0 & e_{N-3} & d_{N-2} & e_{N-2} & 0 \\ 0 & & & 0 & e_{N-2} & d_{N-1} & e_{N-1} \\ 0 & & & & 0 & e_{N-1} & d_N \end{pmatrix} \quad (7.6)$$

where the diagonal entries d_i and above-diagonal entries e_i of the matrix $[P_w]$, and the entries f_i of vector $\{F_w\}$, are given by

$$d_i = \frac{K_{i+1/2}^{j+1,k}}{\Delta t} C_i^{j+1,k} + \frac{K_i^{j+1,k} + K_{i+1}^{j+1,k}}{2\Delta z_i} + \frac{K_i^{j+1,k} + K_{i-1}^{j+1,k}}{2\Delta z_{i-1}} \quad (7.7)$$

$$e_i = -\frac{K_i^{j+1,k} + K_{i+1}^{j+1,k}}{2\Delta z_i} \quad (7.8)$$

$$f_i = \frac{\Delta z}{\Delta t} C_i^{j+1,k} h_i^{j+1,k} - \frac{\theta_i^{j+1,k} - \theta_i^j}{\Delta t} + \frac{K_{i+1}^{j+1,k} - K_{i-1}^{j+1,k}}{2} - S_i^j \Delta z \quad (7.9)$$

The tridiagonal matrix $[P_w]$ is symmetric and therefore the below-diagonal entries are equal to the above-diagonal entries. The entries d_1, e_1, f_1 , and e_{N-1}, d_N, f_N are dependent upon the prescribed boundary conditions.

7.2. Treatment of Pressure Head Boundary Conditions

If a first-type (Dirichlet) boundary condition is specified at the top or bottom of the soil profile, then the terms d , or d_N are equal to unity, e_1 or e_{N-1} reduce to zero, and f_1 or f_N are equal to the prescribed pressure head, h_0 . Some additional rearrangement of the matrix $[P_w]$ is also necessary to preserve its symmetry. The appropriate entries in the second or $(N-1)$ st equations containing the prescribed boundary pressure head h_0 in the left-hand side matrix must then be incorporated into the known vector on the right-hand side of the global matrix equation. When done properly, this rearrangement will restore symmetry in $[P_w]$.

7.3. Treatment of Flux Boundary Conditions

If the third-type (Neumann) boundary condition at the bottom of the profile is specified, then the individual entries are obtained by discretization of Darcy's law, i.e.,

$$q_w = -K \frac{\partial h}{\partial z} - K \quad (7.10)$$

such that d_1 and f_1 in $[P_w]$ attain the values

$$d_1 = \frac{K_1^{j+1,k} + K_2^{j+1,k}}{2 \Delta z_1} \quad (7.11)$$

$$f_1 = \frac{K_1^{j+1,k} + K_2^{j+1,k}}{2} + q_0^{j+1} \quad (7.12)$$

where q_0 is the prescribed boundary flux $[LT^{-1}]$ and where e_1 is described by (7.8). A similar discretization of Darcy's law is also possible to incorporate the flux boundary condition at the top of the soil profile. This approach, however, can quickly lead to relatively unstable solutions when the boundary fluxes at the soil surface vary greatly with time (variable irrigation or rainfall rates). A more stable and mass-conservative solution results when the mass balance equation

$$\frac{\partial \theta_w}{\partial t} = - \frac{\partial q_w}{\partial z} - S \quad (7.13)$$

instead of Darcy's law is discretized. Discretization of (7.13) gives

$$\frac{\theta_N^{j+1,k+1} - \theta_N^j}{\Delta t} = - \frac{2(q_N^{j+1} - q_{N-1/2}^{j+1,k})}{\Delta z_{N-1}} - S_N^j \quad (7.14)$$

Expanding the time derivative on the left hand side of (7.14) as in (7.3), and using the discretized form of Darcy's law for $q_{N-1/2}$ leads to

$$d_N = \frac{\Delta z_{N-1}}{2 \Delta t} C_N^{j+1,k} + \frac{K_N^{j+1,k} + K_{N-1}^{j+1,k}}{2 \Delta z_{N-1}} \quad (7.15)$$

$$f_N = \frac{\Delta x_{N-1}}{2 \Delta t} C_{NN}^{j+1,k} h_N^{j+1,k} - \frac{\theta_N^{j+1,k} - \theta_N^j}{\Delta t} - \frac{K_N^{j+1,k} + K_{N-1}^{j+1,k}}{2} - \frac{\Delta x_{N-1}}{2} S_N^j - q_N^{j+1} \quad (7.16)$$

where q_N is the prescribed soil surface boundary flux. Implementation of a third-type boundary condition always preserves symmetry of the matrix $[P_w]$.

7.4. Numerical Solution Strategy

7.4.1. Iterative Process

Because of the nonlinear nature of (7.5), an iterative process must be used to obtain solutions of the global matrix equation at each new time step. For each iteration a system of linearized algebraic equations is first derived from (7.5) which, after incorporation of the boundary conditions, is solved using Gaussian elimination. The Gaussian elimination process takes advantage of the tridiagonal and symmetric features of the coefficient matrix in (7.5). After solving (7.5) the first time, the coefficients in (7.5) are re-evaluated using the first solution, and the new equations are again solved. The iterative process continues until a satisfactory degree of convergence is obtained, i.e., until at all nodes in the saturated (or unsaturated) region the absolute change in pressure head (or water content) between two successive iterations becomes less than some small value determined by the imposed absolute pressure head (or water content) tolerance. The first estimate (at zero iteration) of the unknown pressure heads at each time step is obtained by extrapolation from the pressure head values at the previous two time levels.

7.4.2. Time Control

Three different time discretizations are introduced in UNSCHEM: (1) time discretizations associated with the numerical solution, (2) time discretizations associated with the implementation of boundary conditions, and (3) time discretizations which provide printed output of the simulation results (e.g., nodal values of dependent variables, water, CO, and solute mass balance components, and other information about the flow regime).

Discretizations 2 and 3 are mutually independent; they generally involve variable time steps as described in the input data file. Discretization 1 starts with a prescribed initial time increment. At this time increment is automatically adjusted at each time level according to the

following rules [Mls, 1982; Šimůnek et al., 1992]:

- a. Discretization 1 must coincide with time values resulting from time discretizations 2 and 3.
- b. Time increments cannot become less than a preselected minimum time step, Δt_{min} , nor exceed a maximum time step, Δt_{max} , (i.e., $\Delta t_{min} \leq \Delta t \leq \Delta t_{max}$).
- c. If, during a particular time step, the number of iterations necessary to reach convergence is ≤ 3 , the time increment for the next time step is increased by multiplying Δt by a predetermined constant >1 (usually between 1.1 and 1.5). If the number of iterations is > 3 , Δt for the next time level is multiplied by a constant <1 (usually between 0.3 and 0.9).
- a. If, during a particular time step, the number of iterations at any time level becomes greater than a prescribed maximum (usually between 10 and 50), the iterative process for that time level is terminated. The time step is subsequently reset to $\Delta t/3$, and the iterative process restarted.

7.4.3. Atmospheric Boundary Conditions and Seepage Faces

Atmospheric boundaries are simulated by applying either prescribed head or prescribed flux boundary conditions depending upon whether equation (2.37) or (2.38) is satisfied [Neuman, 1974]. If (2.38) is not satisfied, boundary node n becomes a prescribed head boundary. If, at any point in time during the computations, the calculated flux exceeds the specified potential flux in (2.37), the node will be assigned a flux equal to the potential value and treated again as a prescribed flux boundary.

If a seepage face is considered as the lower boundary condition and if during each iteration the lower part of the soil profile is saturated then the last node is treated as a prescribed pressure head boundary with $h=0$. However, if this node is unsaturated then a prescribed flux boundary with $q_w=0$ is imposed at the lower boundary.

7.4.4. Water Balance Computations

The UNSCHEM code performs water balance computations at prescribed times for several preselected subregions of the flow domain. The water balance information for each subregion consists of the actual volume of water, V , in that subregion, and the rate, O [LT^{-1}], of inflow or outflow to or from the subregion. These variables V and O are evaluated in UNSCHEM by means of

$$V = \sum_e \Delta z_i \frac{\theta_i + \theta_{i+1}}{2} \quad (7.17)$$

and

$$O = \frac{V_{new} - V_{old}}{\Delta t} \quad (7.18)$$

respectively, where θ_i and θ_{i+1} are water contents evaluated at the corner nodes of element e , Δz_i is the size of the element, and V_{new} and V_{old} are volumes of water in the subregion computed at the current and previous time levels, respectively. The summation in (7.17) is taken over all elements within the subregion.

The absolute error in the mass balance is calculated as

$$\epsilon_a^w = V_t - V_0 + \int_0^t T_a dt - \int_0^t (q_{w0} - q_{wN}) dt \quad (7.19)$$

where V_t and V_0 are the volumes of water in the flow domain, Eq. (7.17), evaluated at time t and zero, respectively. The third term on the right-hand side of (7.19) represents the cumulative root water uptake amount, while the fourth term gives the net cumulative flux through both boundaries.

The accuracy of the numerical solution is evaluated by the relative error, ϵ_r^w [%], in the water mass balance as follows:

$$\epsilon_r^w = \frac{|\epsilon_a^w|}{\text{max} \left[\sum_e |V_t^e - V_0^e|, \int_0^t T_a dt + \int_0^t (|q_{wN}| + |q_{w0}|) dt \right]} 100 \quad (7.20)$$

where V_t^e and V_0^e are the volumes of water in element e at times t and zero, respectively. Note that UNSCHEM does not relate the absolute error to the volume of water in the flow domain, but instead to the maximum value of two quantities. The first quantity represents the sum of the absolute changes in water content over all elements, whereas the second quantity is the sum of the absolute values of all fluxes in and out of the flow domain.

7.4.5. Computation of Nodal Fluxes

Components of the Darcian flux are computed at each time level during the simulation only when the water flow and solute (or CO, or heat) transport equations are solved simultaneously. When the flow equation alone is solved, the flux components are calculated only at selected print times. The z-components of the nodal fluxes are computed for each node n according to

$$q_1^{j+1} = -K_{1+1/2}^{j+1} \left[\frac{h_2^{j+1} - h_1^{j+1}}{\Delta z_i} + 1 \right]$$

$$q_i^{j+1} = \frac{-K_{i+1/2}^{j+1} \left[\frac{h_{i+1}^{j+1} - h_i^{j+1}}{\Delta z_i} + 1 \right] \Delta z_{i-1} - K_{i-1/2}^{j+1} \left[\frac{h_i^{j+1} - h_{i-1}^{j+1}}{\Delta z_{i-1}} + 1 \right] \Delta z_i}{\Delta z_{i-1} + \Delta z_i} \quad (7.21)$$

$$q_N^{j+1} = -K_{N-1/2}^{j+1} \left[\frac{h_N^{j+1} - h_{N-1}^{j+1}}{\Delta z_{N-1}} + 1 \right] - \frac{\Delta z_{N-1}}{2} \left[\frac{\theta_N^{j+1} - \theta_N^j}{\Delta t} + S_N^j \right]$$

7.4.6. Water Uptake by Plant Roots

UNSCHEM considers the root zone to consist of all nodes, n , for which the potential root water uptake distribution, b (see Section 2.2), is greater than zero. The root water extraction rate is assumed to vary linearly over each element. The values of actual root extraction rate S_i in (7.1) are evaluated with (2.2). UNSCHEM calculates the total rate of transpiration using the equation

$$T_a = \sum_e \Delta z_i \frac{S_i + S_{i+1}}{2} \quad (7.22)$$

in which the summation takes place over all elements within the root zone, and where S_i and S_{i+1} are the root water uptake rates evaluated at the corner nodes of element e .

7.4.7. Evaluation of the Soil Hydraulic Properties

At the beginning of a simulation, UNSCHEM generates, for each soil type in the flow domain, a table of water contents, hydraulic conductivities, and specific water capacities from the specified set of hydraulic parameters [Vogel, 1987]. The values of θ_p , K_i and C , in the table are evaluated at prescribed pressure heads h , within a specified interval (h_a, h_b) . The entries in the table are generated such that

$$\frac{h_{i+1}}{h_i} = \text{constant} \quad (7.23)$$

which means that the spacing between two consecutive pressure head values increases in a logarithmic fashion. Values for the hydraulic properties, $\theta_w(h)$, $K(h)$ and $C(h)$, are computed during the iterative solution process using linear interpolation between the entries in the table. If an argument h falls outside the prescribed interval (h_a, h_b) , the hydraulic characteristics are evaluated directly from the hydraulic functions, i.e., interpolation is not possible. The above interpolation technique was found to be much faster computationally than direct evaluation of the hydraulic functions over the entire range of pressure heads, except when very simple hydraulic

models were used.

8. NUMERICAL SOLUTION OF THE TRANSPORT EQUATIONS

The Galerkin finite element method with linear basis functions is used to solve the solute, heat, and the CO, transport equations (3.1), (4.1), and (5.6), respectively, subject to the imposed initial and boundary conditions. Since the solute, heat, and CO, transport equations have the same form (in their linear form), the numerical solution is given only once for the following convection-dispersion equation

$$-\frac{\partial}{\partial t}(Ac) - \frac{\partial}{\partial x}(Bc) + \frac{\partial}{\partial x}E \frac{\partial c}{\partial x} + Fc + G = 0 \quad (8.1)$$

where c in this section stands for all three unknown variables c , c_w , and T , and where for solute transport

$$\begin{aligned} A &= \theta_w \\ B &= q_w \\ \mathbf{E} &= \theta_w D \\ F &= 0 \\ G &= -\rho \frac{\partial \bar{c}}{\partial t} - \rho \frac{\partial \hat{c}}{\partial t} \end{aligned} \quad (8.2)$$

for heat transport

$$\begin{aligned} A &= C_p(\theta_w) \\ B &= C_w q_w \\ E &= \lambda \\ F &= 0 \\ G &= 0 \end{aligned} \quad (8.3)$$

and finally for CO, transport

$$\begin{aligned}
A &= R_f = \theta_a + \theta_w K_{\text{CO}_2} R T \\
B &= q_E = 4, + q_w K_{\text{CO}_2} R T \\
E &= D_E = \theta_a D_a + \theta_w D_w K_{\text{CO}_2} R T \\
F &= -S^* = -S K_{\text{CO}_2} R T \\
G &= P
\end{aligned} \tag{8.4}$$

Since the Galerkin method is relatively standard and has been covered in detail elsewhere [Pinder and Gray, 1977, van Genuchten, 1978, 1987], only the most pertinent steps in the solution process are given here.

8.1. Space Discretization

The finite element method assumes that the dependent variable, the function $c(z,t)$, can be approximated by a finite series $c'(z,t)$ of the form

$$c'(z,t) = \sum_{m=1}^N \phi_m(z) c_m(t) \tag{8.5}$$

where ϕ_m are selected linear basic functions that fulfill the condition $\phi_m(z_n) = \delta_{nm}$, δ_{nm} is Kronecker delta ($\delta_{nm} = 1$ for $m=n$, and $\delta_{nm} = 0$ for $m \neq n$), c_m , are unknown time-dependent coefficients which represent the solution of (8.1) at the finite element nodal points, and N is the total number of nodal points. Linear basis functions have the following form:

$$\begin{aligned}
\phi_1 &= 1 - \xi \\
\phi_2 &= \xi
\end{aligned} \tag{8.6}$$

where ξ is the distance in the local coordinate system [-]. In the global coordinate system ξ is defined as

$$\xi = \frac{z - z_1}{\Delta z} \quad z_1 \leq z \leq z_2, \quad (8.7)$$

where $\Delta z (=z_2-z_1)$ is the size of a finite element [L], i.e., the distance between two neighboring nodal points. The approximate solution $c'(x,t)$ converges to the correct solution $c(x,t)$ as the number of basis functions N increases.

Application of the Galerkin method which postulates that the differential operator associated with the transport equation is orthogonal to each of the N basis functions, we obtain the following system of N time-dependent differential equations with N unknown values $c_n(t)$.

$$\int_0^L \left[-\frac{\partial A c}{\partial t} + \frac{\partial}{\partial z} \left(E \frac{\partial c}{\partial z} - B c \right) + F c + G \right] \phi_n dz = 0 \quad (8.8)$$

Integrating by parts the terms containing spatial derivatives leads to the following equation

$$\int_0^L \left[-\frac{\partial A c}{\partial t} + F c + G \right] \phi_n dz - \int_0^L \left[E \frac{\partial c}{\partial z} - B c \right] \frac{\partial \phi_n}{\partial z} dz - q_{s_r} \phi_n(L) + q_{s_u} \phi_n(0) = 0 \quad (8.9)$$

where q_{s_0} and q_{s_l} are the material or energy fluxes across the lower and upper boundaries, respectively. By substituting $c_{,,}(t)$ for $c(z,t)$ we obtain

$$\int_0^L \left[-\frac{\partial A c_m}{\partial t} \phi_m + F c_m \phi_m + G \phi_n dz - \int_0^L \left[E c_m \frac{\partial \phi_m}{\partial z} - B c_m \phi_m \right] \frac{\partial \phi_n}{\partial z} dz - q_{s_r} \phi_n(L) + q_{s_u} \phi_n(0) = 0 \quad (8.10)$$

Equation (8.10) can be rewritten in the matrix form as

$$\frac{d([\mathcal{Q}]\{c\})}{dt} + [S]\{c\} = \{f\} \quad (8.11)$$

where vector $\{c\}$ contains the unknown values of the nodal concentrations, and where

$$Q_{mm} = \int_0^L A \phi_m \phi_n dz \quad (8.12)$$

$$S_{mm} = \int_0^L [E \frac{d\phi_m}{dz} \frac{d\phi_n}{dz} - B \frac{d\phi_n}{dz} \phi_m - F \phi_m \phi_n] dz \quad (8.13)$$

$$f_n = \int_0^L G \phi_n dz - q_{s_L} \phi_n(L) + q_{s_0} \phi_n(0) \quad (8.14)$$

8.2. Time Discretization

The Galerkin method is used only for approximating the spatial derivatives while the time derivatives are discretized by means of finite differences. The derivation leads to the following matrix equation with asymmetric tridiagonal matrices $[P_c]$ and $[Q_c]$, and vectors $\{c\}$ and $\{F_c\}$

$$[P_c]^{j+1} \{c\}^{j+1} = [Q_c]^j \{c\}^j + \{F_c\} \quad (8.15)$$

where $\{c\}^{j+1}$ is a vector of unknown concentration or temperature and where

$$\begin{aligned} [P_c]^{j+1} &= \frac{1}{\Delta t} [Q]^{j+1} + \epsilon [S]^{j+1} \\ [Q_c]^j &= \frac{1}{\Delta t} [Q]^j - (1 - \epsilon) [S]^j \\ \{F_c\} &= \epsilon \{f\}^{j+1} + (1 - \epsilon) \{f\}^j \end{aligned} \quad (8.16)$$

If the Crank-Nicholson implicit scheme is used for the time discretization then $\epsilon=0.5$. The diagonal entries d_i , and off-diagonal entries b_i and e_i , of the matrix $[P_c]$ are then calculated as described in Table 8.1.

Table 8. Values of the diagonal entries d_i , and off-diagonal entries b_i and e_i of the matrix $[P_c]$ for linear finite elements.

$$d_1 = \frac{\Delta z_1}{12\Delta t}(3A_1 + A_2) + \frac{\epsilon}{2\Delta z_1}(E_1 + E_2) + \frac{\epsilon}{6}(2B_1 + B_2) + \frac{\epsilon\Delta z_1}{12}(3F_1 + F_2) \quad (8.17)$$

$$b_i = \frac{\Delta z_{i-1}}{12\Delta t}(A_{i-1} + A_i) - \frac{\epsilon}{2\Delta z_{i-1}}(E_{i-1} + E_i) - \frac{\epsilon}{6}(2B_{i-1} + B_i) + \frac{\epsilon\Delta z_{i-1}}{12}(F_{i-1} + F_i) \quad (8.18)$$

$$d_i = \frac{\Delta z_{i-1}}{12\Delta t}(A_{i-1} + 3A_i) + \frac{\Delta z_i}{12\Delta t}(3A_i + A_{i+1}) + \frac{\epsilon}{2\Delta z_{i-1}}(E_{i-1} + E_i) + \frac{\epsilon}{2\Delta z_i}(E_i + E_{i+1}) + \frac{\epsilon}{6}(B_{i+1} + B_{i-1}) + \frac{\epsilon\Delta z_{i-1}}{12}(F_i + 3F_i + F_{i+1}) \quad (i=2, \dots, n-1) \quad (8.19)$$

$$e_i = \frac{\Delta z_i}{12\Delta t}(A_i + A_{i+1}) + \frac{\epsilon}{2\Delta z_i}(E_i + E_{i+1}) + \frac{\epsilon}{6}(2B_{i+1} + B_i) + \frac{\epsilon\Delta z_i}{12}(F_i + F_{i+1}) \quad (8.20)$$

$$d_N = \frac{\Delta z_{N-1}}{12\Delta t}(A_{N-1} + 3A_N) + \frac{\epsilon}{2\Delta z_{N-1}}(E_{N-1} + E_N) + \frac{\epsilon}{6}(B_{N-1} + 2B_N) + \frac{\epsilon\Delta z_{N-1}}{12}(F_{N-1} + 3F_N) \quad (8.21)$$

Table 8.2. Values of the diagonal entries d_i , and off-diagonal entries b_i and e_i of the matrix $[P_\epsilon]$ for finite differences.

$$d_1 = \frac{\Delta z_1}{2\Delta t} A_1 + \frac{\epsilon}{2\Delta z_1} (E_1 + E_2) + \frac{\epsilon}{6} (2B_1 + B_2) + \frac{\epsilon \Delta z_1}{12} (3F_1 + F_2) \quad (8.22)$$

$$b_i = \frac{\epsilon}{2\Delta z_{i-1}} (E_{i-1} + E_i) - \frac{\epsilon}{6} (2B_{i-1} + B_i) + \frac{\epsilon \Delta z_{i-1}}{12} (F_{i-1} + F_i) \quad (8.23)$$

$$d_i = \frac{\Delta z}{\Delta t} A_i + \frac{\epsilon}{2\Delta z_{i-1}} (E_{i-1} + E_i) + \frac{\epsilon}{2\Delta z_i} (E_i + E_{i+1}) + \frac{\epsilon}{6} (B_{i-1} + B_i) + \frac{\epsilon \Delta z_{i-1}}{12} (F_{i-1} + 3F_i) + \frac{\epsilon \Delta z_i}{12} (3F_i + F_{i+1}) \quad i = 2, \dots, n \quad (8.24)$$

$$e_i = \frac{\Delta z_i}{12\Delta t} (A_i + A_{i+1}) - \frac{\epsilon}{2\Delta z_i} (E_i + E_{i+1}) + \frac{\epsilon}{6} (2B_{i+1} + B_i) + \frac{\epsilon \Delta z_i}{12} (F_i + F_{i+1}) \quad (8.25)$$

$$\frac{\Delta}{2} \quad \text{---} \quad \frac{\epsilon}{6} \quad \frac{\Delta}{1}$$

Table 8.3. Values of the diagonal entries d_i , and off-diagonal entries b_i and e_i of the matrix $[P_\epsilon]$ for linear finite elements with upstream weighting.

$$d_1 = \frac{\Delta z_1}{12\Delta t}(3A_1 + A_2) + \frac{\epsilon}{2\Delta z_1}(E_1 + E_2) + \frac{\epsilon}{6}[(2 + 3\alpha^+)B_1 + B_2] + \frac{\epsilon \Delta z_1}{12}(3F_1 + F_2) \quad (8.27)$$

$$b_i = \frac{\Delta z_{i-1}}{12\Delta t}(A_{i-1} + A_i) - \frac{\epsilon}{2\Delta z_{i-1}}(E_{i-1} + E_i) - \frac{\epsilon}{6}[(2 + 3\alpha^-)B_{i-1} + B_i] + \frac{\epsilon \Delta z_{i-1}}{12}(F_{i-1} + F_i) \quad (8.28)$$

$$d_i = \frac{\Delta z_{i-1}}{12\Delta t}(A_{i-1} + 3A_i) + \frac{\Delta z_i}{12\Delta t}(3A_i + A_{i+1}) + \frac{\epsilon}{2\Delta z_{i-1}}(E_{i-1} + E_i) + \frac{\epsilon}{2\Delta z_i}(E_i + E_{i+1}) + \frac{\epsilon}{6}[B_{i+1} + 3B_i(\alpha^+ + \alpha^-) - B_{i-1}] + \frac{\epsilon \Delta z_{i-1}}{12}(F_{i-1} + 3F_i) + \frac{\epsilon \Delta z_i}{12}(3F_i + F_{i+1}) \quad (i = 2, \dots, n-1) \quad (8.29)$$

$$e_i = \frac{\Delta z_i}{12\Delta t}(A_i + A_{i+1}) - \frac{\epsilon}{2\Delta z_i}(E_i + E_{i+1}) + \frac{\epsilon}{6}[(2 - 3\alpha^+)B_{i+1} + B_i] + \frac{\epsilon \Delta z_i}{12}(F_i + F_{i+1}) \quad (8.30)$$

$$d_N = \frac{\Delta z_{N-1}}{12\Delta t}(A_{N-1} + 3A_N) + \frac{\epsilon}{2\Delta z_{N-1}}(E_{N-1} + E_N) - \frac{\epsilon}{6}[B_{N-1} + (2 - \alpha^-)B_N] + \frac{\epsilon \Delta z_{N-1}}{12}(F_{N-1} + 3F_N) \quad (8.31)$$

The matrix $[Q_c]$ is exactly the same as $[P_c]$, except that \mathbf{E} , \mathbf{B} and F must be replaced by $(-E)$, $(-\mathbf{B})$ and $(-F)$, respectively. The entries f_i of vector $\{F_c\}$ are given by

$$f_1 = \frac{\Delta z_1}{6} [\epsilon (2G_1 + G_2)^{j+1} + (1 - \epsilon)(2G_1 + G_2)^j] + \epsilon q_{s_0}^{j+1} + (1 - \epsilon)q_{s_0}^j \quad (8.32)$$

$$f_i = \frac{\Delta z_{i-1}}{6} [\epsilon (G_{i-1} + 2G_i)^{j+1} + (1 - \epsilon)(2G_i + G_{i+1})^j] + \frac{\Delta z_i}{6} [\epsilon (G_{i-1} + 2G_i)^{j+1} + (1 - \epsilon)(2G_i + G_{i+1})^j] \quad (8.33)$$

$$f_N = \frac{\Delta z_{N-1}}{6} [\epsilon (G_{N-1} + 2G_N)^{j+1} + (1 - \epsilon)(G_{N-1} + 2G_N)^j] - \epsilon q_{s_N}^{j+1} - (1 - \epsilon)q_{s_N}^j \quad (8.34)$$

Implementation of boundary fluxes is achieved by incorporating these fluxes into the vector $\{F_c\}$. If the first-type (Dirichlet) boundary condition is specified for upper or lower boundary condition, then the terms d_1 or d_N are set equal to unity, e_1 or b_N equal to zero, and f_1 or f_N equal to the prescribed boundary fluxes, respectively. No additional rearrangement of the matrix $[P_c]$ is necessary since this matrix is generally asymmetric due to the convective term.

Higher-order approximations for the time derivative in the transport equation were derived by *van Genuchten* [1976,1978]. The higher-order effects may be incorporated into the transport equation by introducing time-dependent dispersion corrections as follows

$$E^- = E - \frac{B^2 \Delta t}{6A} \quad (8.35)$$

$$E^+ = E + \frac{B^2 \Delta t}{6A}$$

where the superscripts + and - indicate evaluation at the old and new time levels, respectively.

Higher precision in terms of the mass balances can be obtained by using the finite difference method for the first term of the transport equation (8.1) (see Table 8.2).

8.3. Numerical Solution Strategy

8.3.1. Solution Process

The solution process at each time step proceeds as follows. First, an iterative procedure is used to obtain the solution of the Richards' equation (2.1) (see Section 7.4.1). After achieving convergence, the solution of the transport equations (8.15) is sequentially implemented, first for temperature, then for CO, and finally for multicomponent solute transport. This is done by first determining the nodal values of the fluid flux from nodal values of the pressure head by applying Darcy's law. Nodal values of the water content and the fluid flux at the previous time level are already known from the solution at the previous time step. Values for the water content and the fluid flux are subsequently used as input to the heat transport equation, leading to the system of linear algebraic equations corresponding to (8.15). The structure of the final set of equations depends upon the value of the temporal weighing factor, ϵ . The explicit ($\epsilon=0$) and fully implicit ($\epsilon=1$) schemes require that the global matrices $[P_c]$ and $[Q_c]$, and the vector $\{F_c\}$ be evaluated at only one time level (the previous or current time level). All other schemes require evaluation at both time levels. Also, all schemes except for the explicit formulation ($\epsilon=0$) lead to an asymmetric banded matrix $[P,]$. The associated set of algebraic equations is solved using a standard asymmetric matrix equation solver. By contrast, the explicit scheme leads to a diagonal matrix $[P_c]$ which is much easier to solve (but generally requires smaller time steps). Since heat transport equation (4.1) is linear, an iterative procedure is not necessary. The nodal values of water content, velocity and temperature, obtained from the solution of water flow and heat transport equations, are then used to evaluate the coefficients of the discretized CO, transport equation (5.6). The CO, transport equation (5.6) is not linear because the production term P is dependent on CO, concentration. To avoid the necessity to iterate, we evaluate this term with the CO, concentration from the earlier time step. Finally, the multicomponent solute transport is solved based on the knowledge of the water contents, velocities, temperatures and CO, concentrations from the previous solution. The solution of the multicomponent chemical system and its coupling with solute transport will be dealt with in Section 9.2. The water flow is considered to be invariant with respect to temperature, CO, and solute transport. and similarly

heat transport is considered to be invariant with respect to both CO, and solute transport, and finally CO, transport is assumed to be independent of multicomponent solute transport. Using these assumptions, it is not necessary to solve all the equations simultaneously; rather we can solve them sequentially.

8.3.2. *Upstream Weighted Formulation*

Upstream weighing is provided as an option in UNSCHEM to minimize some of the numerical oscillation associated with the solution of the solute transport equation when relatively steep concentration fronts are being simulated. This option is not used for the solution of the heat or CO, transport equations since the Peclet numbers (see Section 8.3.6) for both equations usually have very small values, due to the high values of the apparent thermal conductivity coefficients and effective dispersion coefficients, respectively. For this purpose the second (flux) term of equation (8.1) is not weighted by regular linear basis functions ϕ_n , but instead using the nonlinear functions ϕ_n'' [Huyakorn and Nilkuha. 1979]:

$$\begin{aligned}\phi_1'' &= \phi_1 - 3\alpha'' \phi_1 \phi_2 \\ \phi_2'' &= \phi_2 + 3\alpha'' \phi_1 \phi_2\end{aligned}\tag{8.36}$$

Evaluating integrals (8.12) through (8.14) we get the coefficients described in Table 8.3.

8.3.3. *Reverse Back-Step Particle Tracking*

The reverse back-step particle tracking method is another approach which stabilizes the numerical solution of the convective-dispersive equation. A two-step procedure is followed for this mixed Lagrangian-Eulerian approach. First, convective transport is considered using a Lagrangian approach in which lagrangian concentrations are estimated from particle trajectories. Subsequently, all other processes including sinks and sources are modeled using the standard Eulerian approach involving the finite element method, thus leading to the final concentrations.

In a single-step reverse particle tracking method [Molz, 1981], the initial position of particles arriving at the end of a time step at fixed nodal points is calculated at each time step

as follows

$$z_n' = z_n - \int_{t_k}^{t_{k+1}} v^* dt \quad (8.37)$$

where v^* represents the pore-water velocity (v/R) which takes into account all the retardation processes. This equation states that a particle leaving location z_n' at time t_k will reach the grid point location z_n exactly at time t_{k+1} . The concentration at location z_n' at time t_k is then used in a discretized transport equation.

8.3.4. Solute Mass Balance Calculations

The total amount of mass in the entire flow domain, or in a preselected subregion, in solvent (M_l), mineral phase (M_p), and surface species (M_s) is given by

$$\begin{aligned} M_l &= \sum_e \int \theta c dz = \sum_e \Delta z_i \frac{\theta_i c_i + \theta_{i+1} c_{i+1}}{2} \\ M_p &= \sum_e \int \rho \bar{c} dz = \sum_e \Delta z_i \frac{\rho_i \bar{c}_i + \rho_{i+1} \bar{c}_{i+1}}{2} \\ M_s &= \sum_e \int \rho \hat{c} dz = \sum_e \Delta z_i \frac{\rho_i \hat{c}_i + \rho_{i+1} \hat{c}_{i+1}}{2} \end{aligned} \quad (8.38)$$

where $\theta_i, \theta_{i+1}, \rho_i, \rho_{i+1}, c_i, c_{i+1}, \hat{c}_i, \hat{c}_{i+1}$, and \bar{c}_i, \bar{c}_{i+1} represent, respectively, water contents, bulk densities and aqueous, mineral phase and surface concentrations evaluated at the corner nodes of element e . The summation is taken over all elements within the specified region. The total amount of solute in the entire flow domain, M_T [ML⁻³], is then calculated as

$$M_T = M_l + M_p + M_s \quad (8.39)$$

Finally, when all boundary material fluxes have been computed, the following mass balance should hold for the flow domain as a whole:

$$M_t - M_0 = \int_0^t (q_{s_n} - q_{s_v}) dt \quad (8.40)$$

where M_t and M_0 are the amounts of solute in the flow region at times t and zero, respectively, as calculated with (8.39). The difference between the left- and right-hand sides of (8.40) represents the absolute error, ϵ_a^c , in the solute mass balance. Similarly as for water flow, the accuracy of the numerical solution for solute transport is evaluated by using the relative error, ϵ_r^c [%], in the solute mass balance as follows

$$\epsilon_r^c = \frac{100 |\epsilon_a^c|}{\max \left[\sum_e |M_t^e - M_0^e|, \int_0^t (|q_{s_n}| + |q_{s_v}|) dt \right]} \quad (8.41)$$

where M_0^e and M_t^e are the amounts of solute in element e at times 0 and t , respectively. The relative errors are calculated only for the hypothetical tracer. Note again that UNSCHEM does not relate the absolute error to the total amount of mass in the flow region. Instead, the program uses as a reference the maximum value of (1) the absolute change in element concentrations as summed over all elements, and (2) the sum of the absolute values of all cumulative solute fluxes across the flow boundaries.

8.3.5. Carbon Dioxide Mass Balance Calculations

Total amount of carbon dioxide in the entire flow domain M_{CO} [L], or in a preselected subregion, is given by

$$M_{CO} = \sum_e \int (\theta_w c_w + \theta_a c_a) dz = \sum_e \Delta z_i \frac{c_{a_i} (\theta_{a_i} + K_{CO_2} RT_i \theta_{w_i}) + c_{a_{i+1}} (\theta_{a_{i+1}} + K_{CO_2} RT_{i+1} \theta_{w_{i+1}})}{2} \quad (8.42)$$

The absolute error in the carbon dioxide mass balance ϵ_a^{CO} at time t is given as

$$\epsilon_a^{\text{CO}} = M_{\text{CO}}' - M_{\text{CO}}^0 - \int_0^t (q_0^{\text{CO}} - q_L^{\text{CO}} + P - Sc_w) dt \quad (8.43)$$

where M_{CO}^0 and M_{CO}' are the amounts of carbon dioxide in the flow region at times zero and t respectively, and the integral represents the amount of carbon dioxide added/removed from the flow region by boundary fluxes, CO₂ production and CO₂ root uptake.

8.3.6. Oscillatory Behavior

Numerical solutions of the transport equation often exhibit oscillatory behavior and/or excessive numerical dispersion near relatively sharp concentration fronts. These problems can be especially serious for convection-dominated transport characterized by small dispersivities. One way to partially circumvent numerical oscillations is to use upstream weighing or reverse back-step particle tracking as discussed in Section 8.3.2 and 8.3.3, respectively. Undesired oscillations can often be prevented also by selecting an appropriate combination of space and time discretizations. Two dimensionless numbers may be used to characterize the space and time discretizations. One of these is the grid Peclet number, Pe_c , which defines the predominant type of solute transport (notably the ratio of the advective and dispersive transport terms) in relation to coarseness of the finite element grid:

$$Pe_c = \frac{q_w \Delta z}{\theta_w D} \quad (8.44)$$

where Δz is the characteristic length of a finite element. The Peclet number increases when the convective part of the transport equation dominates the dispersive part, i.e., when a relatively steep concentration front is present. To achieve acceptable numerical results, the spatial discretization must be kept relatively fine to maintain a low Peclet number. Numerical oscillation can be virtually eliminated when the local Peclet numbers do not exceed about 5. However, acceptably small oscillations may be obtained with local Peclet numbers as high as 10 [Huyakorn and Pinder, 1983]. Undesired oscillation for higher Peclet numbers can be effectively eliminated by using upstream weighing or reverse back-step particle tracking methods (see Sections 8.3.2

and 5.3.3).

A second dimensionless number which characterizes the relative extent of numerical oscillations is the Courant number, Cr_c . The Courant number is associated with the time discretization as follows

$$Cr_c = \frac{q_w \Delta t}{\theta_w R \Delta z} \quad (8.45)$$

Four stabilizing options are used in UNSCHEM to avoid oscillations in the numerical solution of the solute transport equation [Šimůnek and van Genuchten, 1994]. The first two options are upstream weighing (see Section 8.3.2) and reverse back-step particle tracking (see Section 8.3.3), which effectively eliminate undesired oscillations at relatively high Peclet numbers. A third option for minimizing numerical oscillations uses the criterion developed by Perrochet and Berod [1993]

$$Pe \cdot Cr \leq \omega_s \quad (= 2) \quad (8.46)$$

where ω_s is the performance index [-]. This criterion indicates that convection-dominated transport problems having large Pe numbers can be properly simulated provided Cr is reduced according to (8.46) [Perrochet and Berod, 1993]. When small oscillations in the solution can be tolerated, ω_s can be increased to about 5 or 10.

A fourth stabilization option implemented in UNSCHEM also utilizes criterion (5.46). However, instead of decreasing Cr to satisfy equation (8.46), this option introduces artificial dispersion to decrease the Peclet number. The amount of additional longitudinal dispersion, \bar{D}_L [L], is given by [Perrochet and Berod, 1993]

$$\bar{D}_L = \frac{|q_w| \Delta t}{R \theta_w \omega_s} - D_L - \frac{\theta_w D_w \tau_w}{|q_w|} \quad (8.47)$$

The maximum permitted time step is calculated for all three options. as well as with the additional requirement that the Courant number must remain less than or equal to 1. The time step calculated in this way is subsequently used as one of the time discretization rules (rule No. B) discussed in section 7.3.3.

9. SOLUTION OF THE CHEMICAL SYSTEM AND COUPLING

9.1. *Solution of the Chemical System*

Computation of the equilibrium solution species distribution is accomplished in a fairly similar way as in the chemical model WATEQ [Truesdell and Jones, 1974], which, however, was a speciation model and did not consider solid and adsorbed species. The inputs into the model are the analytical concentrations of major ions, alkalinity, adsorbed and solid phase concentrations, water content, temperature, bulk density of the soil and CO₂ partial pressure. The model is divided into three major blocks, all of which have their own internal iteration criteria and which are coupled together by two additional global criteria. The first global criterium is the test on the electrical neutrality and the second is on the ionic strength. All iteration criteria have a precision level of 0.1 %.

At the beginning of the first block, the ionic strength, activity coefficients and the temperature dependent equilibrium constants are calculated. The appropriate model for the activity coefficients is chosen according to the ionic strength. For ionic strengths smaller than some specified value (e.g. 0.5 mol kg⁻¹) the extended form of the Debye-Hückel equation (6.49) is used. For solutions with ionic strength higher than this value the equations (6.53), based on Pitzer's theory are used. Next, anionic weak acid species (silicate ions - equation (6.14)), carbonate-bicarbonate distribution and *pH* are calculated and all mineral phases considered in the equilibrium system are checked for their saturation index values and precipitated or dissolved (if present) accordingly. The iteration criterium in this block is the second dissociation constant of carbonic acid.

The second block solves for ion pairs and complexes and consists of six subblocks for calcium, magnesium, sodium, potassium, sulfate and carbonate. The iteration criterium within each subblock is the total analytical concentration of the respective species. The main criterium for the whole block is again the second dissociation constant of carbonic acid. The whole block is skipped if the Pitzer expressions are used to calculate activity coefficients.

The third block involves the calculation of the equilibrium between the soil solution and the adsorbed concentrations on the soil solid. The iteration criterium in this block is the charge

balance of free metal cations.

Redistribution between the ion pairs, the free ions, solid phases and adsorbed species changes the ionic strength and consequently the activity coefficients, which results in the need for another iteration. Therefore, after the completion of the third block the global criteria are checked, and if not fulfilled, a new iteration is begun.

The iteration process must be accomplished for each node, at each time level and each iteration between the solute transport part and equilibrium part of the model (see next section) once or twice depending on whether the kinetic precipitation-dissolution of calcite is considered and if the *Plummer et al.* [1978] relation is used. If calcite is assumed to be at equilibrium with the solution then the iteration process is performed as described above. However, when the nonequilibrium relation is considered, then the whole process must be completed twice in order to obtain variables for the *Plummer et al.* [1978] rate equation (6.41). First to calculate the H^+ activity at the calcite surface with the assumption that the activities of $H_2CO_3^*$ and H_2O at the calcite surface are equal to their bulk fluid values. This is accomplished by including calcite into the equilibrium system and excluding all other minerals and adsorbed species. During the second calculation calcite is not considered part of the equilibrium system and the calculated activities are used for calculation of the reaction rate.

9.2. Coupling the Chemical and Solute Transport Modules

The governing solute transport equation (3.1) contains three time derivative terms. The first is the time derivative of the total dissolved concentration of the aqueous component, the second and the third are time derivatives of the surface and mineral phase concentrations, respectively. For the numerical solution, the second and third terms are lumped together into the term G (see (8.2)). Because of this term the solute transport equation (3.1) is highly nonlinear and the iterative process must be applied to obtain its solution. Both time changes of the surface and mineral phase concentrations can be obtained directly from the chemical equilibrium submodel when all the reactions are considered to reach equilibrium. When the kinetic expressions for the precipitation-dissolution of calcite and dolomite are used, the chemical submodel provides also the rate constants for these reactions. The contribution from the

precipitation-dissolution of calcite and dolomite to the time derivative of the mineral phase concentration of a particular component can then be calculated as follows:

$$\rho \frac{\partial \hat{c}}{\partial t} = -R^C A^C - R^D A^D \quad (9.1)$$

where A^C and A^D are the surface areas of the calcite and dolomite ($\text{m}^2 \ell^{-1}$ of soil matrix), respectively, which are input to the program.

The coupling between the transport and chemical submodules which was described by *Walsh et al.* [1984], *Cederberg et al.* [1985], and *Bryant et al.* [1986] and was also used by *Yeh and Tripathi* [1990] is as follows. First, the discretized solute transport equation is solved by setting the G term equal to zero for the equilibrium case or using equation (9.1) for the kinetic case. Then the new aqueous concentrations are compared with the initial concentrations for this iteration and the chemical module is called for those nodes where changes in concentrations were higher than some prescribed concentration tolerance. When the kinetic reactions for calcite or dolomite are used then the chemical module is called for all nodes at the first iteration. The chemical module provides us with the updated values of aqueous, surface and mineral phase concentrations and new values of the term G. The new aqueous concentrations are checked against those before the chemical module is called and if different, a new iteration is started. This iteration process continues until, at one of the check points, the new and the old concentrations in all nodes differ less than some prescribed concentration tolerance.

IO. PROBLEM DEFINITION

10.1. Construction of Finite Element Grid

The finite element mesh is constructed by dividing the soil profile into linear elements whose sizes are defined by the z -coordinates of the nodes that form the element corners. Neighboring elements should have approximately the same size. The ratio of the sizes of two neighboring elements is not recommended to exceed about 1.5. The nodes are numbered sequentially from 1 to $NumNP$ (total number of nodes) from the bottom of the soil profile to the soil surface.

The element dimensions must be adjusted to a particular problem. They should be made relatively small at locations where large hydraulic gradients are expected. Such a region is usually located close to the soil surface, where highly variable meteorological factors can cause rapid changes in the soil water content and corresponding pressure heads. Therefore it is usually recommended to use relatively small elements near the soil surface, and gradually larger sizes with depth. The element dimensions are also dependent on soil hydraulic properties. Coarse textured soils generally require finer discretization than fine-textured soils (loams, clays). No special restrictions are necessary within the soil root zone.

10.2. Coding of Soil Types and Subregions

Soil Types - An integer code beginning with 1 and ending with $NMat$ (the total number of soil materials) is assigned to each soil type in the flow region. The appropriate material code is subsequently assigned to each nodal point n of the finite element mesh.

Interior material interfaces do not coincide with element boundaries. When different material numbers are assigned to the nodes of a certain element, the finite element algorithm will assume that the material properties will change linearly over the element. This procedure will somewhat smooth soil interfaces. A set of soil hydraulic parameters, and CO_2 , solute and heat transport characteristics must be specified for each soil material.

Subregions - Water, CO₂, heat, and solute mass balances are computed separately for each specified subregion. The subregions may or may not coincide with the material regions. Subregions are characterized by an integer code which runs from 1 to N_{Lay} (the total number of subregions). A subregion code is assigned to each element in the flow domain.

10.3. Coding of Boundary Conditions

Boundary codes $KodTop$ and $KodBot$ must be assigned to surface and bottom boundary nodes, respectively. If a boundary node is to have a prescribed pressure head during a time step (a Dirichlet boundary condition), $KodTop$ and $KodBot$ must be set positive during that time step. If the volumetric flux of water entering or leaving the system is prescribed during a certain time step (a Neumann boundary condition), $KodTop$ and $KodBot$ must be negative or zero.

Constant Boundary Conditions - The values of constant boundary conditions for a particular boundary node, n , are given by the initial values of the pressure head, $h(n)$, in case of Dirichlet boundary conditions, or by the initial values of the recharge/discharge flux, $rTop$ or $rBot$ in case of Neumann boundary conditions. Table 10.1 summarizes the use of the variables $KodTop$ ($KodBot$), $rTop$ ($rBot$), and $h(n)$ for various types of nodes.

Table 10.1. Initial settings of $KodTop$ ($KodBot$), $rTop$ ($rBot$), and $h(n)$ for constant boundary conditions.

Node Type	$KodTop$ ($KodBot$)	$rTop$ ($rBot$)	$h(n)$
Specified Head Boundary	1	0.0	Prescribed
Specified Flux Boundary	-1	Prescribed	Initial Value

Variable Boundary Conditions - Three types of variable boundary conditions can be imposed:

1. Atmospheric boundary conditions for which $TopInf=AtmBC=.true.$,
2. Variable pressure head boundary conditions for which $TopInf=.true.$ and $KodTop=+3$, or $BotInf=.true.$ and $KodBot=+3$, or
3. Variable flux boundary conditions for which $TopInf=.true.$ and $KodTop=-3$, or $BotInf=.true.$ and $KodBot=-3$.

Initial settings of the variables $KodTop$ ($KodBot$), $rTop$ ($rBot$), and $h(n)$ for the time-dependent boundary conditions are given in Table 10.2.

Table 10.2. Initial settings of $KodTop$ ($KodBot$), $rTop$ ($rBot$), and $h(n)$ for variable boundary conditions.

Node Type	KodTop ($KodBot$)	$rTop$ ($rBot$)	$h(n)$
Atmospheric Boundary	- 4	0.0	Initial Value
Variable Head Boundary	+3	0.0	Initial Value
Variable Flux Boundary	- 3	0.0	Initial Value

Atmospheric boundary conditions are implemented when $TopInf=AtmBC=.true.$, in which case time-dependent- input data for the precipitation, $Prec$, and evaporation, $rSoil$, rates must be specified in the input file ATMOSP.H.IN. The potential fluid flux across the soil surface is determined by $rAtm=rSoil-Prec$. The actual surface flux is calculated internally by the program. Two limiting values of surface pressure head must also be provided: $hCritS$ which specifies the maximum allowed pressure head at the soil surface (usually 0.0), and $hCritA$ which specifies the minimum allowed surface pressure head (defined from equilibrium conditions between soil water and atmospheric vapor). The program automatically switches the value of $KodTop$ from -4 to +4 if one of these two limiting points is reached. Table 10.3 summarizes the use of the variables $rAtm$, $hCritS$ and $hCritA$ during program execution.

Table 10.3. Definition of the variables $KodTop$, $rTop$, and $h(n)$ when an atmospheric boundary condition is applied.

$KodTop$	$rTop$	$h(n)$	Event
-4	$rAtm$	Unknown	$rAtm=rSoil-Prec$
+4	Unknown	$hCritA$	Evaporation capacity is exceeded
+4	Unknown	$hCritS$	Infiltration capacity is exceeded

Variable head or flux boundary conditions on the soil surface (bottom of the soil profile) are implemented when $KodTop$ ($KodBot$)=+3 or -3 and $TopInf$ ($BotInf$)=**true.**, respectively. In that case, the input file ATMOSP.H.IN must contain the prescribed time-dependent values of the pressure head, hT (hB), or the flux, rT (rB), imposed on the boundary. The values of hT (hB) or rT (rB) are assigned to particular nodes at specified times according to rules given in Table 10.4.

Table 10.4. Definition of the variables $KodTop$ ($KodBot$), $rTop$ ($rBot$), and $h(n)$ when variable head or flux boundary conditions are applied.

Node Type	$KodTop$ ($KodBot$)	$rTop$ ($rBot$)	$h(n)$
Variable Head Boundary	+3	U n k n o w n	hT (hB)
Variable Flux Boundary	- 3	rT (rB)	Unknown

Water Uptake by Plant Roots - The program calculates the rate at which plants extract water from the root zone by evaluating equation (2.2). Values of the potential transpiration rate, $rRoot$, must be specified at preselected times in the input file ATMOSP.H.IN. These time dependent values must be provided by the user and can be calculated in various ways such as from the temperature and crop coefficients. Actual transpiration rates are calculated internally

by the program as discussed in Section 2.2. The root uptake parameters are taken from an input file, SELECTOR.IN. Values of the function $Beta(n)$, which describes the potential water uptake distribution over the root zone, must be specified for each node in the flow domain (see the description of input Block I in Table 12.9 of Section 12). If the root growth model is used then one of two functional expressions for the spatial distribution of the potential root water uptake is used (equation (2.7) or (2.8)) (see the description of input Block D in Table 12.4 of Section 12). All parts of the flow region where $Beta(n) > 0$ are treated as the soil root zone.

Root Growth Model - The program calculates the time variable rooting depth if the logical variable *lRoot* in input file SELECTOR.IN is equal to **.true.**. Either the Verhulst-Pearl logistic function (2.13) ($kRoot=0$) or its combination with the degree day concept (2.11) ($kRoot=1$) is used depending on the value of the integer variable *kRoot* (see Section 2.2). Either van Genuchten's (2.8) ($kBeta=0$) or an exponential (2.7) ($kBeta=1$) spatial distribution of the root water uptake is used with time-variable rooting depth, depending on the integer variable *kBeta*. If the Verhulst-Pearl logistic function is used, then the root growth factor, *r*, can be calculated either from the known value of root depth (*xRMed*) at a specified time (*tRMed*) or from the assumption that 50% of the rooting depth is reached after 50% of the growing season.

When a root growth model is used and when logical variable *lSurf* specified in input file ATMOSPHERE.IN is equal to **.true.**, the input variable, *rRoot*, from the same file is considered as potential evapotranspiration and is divided between potential transpiration, *rRoot*, and potential evaporation, *rSoil*, proportionally to the ratio between the actual and maximum rooting depth.

Deep Drainage from the Soil Profile - Vertical drainage, $q_{,,}(h)$, across the lower boundary of the soil profile is sometimes approximated by a $flux$ which depends on the position of the groundwater level (e.g., *Hopmans and Stricker, 1989*). If available, such a relationship can be implemented in the form of a variable flux boundary condition for which the code internally set variable *KodBot* equal to -7. This boundary condition is implemented in UNSCHEM by setting the logical variable *qGWL* in the input file SELECTOR.IN equal to **.true.**. The discharge rate $q_{,,}(n)$ assigned to the bottom node *n* is determined by the program as $q_{,,}(n) = q_{,,}(h)$, where *h* is the local value of the pressure head, and $q_{,,}(h)$ is given by

$$q(h) = -A_{qh} \exp(B_{qh} |h - GWLOL|) \quad (10.1)$$

where A_{qh} , and B_{qh} are empirical parameters which must be specified in the input file SELECTOR.IN, together with $GWLOL$ which represents the reference position of the groundwater level (usually set equal to the z-coordinate of the soil surface).

Free Drainage - The unit vertical hydraulic gradient boundary condition can be implemented in the form of a variable flux boundary condition for which the program set internally variable $KodBot$ equal to -5. This boundary condition is implemented in UNSCHEM by setting the logical variable $FreeD$ in the input file SELECTOR.IN equal to **.true.**. The discharge rate $q_w(n)$ assigned to bottom node n is determined by the program as $q_w(n) = -K(h)$, where h is the local value of the pressure head, and $K(h)$ is the hydraulic conductivity corresponding to this pressure head.

Seepage Faces - The initial settings of the variables $KodBot$, $rBot$ and $h(n)$ for a node on a seepage face are summarized in Table 10.5. This boundary condition is implemented in UNSCHEM by setting the logical variable $SeepF$ in the input file SELECTOR.IN, equal to **.true.**.

Table 10.5. Initial setting of $KodBot$, $rBot$, and $h(n)$ for seepage faces.

Node Type	$KodBot$	$rBot$	$h(n)$
Seepage Face (initially saturated)	+1	0.0	0.0
Seepage Face (initially unsaturated)	-1	0.0	Initial Value

Heat Transport Boundary Conditions - The type of applied boundary condition is specified by the input variables $kTopT$ and $kBotT$ for the upper and lower boundary conditions, respectively. Positive values for these variables means that the first-type boundary condition is

used. When the variable $kTopT$ ($kBotT$) is negative, then the third-type boundary condition is applied. When the variable $kBotT$ is equal to zero, the Neumann boundary condition with zero gradient is used. All initial and boundary conditions must be specified in “C.

Carbon Dioxide Transport Boundary Conditions - The type of applied boundary condition is specified by the input variable $kTopCO$ and $kBotCO$ for the upper and lower CO₂ transport boundary conditions, respectively. Positive values for these variables means, as explained for heat transport, that the first-type boundary condition is used. When the variable $kTopCO$ is negative then the boundary condition with the stagnant boundary layer (5.15) is used. When the variable $kBotCO$ is negative then the third-type boundary condition is applied. When this variable is equal to zero, the Neumann boundary condition with zero gradient is used.

Solute Transport Boundary Conditions - The type of applied boundary condition is specified by the input variable $kTopCh$ and $kBotCh$ for the upper and lower solute transport boundary conditions, respectively. Positive values for these variables means, as discussed for heat transport, that the first-type boundary condition is used. When the variable $kTopCh$ ($kBotCh$) is negative, then the third-type boundary condition is applied. When the variable $kBotCh$ is equal to zero, the Neumann boundary condition with zero gradient is used.

10.4. Program Memory Requirements

One single parameter statement is used at the beginning of the code to define the problem dimensions. All major arrays in the program are adjusted automatically according to these dimensions. This feature makes it possible to change the dimensions of the problem to be simulated without having to recompile all program subroutines. Different problems can be investigated by changing the dimensions in the parameter statement at the beginning of the main program, and subsequently linking all previously compiled subroutines with the main program when creating an executable file. Table 10.6 lists the array dimensions which must be defined in the parameter statement.

Table 10.6. List of the array dimensions.

Dimension	Current setting	Description
<i>NumNPD</i>	1000	Maximum number of nodes in finite element mesh
<i>NMatD</i>	20	Maximum number of materials
<i>NTabD</i>	100	Maximum number of items in the table of hydraulic properties generated by the program for each soil material
<i>NObsD</i>	5	Maximum number of observation nodes

11. EXAMPLE PROBLEMS

The model UNSCHEM is developed from the variably saturated solute transport model HYDRUS-1D [Šimůnek *et al.*, 1997], and thus the water flow and solute transport parts of the model have been tested earlier. Therefore all example problems solved in this section concentrate on the demonstration of the chemical features of the model.

Four example problems are presented in this section. The first example simulates an infiltration process into a relatively dry soil column. This example shows predicted differences between the equilibrium and kinetic precipitation-dissolution model. The second example calculates an irrigation problem with root water uptake and demonstrates the importance of considering the proper model for calcite precipitation-dissolution. The third example simulates an irrigation problem with a periodic upper boundary condition and demonstrates the importance of the CO₂ concentration/transport on the solution chemistry. The last example demonstrates the predictive capabilities of UNSCHEM for carbon dioxide production and transport processes.

11.1. Example 1 - Column Infiltration

This example is based on the one used in the documentation of the code SWMS_2D [Šimůnek *et al.*, 1992] to compare results obtained with the SWMS_2D and UNSAT2 [Davis and Neuman, 1983] codes. It originally simulated a one-dimensional laboratory infiltration experiment discussed by Skaggs *et al.* [1970]. This example was altered for the purposes of this report to include multicomponent chemical transport.

The soil water retention and relative hydraulic conductivity functions of the sandy soil are $\theta_r=0.02$, $\theta_a=-0.02$, $\theta_s=\theta_m=0.35$, $\theta_k=0.2875$, $\alpha=0.0410 \text{ cm}^{-1}$, $n=1.964$, $K_s=0.000722 \text{ c m s}^{-1}$, $K_k=0.000695 \text{ cm s}^{-1}$). The sand was assumed to be at an initial pressure head of -150 cm. The soil hydraulic properties were assumed to be homogenous and isotropic. The column was subjected to ponded infiltration (a Dirichlet boundary condition) at the soil surface, resulting in one-dimensional vertical water flow. The open bottom boundary of the soil column was simulated by implementing a no-flow boundary condition during unsaturated flow ($h < 0$), and a seepage face with $h=0$ when the bottom boundary becomes saturated (this last condition was not

reached during the simulation). The solution composition of the water initially present in the soil profile is that of a calcite supersaturated well water from the Wellton-Mohawk Irrigation District (well # 15 [Suarez, 1977b]: $Ca_T=12.2$, $Mg_T=9.66$, $Na_T=37.5$, $K_T=0.27$, $Cl_T=31.1$, $SO_{4T}=22.1$, alkalinity= $6.5 \text{ mmol}_c\text{L}^{-1}$). Calcite undersaturated Colorado river water from the Grand Valley ([Rhoades and Suarez, 1977]: $Ca_T=2.63$, $Mg_T=1.05$, $Na_T=2.55$, $K_T=0.06$, $Cl_T=1.94$, $SO_{4T}=2.03$, alkalinity= $2.33 \text{ mmol}_c\text{L}^{-1}$) was used as the solution composition of the infiltrating water. The simulation was run at a temperature of $25 \text{ }^\circ\text{C}$ and the soil CO_2 partial pressure was assumed to be equal to 1 kPa . The precipitation-dissolution of calcite was considered either as an equilibrium or kinetic process with a calcite surface area of $0.02 \text{ m}^2\ell^{-1}$ of soil. The bulk density of the soil was taken as 1.3 g cm^{-3} and molecular diffusion as $0.02 \text{ cm}^2\text{s}^{-1}$. Longitudinal dispersivity was equal to zero. Activity coefficients were calculated with the Debye-Hückel equation. Cation exchange was not considered in this example.

Figures 11.1 and 11.2 show the water content and tracer concentration profiles, respectively, at various times. Calcium concentration and alkalinity profiles at various times for both equilibrium and kinetic calcite precipitation-dissolution are shown in Figures 11.3 and 11.4, respectively. Calcite profiles at various times for both equilibrium and kinetic calcite precipitation-dissolution are shown in Figure 11.5.

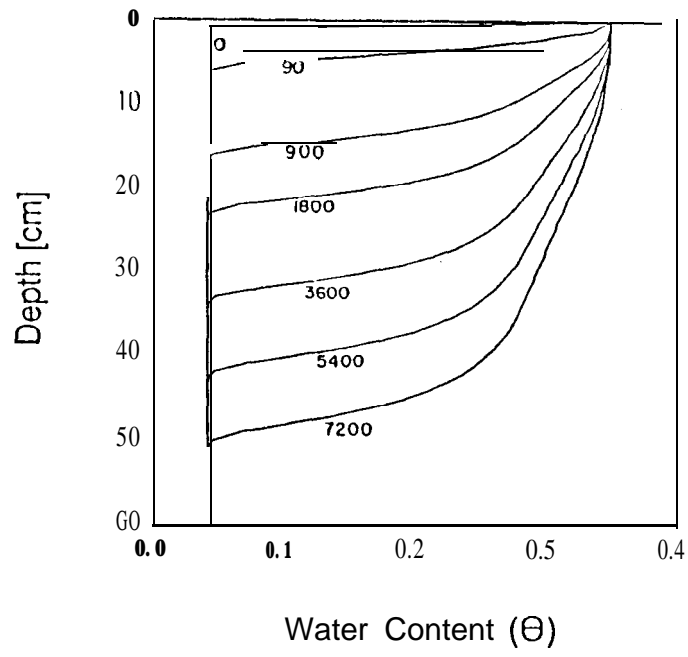


Fig. 11.1. Water content profiles at various times for example 1.

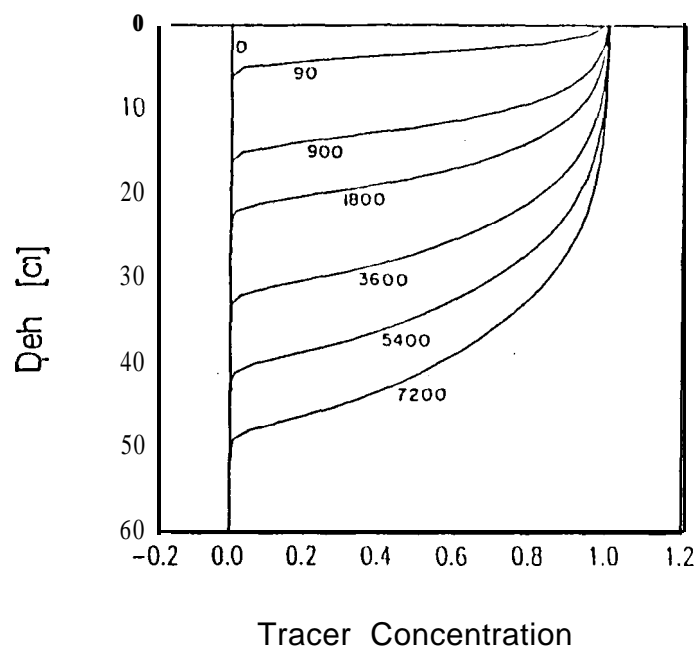


Fig. 11.2. Tracer concentration profiles at various times for example 1.

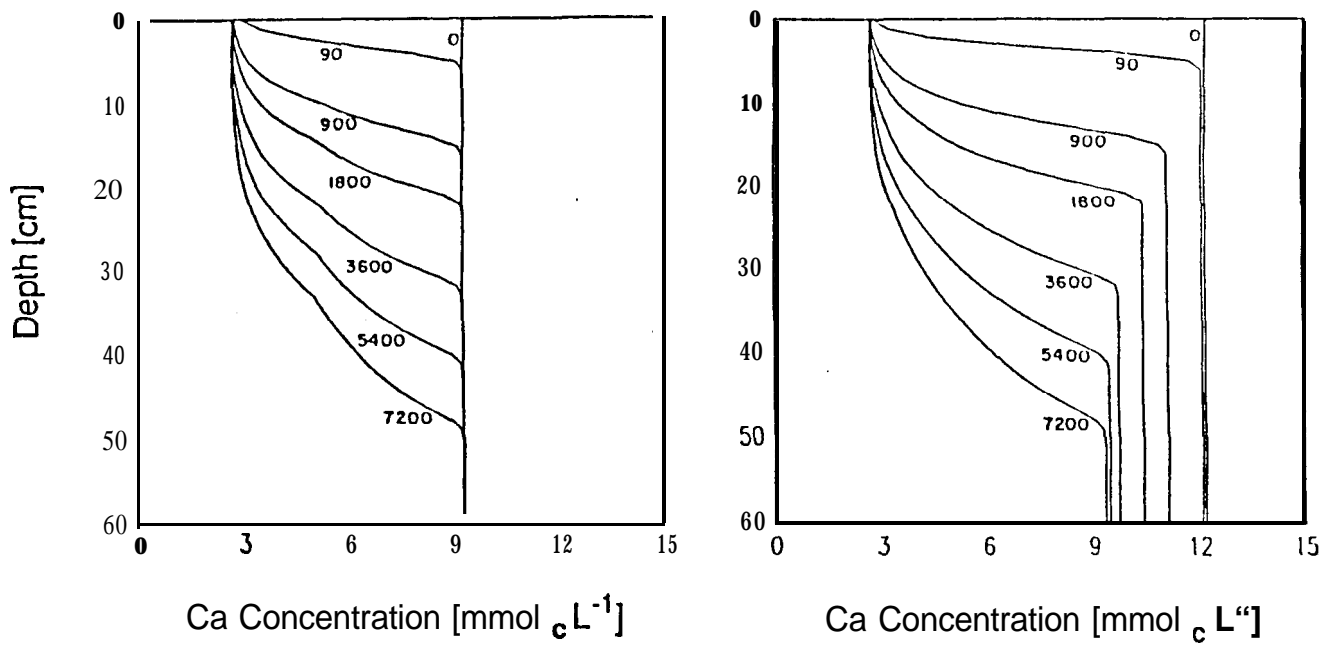


Fig. 11.3. Calcium concentration profiles at various times for a) equilibrium and b) kinetic calcite precipitation-dissolution for example 1.

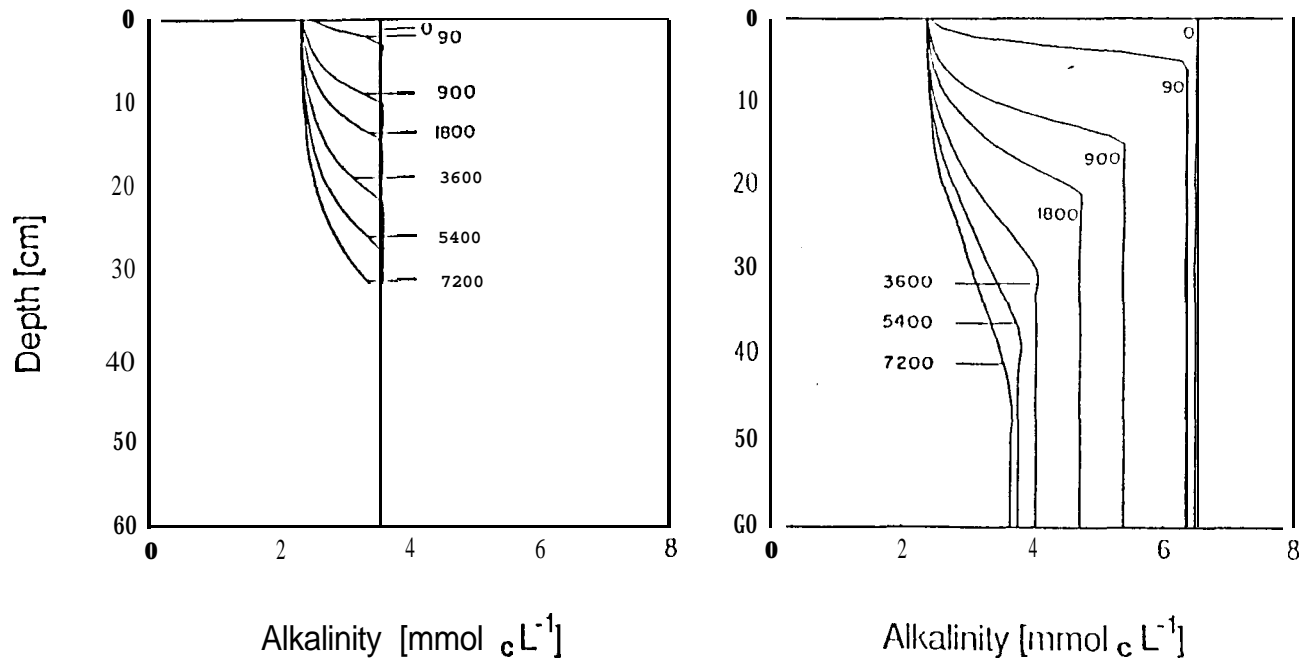


Fig. 11. 4. Alkalinity profiles at various times for a) equilibrium and b) kinetic calcite precipitation-dissolution for example 1.

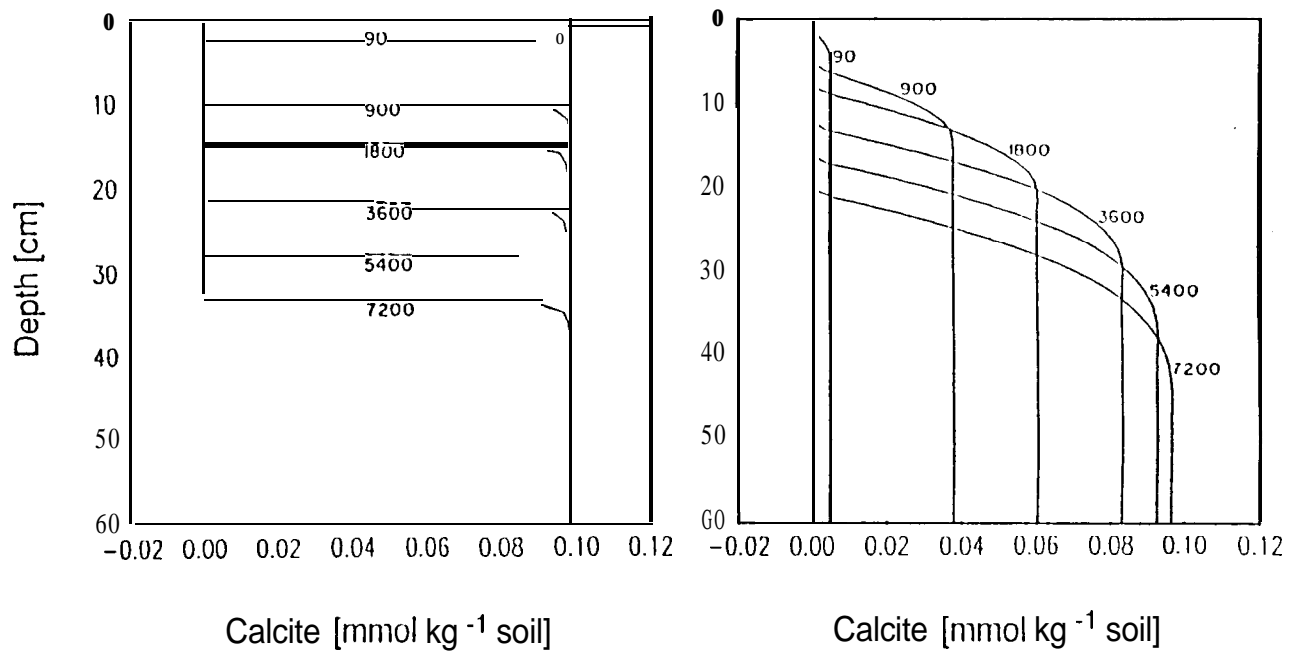


Fig. 11.5. Calcite profiles at various times for a) equilibrium and b) kinetic calcite precipitation-dissolution for example 1.

11.2. Example 2 - One Year Irrigation

In this example we examine differences in solution composition and location of precipitation when simulating calcite precipitation using kinetic as compared to an equilibrium model. We assume a 100 cm deep soil profile with an initial pressure head of -500 cm. The hydraulic parameters of a hypothetical loam soil were derived from the retention curve given by *Hillel and van Bavel* [1976] ($\theta_r=0.000$, $\theta_s=0.480$, $n=1.592$, $\alpha=0.015022 \text{ cm}^{-1}$, and $K_s=60.48 \text{ cm day}^{-1}$). The upper boundary condition was an irrigation intensity of 1 cm day^{-1} , whereas free drainage was utilized as the lower boundary condition. The potential root water uptake was distributed linearly throughout the whole soil profile with a maximum at the soil surface and zero uptake at the bottom of the rootzone. The total water uptake was assumed to be 0.9 cm day^{-1} , which together with the irrigation intensity of 1 cm day^{-1} results in a leaching fraction of 0.1. The water stress response function $a_s(h)$ was assumed to be equal to 1 for all pressure heads, i.e., there was no reduction of the potential root water uptake. Cauchy and Neumann boundary conditions were assumed at the surface and at the bottom of the soil profile, respectively. The bulk density of the soil was taken as 1.3 g cm^{-3} and molecular diffusion as $30 \text{ cm}^2\text{day}^{-1}$. Both longitudinal and transverse dispersivities were equal to zero.

The solution composition of the irrigation water, as well as of the water initially present in the soil profile, was that of a Colorado River derived well water which is already calcite supersaturated (drainage well # 15 from the Wellton-Mohawk Irrigation District in Arizona, as analyzed by *Suarez* [1977b]), as in the first example. The simulation was run at a temperature of 25 °C. The soil CO₂ partial pressure was assumed to be equal to the atmospheric value at the soil surface (33 Pa) and to increase linearly with depth up to 2 kPa at the bottom of the soil profile. Pitzer expressions were used to calculate activity coefficients. Cation exchange was not considered in this example.

A detailed description of the results was given in *Suarez and Šimůnek* [1997]. Figure 11.6 shows the water content profiles at various times during the simulation. The water content in the soil reached steady state after about 100 days. The decrease in water content with depth is due to plant root water uptake. The concentration profiles for the tracer are shown in Figure 11.7. The tracer becomes gradually more concentrated as it moves through the rootzone due to

evapotranspiration, reaching the steady state concentration of 10 at the bottom of the rootzone, as expected for a leaching fraction of 0.1. The Ca concentration profile using the equilibrium model, shown in Figure 11.8a, increases steadily with time reaching steady state after 100 days. At steady state the Ca concentration ranges from 6 mmol_cℓ⁻¹ at the surface to 32 mmol_cℓ⁻¹ at the 60 cm depth. Using the kinetic model with an assumed calcite surface area of 1* 10⁻⁷m²m⁻³ of soil, Ca concentrations are almost doubled near the surface and similar to the equilibrium case at the bottom of the profile. The Ca values are roughly similar to the equilibrium case at the bottom of the profile because of gypsum precipitation at the lower depths. The simulated output for the kinetic model is dependent on the surface area and DOC content of the soil water.

The alkalinity values shown in Figure 11.9 indicate large differences between the two simulations, with the kinetic model again predicting much larger concentrations, especially in the shallow depths but still twice as large at the bottom of the profile. These alkalinity differences are related to the calcite supersaturation throughout the soil profile, as shown in Figure 11.10, which shows the *p*IAP values for CaCO₃ as a function of depth and time. The final steady state *p*IAP values range around 7.0 in the near surface environment to 8.1 at the 100 cm depth, similar to those reported by *Suarez [1985]*. In contrast, the equilibrium model results in calcite equilibrium (*p*IAP=8.47) at all times and locations in the profile.

Due to the initial equilibrium assumption, the kinetic simulation took longer to reach steady state, as evident by the *p*IAP-time relations in Figure 11.10, as well as the comparison of alkalinity-time relations in Figure 11.9. In addition to differences in solution composition, the models also give differences in the carbonate distribution with depth as shown in Figure 11.1 la and b. The equilibrium model predicts a large quantity of calcite precipitation in the first node followed by a very large quantity of calcite dissolution in the shallow depths, followed by slight precipitation at depth. This unrealistic result demonstrates the limitations of a equilibrium model for simulation of calcite precipitation. The result can be partially avoided by the equally unrealistic forcing of the input solution to calcite saturation before initiating the program. In contrast to the equilibrium model, the kinetic model simulates a condition of decreasing precipitation with depth.

Gypsum precipitation using the calcite kinetic model is simulated as occurring in the 60-100 cm zone with a maximum at 67 cm. In contrast. with the equilibrium model, the location

of gypsum accumulation is shifted downward, due to the smaller Ca and alkalinity concentrations for the equilibrium as compared to the kinetic model. Figure 11.12 shows gypsum profiles for the calcite equilibrium model with and without iteration between the solute transport and chemical modules (see Section 9.2). Figure 11.12 indicates relatively small differences with and without the iteration process. The simulation with iteration has a better defined maxima in the precipitation front.

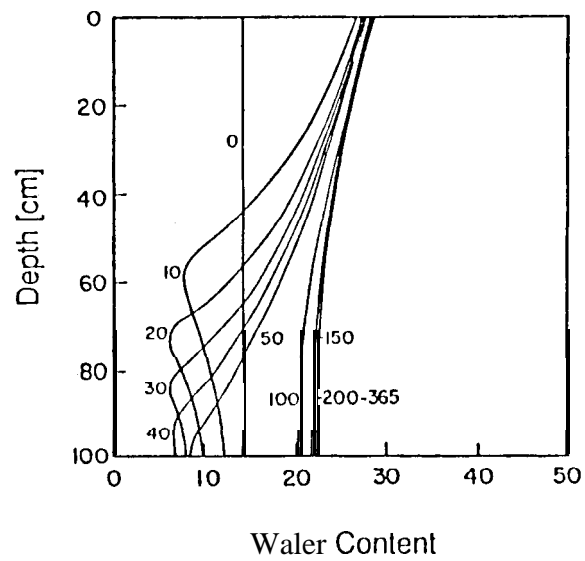


Fig. 11.6. 'Water content profiles at various times for example 2.

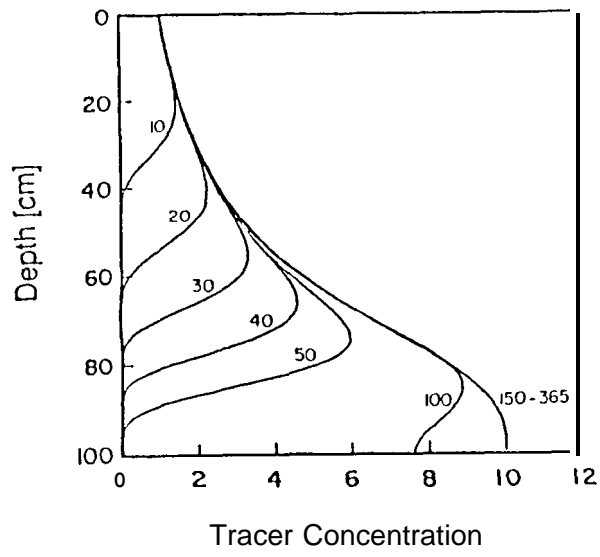


Fig. 1 1.7. Tracer concentration profiles at various times for example 2.

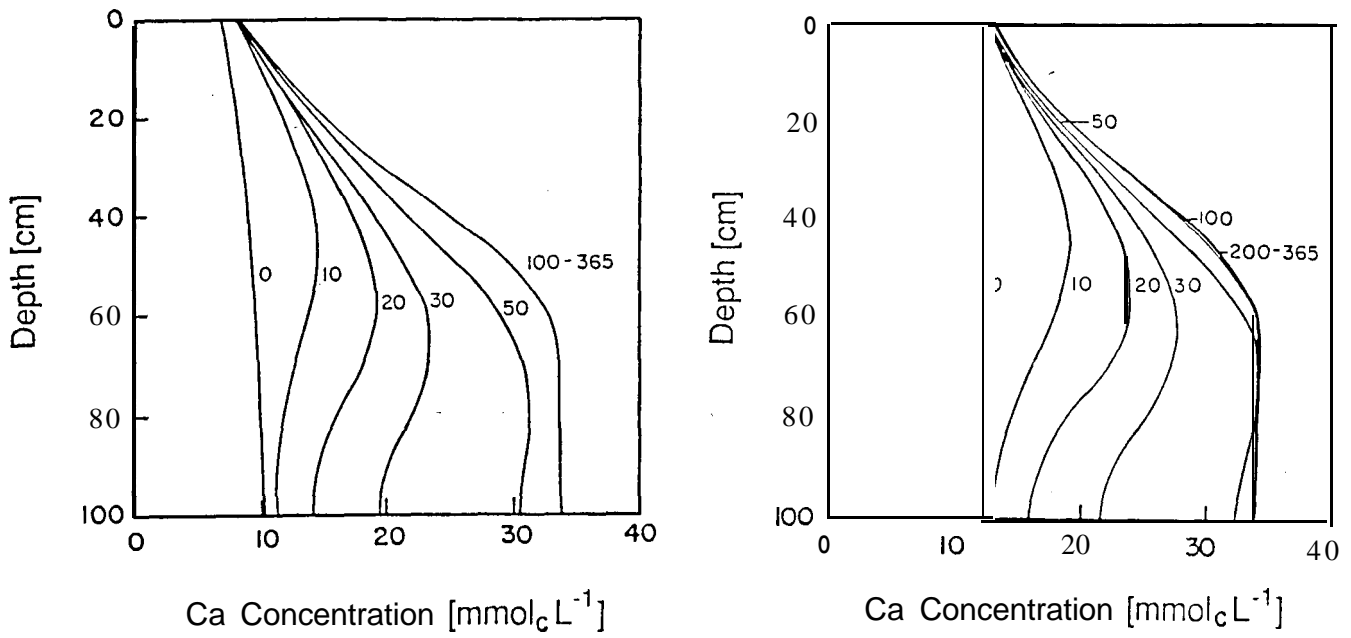


Fig.11.8. Calcium concentration profiles at various times for a) equilibrium and b) kinetic calcite precipitation-dissolution for example 2.

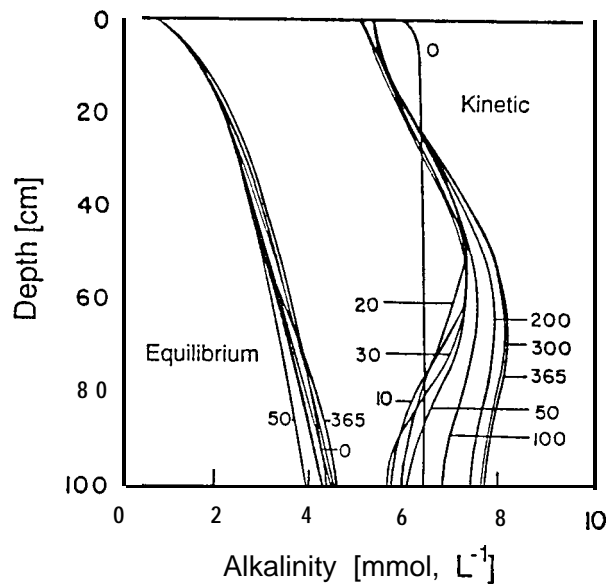


Fig. 11.9. Alkalinity profiles at various times for equilibrium and kinetic calcite precipitation-dissolution for example 2.

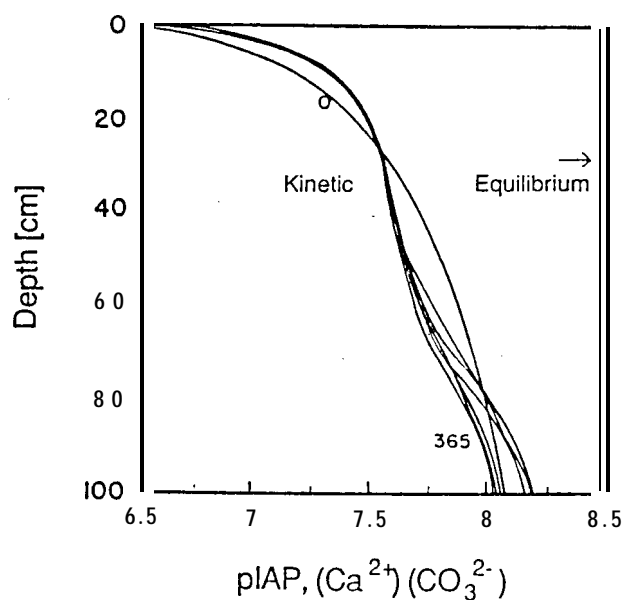


Fig. 11.10. CaCO_3 pIAP profiles at various times for equilibrium and kinetic calcite precipitation-dissolution for example 2.

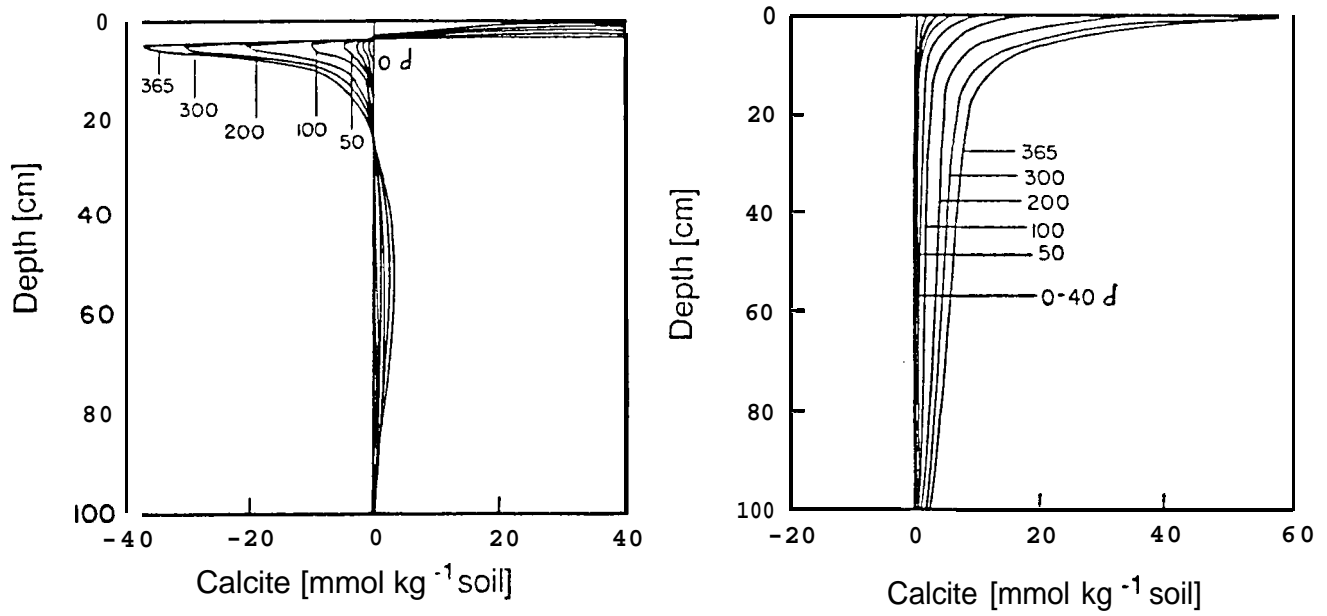


Fig. 1 1.1 1. Calcite concentration profiles at various times for a) equilibrium and b) kinetic calcite precipitation-dissolution for example 2.

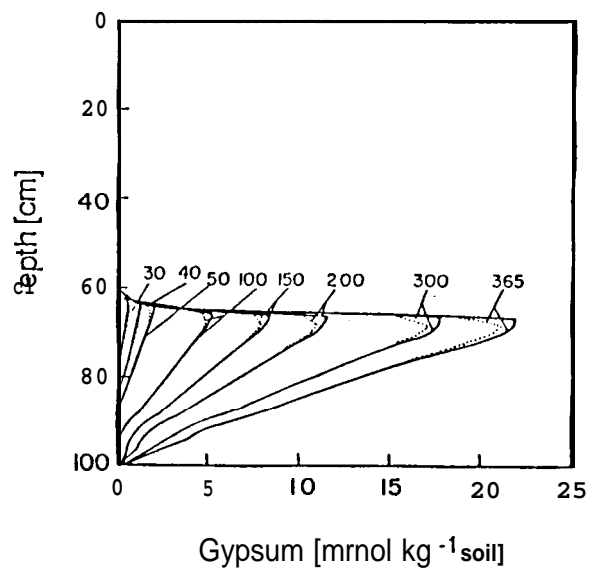


Fig. 11.12. Gypsum concentration profiles at various times without (dashed line) and with (full line) iteration between the solute transport and chemical modules for example 2.

11.3. Example 3 - 10 Day Irrigation Cycle

The third example considers both the interaction of transient water flow and water content, as well as the dynamic CO₂ submodel [Šimůnek and Suarez, 1993], with the equilibrium and kinetic carbonate subroutines [Suarez and Šimůnek, 1997]. In these simulations we considered intermittent irrigation of 10 cm, every 10 days, of Colorado River water (where Ca=2.63, Mg=1.03, Na=2.55, Cl=1.94, alkalinity=2.33 and SO₄=2.0, mmol_cℓ⁻¹). Although the model can calculate CO₂ production as a function of environmental stress, for the purposes of comparing the different simulations we fixed the carbon dioxide production at 0.007 m³m⁻³ which is a realistic field value [Suarez and Šimůnek, 1993].

After 100 days a steady state cycle was reached in that the water content and solution composition cycled between irrigations. Shown in Figure 11.13 is the water content distribution with depth for a 10 day interval between irrigations after 250 days of simulation. After irrigation the water content increases in the shallow soil zone with subsequent redistribution and water uptake by plants. Ten days after an irrigation the water content is back to the initial conditions immediately before the next irrigation. Using the dynamic CO₂ production transport model we simulate changing CO₂ concentrations with depth and time. As shown in Figure 11.14, the CO₂ concentrations are greatest two days after an irrigation when the water content near the surface is still high. High water content restricts gas diffusion, and after sufficient time restricted diffusion results in elevated CO₂ concentrations. Upon drainage, the soil CO₂ distribution quickly reverts back to the pattern shown on days 4-10, with increasing CO₂ concentration with depth to the bottom of the rootzone. These dynamic distributions with space and time in turn produce effects on the soil solution- composition.

The simulations in Figure 11.15 show that the Ca concentration is relatively constant during the 10 day cycle using the equilibrium model at fixed CO₂. Increasing concentration with depth due to root water uptake is moderated by calcite precipitation. In contrast the Ca concentrations changed with time by more than a factor of two in the upper portion of the profile when the kinetic model was utilized. The kinetic model also predicts higher concentrations throughout the profile. At shallow depths this is due to both calcite supersaturation and fluctuations in CO₂; in the lower portions of the profile it is primarily due to calcite

supersaturation during precipitation. The corresponding alkalinity concentrations for the same two simulations are shown in Figure 11.16. Similar to the Ca profiles, the alkalinity concentrations and changes with time, are greater using the kinetic model than the equilibrium model.

The differences in Ca and alkalinity concentrations between the equilibrium and kinetic models are consistent with the $pIAP$ changes presented in Figure 11.17, for the same 10 day cycle. Changes in pH with depth and time are also quite variable, as shown in Figure 11.18 for the kinetic model. This range in pH has important implications for plant nutrition as well as chemical transport.

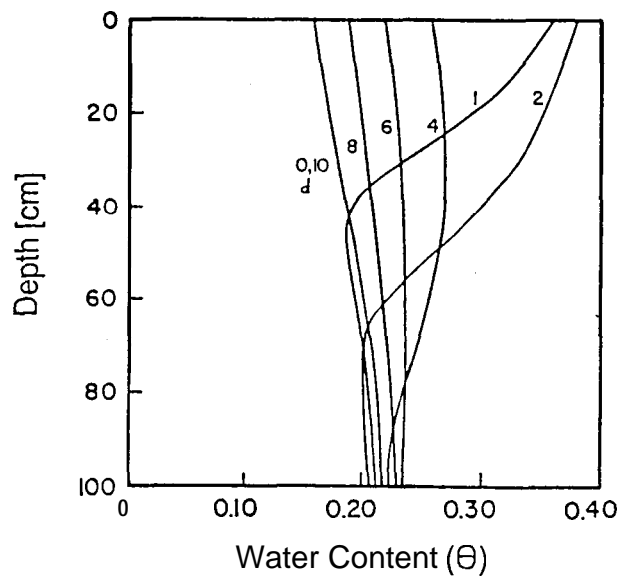


Fig. 11.13. Water content profiles at various times for example 3.

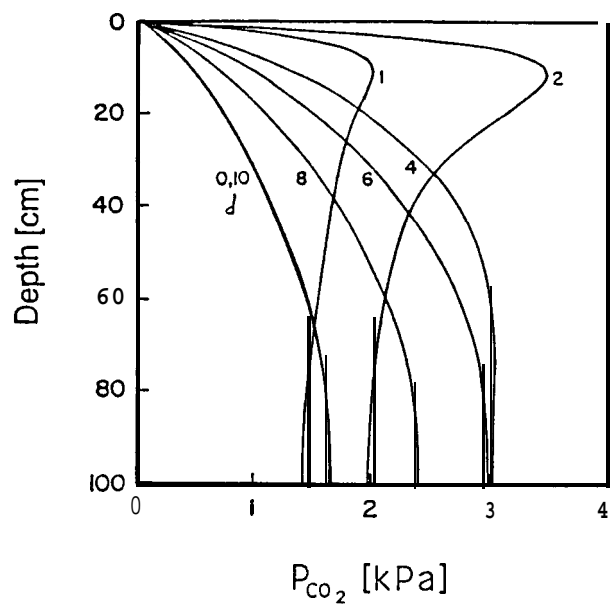


Fig. 11.14. P_{CO_2} profiles at various times for example 3.

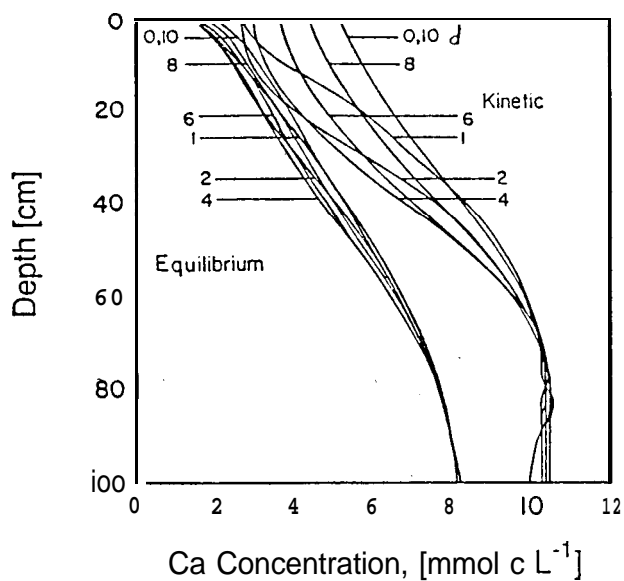


Fig. 11.15. Calcium concentration profiles at various times for equilibrium calcite precipitation with constant CO₂, and kinetic calcite precipitation with variable CO₂ concentrations for example 3.

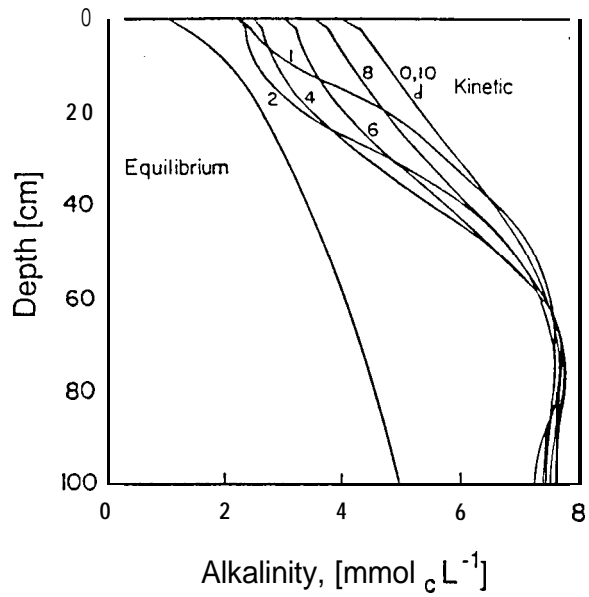


Fig. 1 1.16. Alkalinity profiles at various times for equilibrium calcite precipitation with constant CO_2 and kinetic calcite precipitation with variable CO_2 concentrations for example 3.

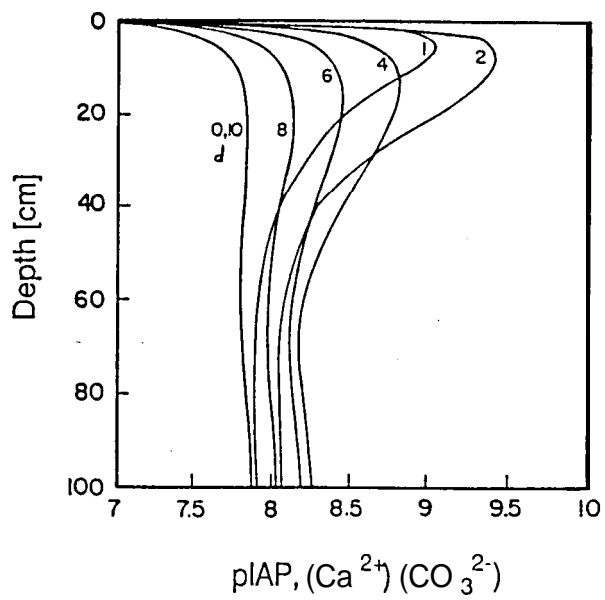


Fig. 1 1.17. CaCO_3 pIAP profiles at various times for a) constant and b) variable CO_2 concentrations for example 3.

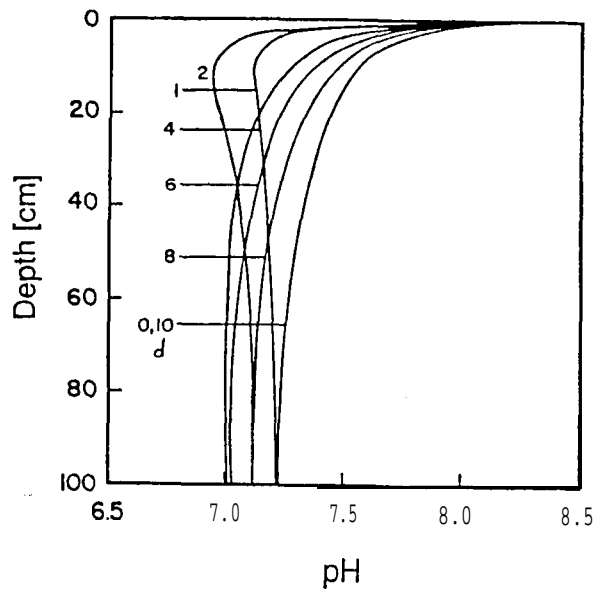


Fig. 11.18. *pH* profiles at various times for a) equilibrium calcite precipitation with constant CO_2 , and b) kinetic calcite precipitation with variable CO_2 concentrations for example 3.

11.4. Example 4 - Missouri CO₂ Experiment

The predictive capabilities of UNSCHEM were further evaluated by comparing simulations to the field data published by *Buyanovsky and Wagner [1983]* and *Buyanovsky et al. [1986]* for wheat, soybeans and corn grown in Missouri. Experimental details, data and model interpretation of this experiment are presented in *Suarez and Šimůnek [1993]*. Since it was our objective to compare the CO₂ concentrations in the soil as well as the simulated and measured CO₂ evolution from the soil, we first generated a prediction for the year 1982 for the soil cultivated to wheat. We initiated the simulation at the beginning of March (the first month with positive air temperatures) and terminated it at the end of October. *Buyanovsky and Wagner [1983]* presented data for daily precipitation and average weekly air temperatures, as well as CO₂ concentrations in the soil air, soil water content and soil temperature at the 20 cm depth. From the air temperatures we calculated values of potential evapotranspiration using Thornthwaite's formula [*de Marsily, 1986*]. *Buyanovsky and Wagner [1983]* reported the textural characteristics of their Mexico silt loam as well as organic matter content, bulk density, and air porosity at field capacity. After inspection of these data we divided the soil profile into three horizons: A, B 1 and B2. Since we did not have the hydraulic characteristics of this soil we used the mean textural characteristics and the linear regression equations reported by *Rawls et al. [1982]* to obtain the soil water contents at 10 different soil water pressure heads. These data were then used to determine regression parameters of the retention equation by nonlinear least-square curve fitting [*van Genzrchten, 1978*]. The calculated retention curves were scaled in order to insure that they correspond to the porosity calculated from the data on bulk density and specific density and to the measured air porosity at field capacity [*Buyanovsky and Wagner, 1983*].

The depth of the root zone as a function of time was again calculated with the root growth model as developed by *Šimůnek and Suarez [1993]* with $T_{bas}=1275^{\circ}\text{C day}$ (base temperature of 4.4°C) calculated from *Pirasteh and Welsh [1980]*. The wheat was planted in the middle of October of 1981, therefore we assigned the root depth at the beginning of the simulation on 1 March to be 5 cm. The wheat was harvested around 10 July. We also assumed, that 65% of the roots are in the top 0.1 m, which leads to the coefficient $a=10.5\text{ m}^{-1}$ for the exponential root distribution. The root-depth distribution selected is consistent with the observations of

Buyanovsky et al. [1986], that about 50% of the roots were located in the upper 0.1 m layer during the early stage of crop development, whereas in the later stages up to 75-80% of the roots were in this layer.

A relatively wet soil profile with a constant pressure head of -1.0 m was used as the initial condition. The lower boundary condition was taken as free drainage at a depth of 1.6 m. Figure 11.19 shows the water content at a depth of 0.2 m as reported by *Buyanovsky and Wagner* [1983] and as predicted by the model. The correspondence of measured and calculated values is quite good in view of the relatively inaccurate methods used for estimation of the hydraulic characteristics and potential evapotranspiration (because of the lack of available data).

Since the Mexico silt loam has a high clay content (from 22 to 53 %), we used the parameters for the thermal conductivity from *Chung and Horton* [1987] for clay ($b_1=-0.197$, $b_2=-0.962$, and $b_3=2.521 \text{ Wm}^{-1}\text{K}^{-1}$). The measured air temperature was taken as the upper boundary condition with a daily amplitude of 5 °C. A zero temperature gradient was used as the lower boundary condition. The measured and calculated temperatures at the 0.2 m depth are shown in Figure 11.20. There is an excellent correspondence between measured and calculated values, which is important since temperature has a significant effect on CO₂ production. Unfortunately experimental data was not available for deeper depths, which would be required for a more rigorous test of the heat transport submodel.

The initial volumetric CO₂ concentration was constant at 1%. The lower boundary condition for CO₂ transport was zero flux. The upper boundary condition at the soil surface was constant CO₂ concentration at the atmospheric value of 0.035%. The CO₂ production and reduction coefficients were selected based on the discussion in Section 5.5. Figure 11.21 shows an excellent agreement between measured and calculated CO₂ concentrations at the 0.2 m depth. There are no statistically significant differences between the measured and predicted CO₂ concentrations at the 90% confidence level. The irregular pattern of the CO₂ concentrations shown in Figure 11.21 reflects the fact that within the dry periods (first half of May, second half of July and all of October), the CO₂ concentrations decrease to very low values, while during the wet periods the CO₂ concentrations are relatively high.

Figure 11.22 shows the comparison of the calculated daily and weekly CO₂ **fluxes to** the atmosphere with the flux measurements of *Buyanovsky et al.* [1986]. The large fluctuations

shown in Figure 11.22 indicate that the accurate determination of flux requires an excessive number of measurements if the surface water content is rapidly changing, as occurs with frequent water applications. As with the CO₂ concentration data, there is an excellent correspondence between measured and calculated flux values.

Further evaluation of the model is possible using CO₂ concentration measurements made by *Buyanovsky and Wagner* [1983] for corn and soybeans grown in 1982, and for wheat grown in 1981 [*Buyanovsky and Wagner, 1983; Buyanovsky et al., 1986*]. The results of these numerical and experimental data were reported in *Suarez and Šimůnek* [1993] and *Šimůnek and Suarez* [1993c] and will not be repeated here.

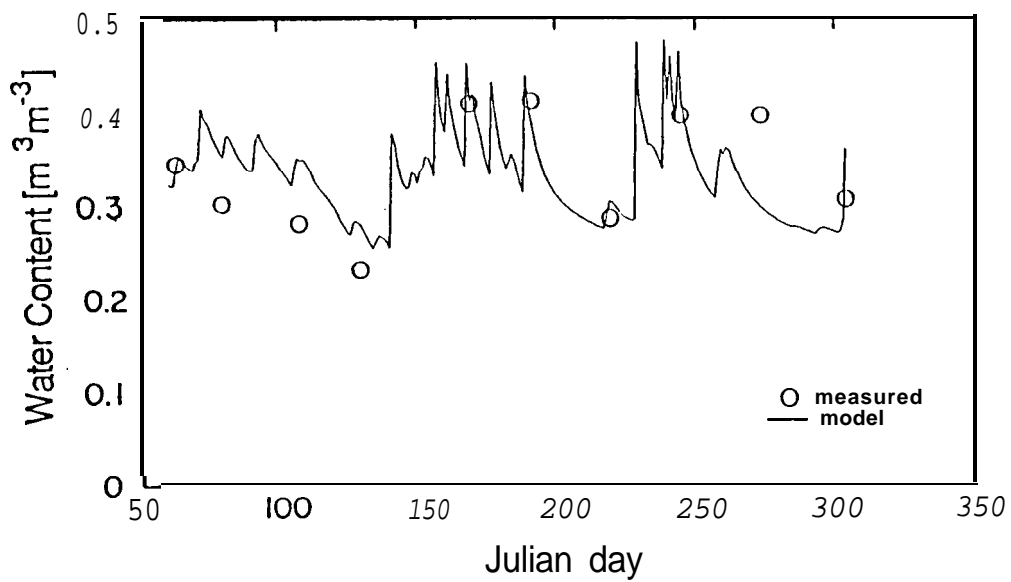


Fig. 11.19. Measured [Buyanovsky and Wagner, 1983] and calculated water contents at a depth of 0.20 m for the Missouri wheat experiment, 1982 (example 4).

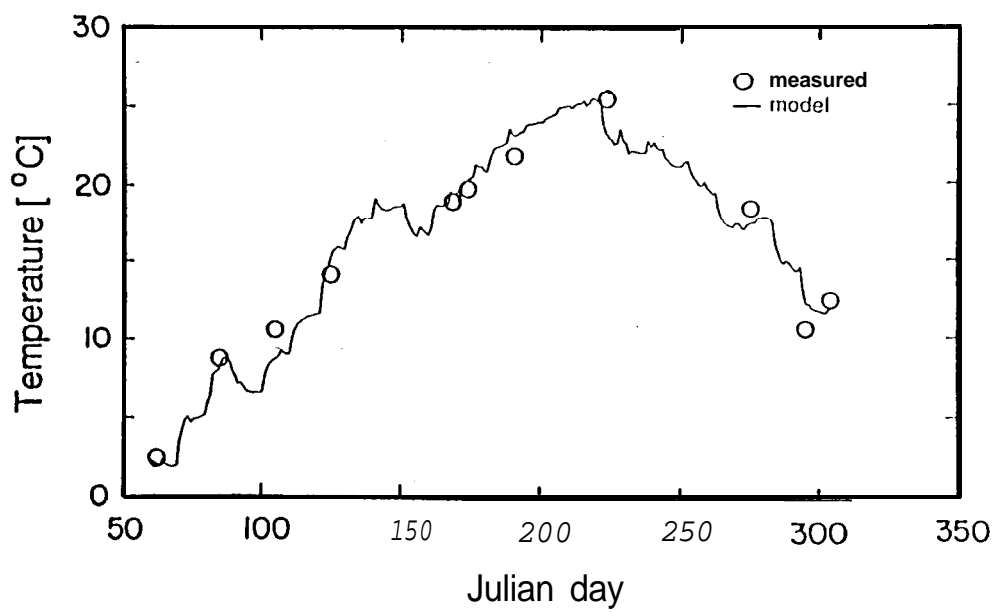


Fig. 11.20. Measured [Buyanovsky and Wagner, 1983] and calculated temperatures at a depth of 0.20 m for the Missouri wheat experiment, 1982 (example 4).

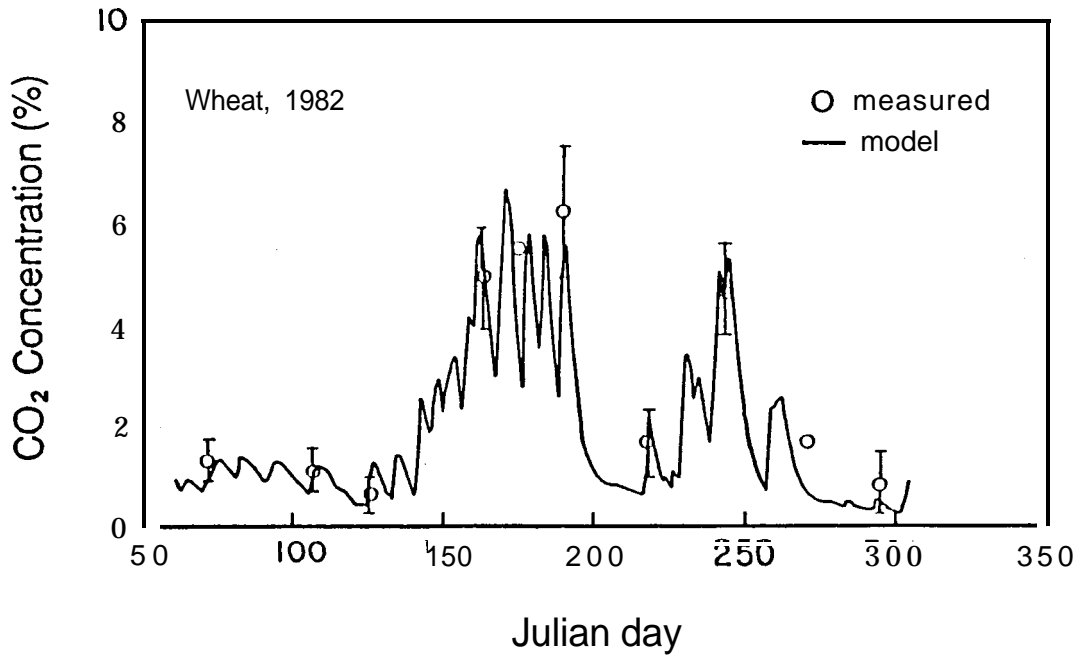


Fig. 1 1.2 1. Measured [Buyanovsky and Wagner, 1983] and calculated CO₂ concentrations at a depth of 0.20 m for the Missouri wheat experiment, 1982 (example 4).

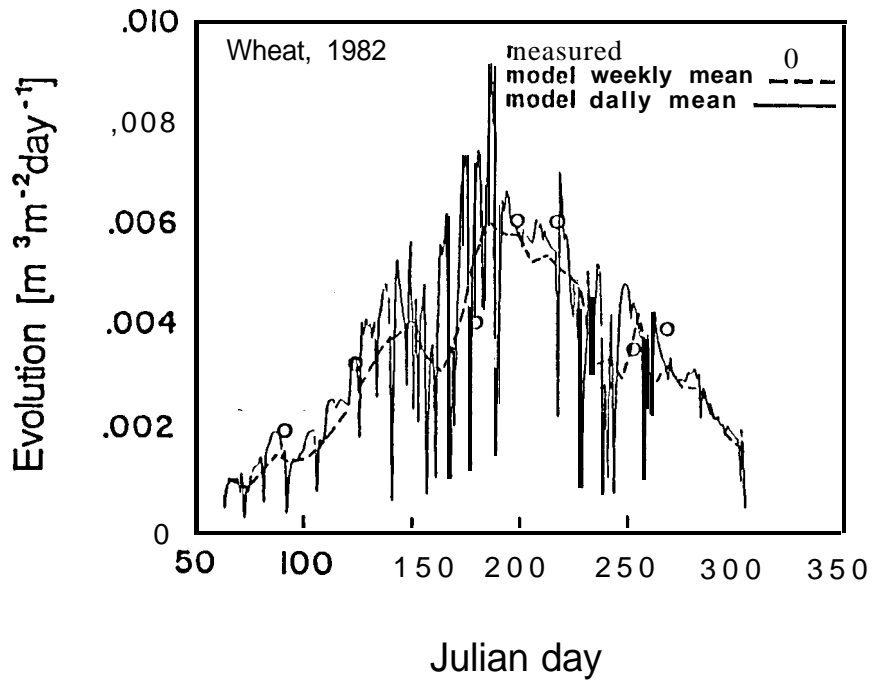


Fig. 1 1.2.2. Measured [Buyanovsky and Wagner, 1986] and calculated daily and weekly CO₂ fluxes to the atmosphere for the Missouri wheat experiment, 1982 (example 4).

12. INPUT DATA

The input data for UNSCHEM are given in seven separate input files. The first four input files give input data for Pitzer' equations and are provided together with the program and should not be changed by the user. These input files which were adopted from *Felmy*[1990] must be placed in the same directory as the executable program.

COMP.DAT	contains the species ID numbers, species names, and species charge (see Table 12.11).
BINARYP.DAT	contains the ID number of each species in each binary interaction considered (e.g., CaHCO_3^+) and the Pitzer ion interaction parameters $\beta^{(0)}$, $\beta^{(1)}$, $\beta^{(2)}$, and C^ϕ for binary systems (see Table 12.12).
TERNARYP.DAT	contains the Pitzer ion-interaction parameters for the common ion ternary systems, θ , and ψ . The first two columns include the cation-cation or anion-anion ID numbers associated with the ion-interaction parameter, θ , in column three. Subsequent columns include the anion or cation ID number and the triple ion-interaction parameter, ψ , associated with that triple ion interaction (see Table 12.13).
LAMBDA.DAT	contains the Pitzer ion-interaction parameters for the neutral species, λ and δ . The first column of this file contains the ID number for the neutral species, and the second column contains the ID number for the cation or anion involved in the neutral-cation or neutral-anion interaction parameterized by the Pitzer λ parameter included in the third column. Subsequent columns are for higher-order neutral interactions (see Table 12.14).

The last three input files consist of one or more input blocks identified by the letters from A through J. The input files and blocks must be arranged as follows:

SELECTOR.IN

- A. Basic information
- B. Water flow information
- C. Time information
- D. Root growth information
- E. Root water uptake information
- F. Heat transport information
- G. Carbon dioxide transport and production information
- H. Solute transport and chemical information

PROFILE.DAT

I. Nodal information

ATMOSP.HIN

J. Atmospheric information

All input files must be placed into one subdirectory. Output files are printed into the same subdirectory. An additional file **Level_Ol.dir** which specifies the path to the input and output file subdirectory must be given in the same directory as the executable **UNSCHEM** code. Another file, **UNSATCH.DAT**, which is not read by the executable code, enables communication between particular modules of the user-interface and will be described in part B of this manual. The input files can be created manually or with the graphics-based user-friendly interface **UNSATCH** also described in part B.

Tables 12.1 through 12.10 describe the data required for each input block. All data are read in using list-directed formatting (free format). Comment lines are provided at the beginning of, and within, each input block to facilitate, among other things, proper identification of the function of the block and the input variables. The comment lines are ignored during program execution; hence, they may be left blank but should not be omitted. The program assumes that all input data are specified in a consistent set of units for mass M, length L, and time T. The exceptions from this rule are the chemical data in Table 12.S (Block H). The units required in this table are mandatory. The input values of temperature are required in degrees Celsius.

Most of the information in Tables 12.1 through 12.10 should be self-explanatory. Table 12.9 (Block I) is used to define, among other things, the nodal coordinates and initial conditions for the pressure head, temperature and CO₂ concentration. When two nodes (e.g., n_1 and n_2), not adjacent to each other, are located such that n_2 is greater than n_1+1 , the program will automatically generate nodes between n_1 and n_2 , provided all of the following conditions are met simultaneously: (1) the values of the input variables $hOld(n)$, $Beta(n)$, $Temp(n)$, and $CO2(n)$ vary linearly between nodes n_1 and n_2 , and (2) the values of $LayNum(n)$, $MatNum(n)$, $nC(n)$, $nS(n)$, and $nX(n)$ are the same for all $n = n_1, n_1+1, \dots, n_2-1$ (see Block I).

Table 12.1. Block A - Basic information.

Record	Type	Symbol	Description
1,2			Comment lines.
3	Char	<i>Hed</i>	Heading.
4			Comment line.
5	Char	<i>LUnit</i>	Length unit (e.g. 'cm').
6	Char	<i>TUnit</i>	Time unit (e.g. 'min').
7	Char	<i>MUnit</i>	Mass unit for the concentration variables (e.g. 'g', 'mol', '-').
8			Comment line.
9	Logical	<i>lWat</i>	Set this logical variable equal to .true. if transient water flow is to be considered. Set equal to .false. if initial condition given in Block I (Table 12.9) is to be kept constant throughout the simulation.
9	Logical	<i>lChem</i>	Set this logical variable equal to .true. if chemical solute transport is to be considered.
9	Logical	<i>lTemp</i>	Set this logical variable equal to .true. if heat transport is to be considered.
9	Logical	<i>lCO2</i>	Set this logical variable equal to .true. if carbon dioxide transport is to be considered.
9	Logical	<i>lSink</i>	Set this variable equal to .true. if the water extraction from the root zone occurs.
9	Logical	<i>lRoot</i>	Set this variable equal to .true. if the root growth is to be considered.
9	Logical	<i>ShortF</i>	.true. if printing of output at each time level (time-level information) is to be suppressed and the information printed only in specified print times, .false. if this information is to be printed on each time level.
9	Logical	<i>lScreen</i>	.true. if information is to be printed on the screen during code execution.
9	Logical	<i>AtmInf</i>	.true. if variable boundary conditions are supplied via the input file ATMOSP.H.IN, .false. if the file ATMOSP.H.IN is not provided (i.e., in case of time independent boundary conditions).
10			Comment line.
11	Integer	<i>NMat</i>	Number of soil materials. Materials are identified by the material number, <i>MatNum</i> , specified in Block I.
11	Integer	<i>NLay</i>	Number of subregions for which separate water balances are being computed. Subregions are identified by the subregion number, <i>LayNum</i> , specified in Block I.
11	Keal	<i>CosAlfa</i>	Cosine of the angle between the flow direction and the vertical axis (i.e., $\cos \alpha = 1$ for vertical flow, $\cos \alpha = 0$ for horizontal flow, and $0 < \cos \alpha < 1$ for inclined flow).

Table 12.2. Block B - Water flow information.

Record	Type	Symbol	Description
1,2			Comment lines.
3	Integer	<i>MaxIt</i>	Maximum number of iterations allowed during any time step (usually 20).
3	Real	<i>TolTh</i>	Absolute water content tolerance for nodes in the unsaturated part of the flow region [-] (its recommended value is 0.0001). <i>TolTh</i> represents the maximum desired absolute change in the value of the water content, θ_w , between two successive iterations during a particular time step.
3	Real	<i>TolH</i>	Absolute pressure head tolerance for nodes in the saturated part of the flow region [L] (its recommended value is 0.1 cm). <i>TolH</i> represents the maximum desired absolute change in the value of the pressure head, h , between two successive iterations during a particular time step.
4			Comment line.
5	Logical	<i>TopInf</i>	.true. if time dependent boundary condition is to be imposed at the top of the profile; data are supplied via input file ATMOSPH.IN. .false. in the case of time independent surface boundary conditions.
5	Logical	<i>WLayer</i>	Set this variable equal to .true. if water can accumulate at the surface with zero surface runoff.
5	Integer	<i>KodTop</i>	Code specifying type of boundary condition (BC) for water flow at the surface. Code number is positive for Dirichlet BC and negative for Neumann BC. In the case of 'Atmospheric BC' set <i>KodTop</i> =-1.
6			Comment line.
7	Logical	<i>BotInf</i>	.true. if time dependent boundary condition is to be imposed at the bottom of the profile; control data are supplied via input file ATMOSPH.IN. .false. in the case of time independent bottom boundary conditions.
7	Logical	<i>qGWLf</i>	Set this variable equal to .true. if the discharge-groundwater level relationship $q_w(GWL)$ is applied as bottom boundary condition.
7	Logical	<i>FreeD</i>	.true. if free drainage is to be considered as bottom boundary condition.
7	Logical	<i>SeepF</i>	.true. if seepage face is to be considered as bottom boundary condition.
7	Integer	<i>KodBot</i>	Code specifying type of boundary condition for water flow at the bottom of the profile. Code number is positive for a Dirichlet BC and negative for a Neumann BC. In case of a seepage face or free drainage BC set <i>KodBot</i> =-1.
8a			Comment line.
9a	Real	<i>rTop</i>	Prescribed top flux [LT^{-1}] (in case of a Dirichlet BC set this variable equal to zero).
9a	Real	<i>rBot</i>	Prescribed bottom flux [LT^{-1}] (in case of a Dirichlet BC set this variable equal to zero).
9a	Real	<i>rRoot</i>	Prescribed potential transpiration rate [LT^{-1}] (if no transpiration occurs or if transpiration is variable in time set this variable equal to zero).

Table 12.2. (continued)

Record	Type	Variable	Description
			Records 8a and 9a are provided only when both boundary conditions are independent of time and at least one of them is a Neumann BC.
8b			Comment line.
9b	Real	G WLOL	Reference position of the groundwater table (e.g., the z-coordinate of the soil surface).
9b	Real	Aqh	Value of the parameter A , [LT ⁻¹] in the $q_w(GWL)$ -relationship, equation (10.1); set to zero if $qGWL = \text{.false.}$
9b	Real	Bqh	Value of the parameter B_{qh} [L ⁻¹] in the $q_w(GWL)$ -relationship, equation (10.1); set to zero if $qGWL = \text{.false.}$
			Records 8b and 9b are provided only when the logical variable $qGWL = \text{.true.}$.
10			Comment line.
11	Real	ha	Absolute value of the upper limit [L] of the pressure head interval below which a table of hydraulic properties will be generated internally for each material (h_a must be greater than 0.0; e.g. 0.001 cm) (see Section 7.4.7).
11	Real	hb	Absolute value of the lower limit [L] of the pressure head interval for which a table of hydraulic properties will be generated internally for each material (e.g. 1000 m). One may assign to h_b the highest (absolute) expected pressure head to be expected during a simulation. If the absolute value of the pressure head during program execution lies outside of the interval [h_a, h_b], then appropriate values for the hydraulic properties are computed directly from the hydraulic functions (i.e., without interpolation in the table).
11	Integer	NPar	Number of parameters specified for each material (i.e., 9 in case of the modified van Genuchten's model).
12			Comment line.
13	Real	Par(1,M)	Parameter θ_r for material M [-].
13	Real	Par(2,M)	Parameter θ_s for material M [-].
13	Real	Par(3,M)	Parameter θ_a for material M [-].
13	Real	Par(4,M)	Parameter θ_m for material A4 [-].
13	Real	Par(5,M)	Parameter α for material M [L ⁻¹].
13	Real	Par(6,M)	Parameter n for material A4 [-].
13	Real	Par(7,M)	Parameter K , for material A4 [LT. ⁻¹].
13	Real	Par(8,M)	Parameter K_k for material M [LT. ⁻¹].
13	Real	Par(9,M)	Parameter θ_k for material A4 [-].
			Record 13 information' is provided for each material M (from 1 to $NMat$).

Table 12.3. Block C - Time information.

Record	Type	Symbol	Description
1,2			Comment lines.
3	Real	<i>dt</i>	Initial time increment Δt [T]. Initial time step should be estimated based on the problem being solved. For problems with high pressure gradients (e.g. infiltration into an initially dry soil), Δt should be relatively small.
3	Real	<i>dtMin</i>	Minimum permitted time increment, Δt_{min} [T].
3	Real	<i>dtMax</i>	Maximum permitted time increment, Δt_{max} [T].
3	Real	<i>dMul</i>	If the number of required iterations at a particular time step is less than or equal to 3, then Δt for the next time step is multiplied by a dimensionless number $dMul \geq 1.0$ (it is recommended that this value not exceed 1.3).
3	Real	<i>dMul2</i>	If the number of required iterations at a particular time step is greater than or equal to 7, then Δt for the next time step is multiplied by $dMul2 \leq 1.0$ (e.g. 0.33).
3	Integer	<i>ItMin</i>	If the number of required iterations at a particular time step is less than or equal to <i>ItMin</i> , then Δt for the next time step is multiplied by a dimensionless number $dMul \geq 1.0$.
3	Integer	<i>ItMax</i>	If the number of required iterations at a particular time step is greater than or equal to <i>ItMax</i> , then Δt for the next time step is multiplied by $dMul2 \leq 1.0$.
3	Integer	<i>MPL</i>	Number of specified print-times at which detailed information about the pressure head, water content, flux, temperature, CO, and solute concentrations, and the water, CO, and solute balances will be printed.
4			Comment line.
5	Real	<i>tInit</i>	Initial time of the simulation [T].
5	Real	<i>tMax</i>	Final time of the simulation [T].
6			Comment line.
7	Real	<i>TPrint(1)</i>	First specified print-time [T].
7	Real	<i>TPrint(2)</i>	Second specified print-time [T].
7	Real	<i>TPrint(MPL)</i>	Last specified print-time [T]. (Maximum six values on one line.)

Table 12.4. Block D - Root growth information.+

Record	Type	Symbol	Description
1,2			Comment lines.
3	Integer	<i>kRoot</i>	Type of the root growth model. =0: Verhulst-Pearl logistic growth function. =1: Degree day concept combined with logistic growth function.
3	Integer	<i>kBeta</i>	Spatial distribution of the root water uptake. =0: van Genuchten's function. = 1: exponential distribution.
4			Comment line (only if <i>kRoot=1</i>).
5	Real	<i>T1</i>	Temperature, T_1 (°C), below which plants register no effective growth.
5	Real	<i>T2</i>	Temperature, T_2 (°C), above which plants register maximum growth which remains unchanged up to a maximum temperature T_3 (°C).
5	Real	<i>T3</i>	Temperature, T_3 (°C), above which increased temperature has a negative effect on growth. Record 5 needs to be supplied only if <i>kRoot=1</i> .
6			Comment line.
7	Integer	<i>iRFak</i>	Method to calculate the root growth factor <i>r</i> . Set equal to zero if <i>kRoot=1</i> . =0; the root growth factor <i>r</i> is calculated based on the assumption that 50% of the rooting depth, $(xRMax+xRMin)/2$, is reached after 50% of the growing season, $(tRHarv+tRMin)/2$. =1; the root growth factor <i>r</i> is calculated from given data [<i>tRMed</i> , <i>xRMed</i>].
7	Real	<i>tRMin</i>	Initial time of the root growth period [T].
7	Real	<i>tRMed</i>	Time of known rooting depth (set equal to zero if <i>iRFak=0</i>) [T].
7	Real	<i>tRHarv</i>	Time at the end of root water uptake period [T].
7	Real	<i>xRMin</i>	Initial value of the rooting depth at the beginning of the growth period (recommended value = 1 cm) [L].
7	Real	<i>xRMed</i>	Value of known rooting depth (set equal to zero if <i>iRFak=0</i>)[L].
7	Real	<i>xRMax</i>	Maximum rooting depth which may be reached at infinite time [L].
7	Real	<i>RDDMax</i>	The value of the cumulative temperature (degree days) when the root depth reaches the maximum value (set equal to zero if <i>kRoot=0</i>) [K].
8			Comment line (only if <i>kBeta=1</i>).
9	Real	<i>alpha</i>	Coefficient of the exponential depth distribution function [L^{-1}] (only if <i>kBeta=1</i>).

† Block D is not read if logical variable *lRoot* (Block A) is set equal to *.false.*.

Table 12.5. Block E - Root water uptake information.+

Record	Type	Symbol	Description
1,2	-		Comment lines.
3	Real	PO	The coefficient b in the root water uptake reduction function due to water stress [-]. The recommended value is 3. (see van <i>Genuchten</i> [1987]).
3	Real	P_{50}	The value h_{50} in the root water uptake reduction function due to water stress [L]. There is a 50% reduction of the root water uptake for this pressure head.
3	Real	P_{phi0}	The coefficient b in the root water uptake reduction function due to salinity stress [-]. The recommended value is 3. (see <i>van Genuchten</i> [1987]).
3	Real	P_{phi50}	The value $h_{\phi50}$ in the root water uptake reduction function due to salinity stress [L]. There is a 50% reduction in the root water uptake for this osmotic head.

† Block E is not read if logical variable *SinkF* (Block A) is set equal to **.false.**.

Table 12.6. Block F - Meat transport information.†

Record	Type	Symbol	Description
1,2	-		Comment lines.
3	Real	$TPar(1,M)$	Volumetric solid phase fraction of material $M, \theta_s [-]$.
3	Real	$TPar(2,M)$	Volumetric organic matter fraction of material $M, \theta_o [-]$.
3	Real	$TPar(3,M)$	Longitudinal thermal dispersivity of material $M, \lambda_L [L]$.
3	Real	$TPar(4,M)$	Coefficient b_1 in the thermal conductivity function $[MLT^{-3}K^{-1}]$ (e.g. $Wm^{-1}K^{-1}$) (see equation (4.6)).
3	Real	$TPar(5,M)$	Coefficient b_2 in the thermal conductivity function $[MLT^{-3}K^{-1}]$ (e.g. $Wm^{-1}K^{-1}$) (see equation (4.6)).
3	Real	$TPar(6,M)$	Coefficient b_3 in the thermal conductivity function $[MLT^{-3}K^{-1}]$ (e.g. $Wm^{-1}K^{-1}$) (see equation (4.6)).
3	Real	$TPar(7,M)$	Volumetric heat capacity of solid phase of material $M, C_s, [ML^{-1}T^{-2}K^{-1}]$ (e.g. $Jm^{-3}K^{-1}$).
3	Real	$TPar(8,M)$	Volumetric heat capacity of organic matter of material $M, C_o, [ML^{-1}T^{-2}K^{-1}]$ (e.g. $Jm^{-3}K^{-1}$).
3	Real	$TPar(9,M)$	Volumetric heat capacity of liquid phase of material $M, C_w, [ML^{-1}T^{-2}K^{-1}]$ (e.g. $Jm^{-3}K^{-1}$).
			Record 3 is required for each soil material A4 (from 1 to $NMat$).
4			Comment line.
5	Real	A_{mpl}	Temperature amplitude at the soil surface [K].
5	Real	t_{Period}	Time interval for completion of one temperature cycle (usually 1 day) [T].
6			Comment line.
7	Integer	$kTopT$	Code which specifies the type of upper boundary condition =1: Dirichlet boundary condition, =-1: Cauchy boundary condition.
7	Real	$tTop$	Temperature of the upper boundary, or temperature of the incoming fluid [$^{\circ}C$].
7	Integer	$kBotT$	Code which specifies the type of lower boundary condition =1: Dirichlet boundary condition, =0: continuous temperature profile, zero gradient, =-1: Cauchy boundary condition.
7	Real	$tBot$	Temperature of lower boundary, or temperature of the incoming fluid [$^{\circ}C$].

† Block F need not be supplied if logical variables $lTemp$ (Block A) is set equal to **false**.

Table 12.7. Block G - Carbon dioxide transport information.+

Record	Type	Symbol	Description
1..2			Comment lines.
3	Logical	<i>lStagn</i>	Set this variable equal to .true. if the gas phase is to be considered stagnant, e.i., there is no gas convection. Otherwise the simplified gas convection expression is considered (see Section 5.1).
4			Comment line.
5	Integer	<i>kTopCO</i>	Code specifying type of boundary condition (BC) for the CO ₂ transport at the soil surface. Code number is positive for Dirichlet BC and negative for stagnant boundary layer at the soil surface.
5	Real	<i>CO2Top</i>	Value of the time independent BC at the surface [L^3L^{-3}]. For <i>kTopCO</i> <0 <i>CO2Top</i> represents the thickness of the stagnant boundary layer [L].
5	Integer	<i>kBotCO</i>	Code specifying type of boundary condition at the bottom of the profile. Code number is positive for Dirichlet and negative for Cauchy BC. In the case of 'Free drainage' set <i>kBotCO</i> =0.
5	Real	<i>CO2Bot</i>	Value of the time independent BC at the bottom of the soil profile [L^3L^{-3}]. In case of 'Free drainage' set <i>CO2Bot</i> =0.
6			Comment line.
7	Real	<i>Par(11,M)</i>	Molecular diffusion coefficient of CO, in air at 20°C, D_a [L^2T^{-1}].
7	Real	<i>Par(12,M)</i>	Molecular diffusion coefficient of CO ₂ in water at 20°C, D_w [L^2T^{-1}].
7	Real	<i>Par(13,M)</i>	Longitudinal dispersivity of CO, of material <i>M</i> , D_L [L]. The same record as above must be provided for each material <i>M</i> (from 1 to <i>NMat</i>).
8			Comment line.
9	Real	<i>GamR0</i>	Optimal CO ₂ production by plant roots for the whole soil profile at 20°C under optimal water, solute, and CO ₂ concentration conditions, γ_{r0} [$L^3L^{-2}T^{-1}$].
9	Real	<i>GamS0</i>	Optimal CO ₂ production by soil microorganisms for the whole soil profile at 20°C under optimal water, solute, and CO ₂ concentration conditions, γ_{s0} [$L^3L^{-2}T^{-1}$].
9	Real	<i>PDDMax</i>	The cumulative value of temperature when the CO ₂ production reaches the maximum value. Set equal to zero if degree day concept is not used to calculate the time reduction coefficient for plant CO ₂ production. In that case the time reduction coefficient is equal to one during the whole season.
9	Integer	<i>kProd</i>	Code specifying the type of spatial distribution function for CO ₂ production by soil microorganisms. =0: Exponential function. =I: van Genuchten's distribution function.
10			Comment line.
11	Real	<i>rAlfa</i>	Coefficient of the exponential function (only if <i>kProd</i> =0) [L^{-1}].

Table 12.7. (continued)

Record	Type	Symbol	Description
11	Real	xR	Maximum depth of the CO ₂ soil production (only if $kProd=1$) [L].
12			Comment line.
13	Real	B2	Activation energy of the CO ₂ production by plant roots, E_2 [ML ² T ⁻² M ⁻¹], divided by universal gas constant, R [ML ² T ⁻² K ⁻¹ M ⁻¹]; $B_2=E_2/R$ [K].
13	Real	B1	Activation energy of the CO ₂ production by soil microorganisms, E_1 [ML ² T ⁻² M ⁻¹], divided by universal gas constant, R [ML ² T ⁻² K ⁻¹ M ⁻¹]; $B_1=E_1/R$ [K].
13	Real	cm2	Michaelis' constant of the CO ₂ production by plant roots [L ³ L ⁻³]. It is equal to the CO ₂ concentration at which the CO ₂ production is reduced by half from the optimal value γ_{r0} .
13	Real	<i>cM1</i>	Michaelis' constant of the CO ₂ production by soil microorganisms [L ³ L ⁻³]. It is equal to the CO ₂ concentration at which the CO ₂ production is reduced by half from the optimal value γ_{s0} .
13	Real	<i>hB1</i>	Value of the pressure head at which the CO ₂ production by soil microorganisms is at the optimal level [L].
13	Real	<i>hB2</i>	Value of the pressure head below which the CO ₂ production by soil microorganisms ceases [L].
13	Real	<i>P0c</i>	The coefficient b in the CO ₂ soil production reduction function due to salinity stress [-]. The recommended value is 3.
13	Real	<i>P50c</i>	The value $h_{\phi,50}$ in the CO ₂ soil production reduction function due to salinity stress [L]. There is a 50% reduction of the CO ₂ production by soil microorganisms for this osmotic head.

† Block G need not be supplied if the logical variable *lCO2*(Block A) is set equal to *.false*.

Table 12.8. Block H - Solute transport and chemical information.'

Record	Type	Variable	Description
1,2			Comment lines.
3	Real	<i>Epsi</i>	Temporal weighing' coefficient. =0.0 for an explicit scheme. =0.5 for a Crank-Nicholson implicit scheme. =1.0 for a fully implicit scheme.
3	Logical	<i>lUpW</i>	.true. if upstream weighing formulation is to be used (see Section 8.3.2). .false. if the original Galerkin formulation is to be used .
3	Logical	<i>lArtD</i>	.true. if artificial dispersion is to be added in order to fulfill the stability criterion <i>PeCr</i> (see Section 8.3.6). .false. otherwise.
3	Logical	<i>lLagr</i>	.true. if Eulerian-Lagrangian approach of a single-step reverse particle tracking technique is to be used to solve the solute transport equation. This method is useful for convection dominated problems (see Section 8.3.3). .false. if Eulerian approach of finite differences is to be used to solve the solute transport equation.
3	Real	<i>PeCr</i>	Stability criteria (see Section 8.3.6). Set equal to zero when <i>lUpW</i> is equal to .true. .
3	Logical	<i>lTort</i>	.true. if tortuosity factor [<i>Millington arm' Quirk,1961</i>] is to be used. .false. if tortuosity factor is assumed to be equal to one.
4			Comment line.
5	Logical	<i>lRate</i>	Set this logical variable equal to .true. if kinetic precipitation-dissolution of calcite and kinetic dissolution of dolomite is to be considered. Set this logical variable equal to .false. if only equilibrium reactions are to be considered.
5	Logical	<i>lSilic</i>	Set this logical variable equal to .true. if silica content in solution is to be calculated based on the solution pH. Set this logical variable equal to .false. if silica content in solution is not considered.
5	Real	<i>UCrit</i>	The value of ionic strength below which the extended Debye-Hückel equation is used to calculate ion activity coefficients. Pitzer's virial-type equations are used above this value. It is suggested that either one or the other be used.
5	Integer	<i>MaxCh</i>	Maximum number of iterations allowed during any time step between the solute transport and chemical modules. When the maximum number of iterations is reached for <i>MaxCh</i> >5 then the time step is divided by three and the particular time' level is restarted again. When maximum number of iterations is reached for <i>MaxCh</i> ≤5 then the code continues on the new time level. Recommended value (from our experience) is 5. Set equal to one if no iteration is required.
5	Real	<i>xConv</i>	Length conversion lfactor. Multiplication factor to convert the length unit <i>LUnit</i> into meters.

Table 12.8. (continued)

Record	Type	Variable	Description
5	Real	<i>tConv</i>	Time conversion factor. Multiplication factor to convert the time unit <i>TUnit</i> into seconds.
6			Comment line.
7	Real	<i>ChPar(1,M)</i>	Bulk density of material <i>M</i> [ML ⁻³].
7	Real	<i>ChPar(2,M)</i>	Molecular diffusion coefficient in free water, D_w [L ² T ⁻¹].
7	Real	<i>ChPar(3,M)</i>	Longitudinal dispersivity for material type <i>M</i> , D_L [L].
7	Real	<i>ChPar(4,M)</i>	Cation exchange capacity for material type <i>M</i> , \bar{c}_T (mmol _c kg ⁻¹ of soil).
7	Real	<i>ChPar(5,M)</i>	Calcite surface area A'' (m ² ℓ ⁻¹ of soil matrix). Set this variable equal to zero when <i>IRate</i> = false .
7	Real	<i>ChPar(6,M)</i>	Dolomite surface area A^D (m ² ℓ ⁻¹ of soil matrix). Set this variable equal to zero when <i>IRate</i> = false . or dolomite is not present in the soil profile.
7	Real	<i>ChPar(7,M)</i>	Dissolved organic carbon (μmol ℓ ⁻¹). This variable is used to calculate the reduction of the precipitation-dissolution rates of calcite.
7	Real	<i>ChPar(8,M)</i>	Gapon' selectivity constant between calcium and magnesium, K_{13} [-].
7	Real	<i>ChPar(9,M)</i>	Gapon' selectivity constant between calcium and sodium, K_{14} [-].
7	Real	<i>ChPar(10,M)</i>	Gapon' selectivity constant between calcium and potassium, K_{15} [-].
			Record 7 information is provided for each material <i>M</i> (from 1 to <i>NMat</i>).
8			Comment line.
9	Integer	<i>kTopCh</i>	Code which specifies the type of upper boundary condition =+ 1: Dirichlet boundary condition, =-1 : Cauchy boundary condition.
9	Integer	<i>nTop</i>	Code which in case of time-independent upper boundary condition (<i>TopInf</i> = false . - see Block A), refers to the field <i>ConcTab</i> for the value of the solute transport boundary condition. <i>ConcTab(nTop,i)</i> is the boundary condition for the soil surface for species <i>i</i> . Permissible values are 1,2,3,..., <i>nSolConc</i> .
9	Integer	<i>kBotCh</i>	Code which specifies the type of lower boundary condition = 1: Dirichlet boundary condition, = 0: Continuous boundary condition, free drainage, =-1: Cauchy boundary condition.
9	Integer	<i>nBot</i>	Code which in case of time-independent upper boundary condition (<i>BotInf</i> = false . - see Block A), refers to the field <i>ConcTab</i> for the value of the solute transport boundary condition. <i>ConcTab(nBot,i)</i> is the boundary condition at the soil surface for species <i>i</i> . Permissible values are 1,2,3,..., <i>nSolConc</i> .
10			Comment line.
II	Integer	<i>nSolConc</i>	Number of different solutions used in a particular application.

Table 12.8. (continued)

Record	Type	Variable	Description
11	Integer	<i>nAdsConc</i>	Number of surface species combinations used in a particular application.
11	Integer	<i>nPrecConc</i>	Number of mineral phase combinations used in a particular application.
12			Comment line.
13	Real	<i>ConcTab(1,1)</i>	Analytical concentration of calcium for the first solution concentration combination, Ca, ($\text{mmol}_c\ell^{-1}$ of solution).
13	Real	<i>ConcTab(1,2)</i>	Analytical concentration of magnesium for the first solution concentration combination, Mg, ($\text{mmol}_c\ell^{-1}$ of solution).
13	Real	<i>ConcTab(1,3)</i>	Analytical concentration of sodium for the first solution concentration combination, Na, ($\text{mmol}_c\ell^{-1}$ of solution).
13	Real	<i>ConcTab(1,4)</i>	Analytical concentration of potassium for the first solution concentration combination, K_T ($\text{mmol}_c\ell^{-1}$ of solution).
13	Real	<i>ConcTab(1,5)</i>	Analytical concentration of alkalinity for the first solution concentration combination, <i>Alk</i> ($\text{mmol}_c\ell^{-1}$ of solution).
13	Real	<i>ConcTab(1,6)</i>	Analytical concentration of sulfate for the first solution concentration combination, SO_4 , ($\text{mmol}_c\ell^{-1}$ of solution).
13	Real	<i>ConcTab(1,7)</i>	Analytical concentration of chloride for the first solution concentration combination, Cl, ($\text{mmol}_c\ell^{-1}$ of solution).
13	Real	<i>ConcTab(1,8)</i>	Analytical concentration of hypothetical tracer for the first solution concentration combination [-].
			In general, one record as described above is required for each solution concentration combination, starting with the first solution concentration combination and continuing in sequence up to the <i>nSolConcth</i> combination.
14			Comment line.
15	Real	<i>XConcTab(1,1)</i>	Adsorbed (surface species) calcium concentration for the first surface species combination, \bar{Ca} ($\text{mmol}_c\text{kg}^{-1}$ of soil matrix).
15	Real	<i>XConcTab(1,2)</i>	Adsorbed magnesium concentration for the first surface species combination, Mg ($\text{mmol}_c\text{kg}^{-1}$ of soil matrix).
15	Real	<i>XConcTab(1,3)</i>	Adsorbed sodium concentration for the first surface species combination, \bar{Na} ($\text{mmol}_c\text{kg}^{-1}$ of soil matrix).
15	Real	<i>XConcTab(1,4)</i>	Adsorbed potassium concentration for the surface species combination, \bar{K} ($\text{mmol}_c\text{kg}^{-1}$ of soil matrix).
			In general, one record as described above is required for each surface species combination, starting with the first surface species combination and continuing in sequence up to the <i>nAdsConcth</i> combination.
16			Comment line.
17	Real	<i>SConcTab(1,1)</i>	Solid phase calcite concentration for the first mineral phnsc combination expressed in mmol_c of Ca per kg of soil matrix, $CaCO_3$, (divide by $2 \cdot 10^{-3}$ to obtain moles of calcite per kg of soil matrix).

Table 12.8. (continued)

Record	Type	Variable	Description
17	Real	$SConcTab(1,2)$	Solid phase gypsum concentration for the first mineral phase combination expressed in mmol_c of Ca per kg of soil matrix. CaSO_4 (divide by $2 \cdot 10^{-3}$ to obtain moles of gypsum per kg of soil matrix).
17	Real	$SConcTab(1,3)$	Solid phase dolomite concentration for the first mineral phase combination expressed in mmol_c of Ca per kg of soil matrix, $\text{CaMg}(\text{CO}_3)_2$ (divide by $2 \cdot 10^{-3}$ to obtain moles of dolomite per kg of soil matrix).
17	Real	$SConcTab(1,4)$	Solid phase hydromagnesite concentration for the first mineral phase combination expressed in mmol_c of Mg per kg of soil matrix, $\text{Mg}_5(\text{CO}_3)_4(\text{OH})_2 \cdot 4\text{H}_2\text{O}$ (divide by 10^{-4} to obtain moles of hydromagnesite per kg of soil matrix).
17	Real	$SConcTab(1,5)$	Solid phase nesquehonite concentration for the first mineral phase combination expressed in mmol_c of Mg per kg of soil matrix, $\text{MgCO}_3 \cdot 3\text{H}_2\text{O}$ (divide by $2 \cdot 10^{-3}$ to obtain moles of nesquehonite per kg of soil matrix).
17	Real	$SConcTab(1,6)$	Solid phase sepiolite concentration for the first mineral phase combination expressed in mmol_c of Mg per kg of soil matrix, $\text{Mg}_2\text{Si}_3\text{O}_7 \cdot 3\text{H}_2\text{O}$ (divide by $4 \cdot 10^{-3}$ to obtain moles of nesquehonite per kg of soil matrix).
			In general, one record as described above is required for each mineral phase combination, starting with the first mineral phase combination and continuing in sequence up to the $nPrecConcth$ combination.

*Block H is not needed when the logical variable $IChem$ in Block A is set equal to `.false.`.

Table 12.9. Block I - Nodal information.

Record	Type	Variable	Description
1	Integer	<i>NFix</i>	Number of fixed nodes.
2	Integer	<i>i</i>	Fixed node.
2	Real	<i>xFix(i)</i>	z-coordinate of the fixed node <i>i</i> .
2	Real	<i>wTop(i)</i>	Nodal density above fixed node <i>i</i> .
2	Real	<i>wBot(i)</i>	Nodal density below fixed node <i>i</i> .
			Record 2 must be specified for each fixed node.
			Records 1 and 2 have relevant information only for the module PROFILE of the user interface. When the code is used without the user interface, then only two fixed points (top and bottom of the soil profile) with unit nodal density have to be specified.
3	Integer	<i>NumNP</i>	Number of nodal points.
4	Integer	<i>n</i>	Nodal number.
4	Real	<i>x(n)</i>	z-coordinate of node <i>n</i> [L].
4	Real	<i>hOld(n)</i>	Initial value of the pressure head at node <i>n</i> [L]. If <i>lWat=.false.</i> in Block A, then <i>hOld(n)</i> represents the pressure head which will be kept constant during simulation.
4	Integer	<i>MatNum(n)</i>	Index for material whose hydraulic and transport properties are assigned to node <i>n</i> .
4	Integer	<i>LayNum(n)</i>	Subregion number assigned to node <i>n</i> .
4	Real	<i>Beta(n)</i>	Value of the water uptake distribution, $h(z)$ [L ⁻¹], in the soil root zone at node <i>n</i> . Set <i>Beta(n)</i> equal to zero if node <i>n</i> lies outside the root zone.
4	Real	<i>CO2(n)</i>	Initial value of the carbon dioxide concentration at node <i>n</i> [L ³ L ⁻³].
4	Real	<i>Temp(n)</i>	Initial value of the temperature at node <i>n</i> [°C] (if <i>lTemp=.false.</i> and <i>lChem=.true.</i> then set equal to any temperature value to be used later for temperature dependent solute transport).
4	Integer	<i>nC(n)</i>	Code which specifies which solution concentration combination (see Block H) is to be used as an initial condition at node <i>n</i> [-] (omit if <i>lChem=.false.</i>).
4	Integer	<i>nX(n)</i>	Code which specifies which surface species combination (see Block H) is to be used as an initial condition at node <i>n</i> [-] (omit if <i>lChem=.false.</i>).
4	Integer	<i>nS(n)</i>	Code which specifies which mineral phase combination (see Block H) is to be used as an initial condition at node <i>n</i> [-] (omit if <i>lChem=.false.</i>).
			In general, record 4 information is required for each node <i>n</i> , starting with <i>n=1</i> and continuing sequentially until <i>n=NumNP</i> . Record 4 information for certain nodes may be skipped if several conditions are satisfied (see beginning of this section).

Table 12.9. (continued)

Record	Type	Variable	Description
5	Integer	<i>NObs</i>	Number of observation nodes for which values of the pressure head, the water content, temperature (for <i>ITemp=.true.</i>), and carbon dioxide (for <i>ICO2=.true.</i>) are printed at each time level.
6	Integer	<i>iObs(1)</i>	Nodal number of the first observation node.
6	Integer	<i>iObs(2)</i>	Nodal number of the second observation node.
6	Integer	<i>iObs(NObs)</i>	Nodal number of the last observation node.

Table 12.10. Block J - Atmospheric information.+

Record	Type	Symbol	Description
1..2			Comment lines.
3	Integer	<i>MaxAl</i>	Number of atmospheric data records.
4			Comment line.
5	Real	<i>hCritS</i>	Maximum allowed pressure head at the soil surface [L].
5	Real	<i>lSurf</i>	Logical variable indicating whether the potential transpiration <i>rRoot(i)</i> is to be divided into both potential evaporation and potential transpiration according to ratio between the actual root depth and the maximum root depth.
6			Comment line.
7	Real	<i>tAtm(i)</i>	Time for which the <i>i</i> -th data record is provided [T].
7	Real	<i>Prec(i)</i>	Precipitation rate [LT^{-1}] (in absolute value).
7	Real	<i>rSoil(i)</i>	Potential soil evaporation rate [LT^{-1}] (in absolute value). Set <i>rSoil</i> equal to zero if <i>lSurf</i> = .true. . In that case <i>rSoil</i> is calculated as a function of <i>rRoot</i> (See Section 7.3).
7	Real	<i>rRoot(i)</i>	Potential transpiration rate [LT^{-1}] (in absolute value) .
7	Real	<i>hCritA(i)</i>	Absolute value of minimum allowed pressure head at the soil surface [L].
7	Real	<i>rB(i)</i>	Bottom flux [LT^{-1}] (set equal to 0 if <i>KodBot</i> is positive or one of logical variables <i>qGWLf</i> or <i>FreeD</i> or <i>SeepF</i> is .true.).
7	Real	<i>hB(i)</i>	Groundwater level [L], or any other prescribed pressure head boundary condition as indicated by a positive value of <i>KodBot</i> (set equal to 0 if <i>KodBot</i> is negative or one of logical variables <i>qGWLf</i> or <i>FreeD</i> or <i>SeepF</i> is .true.).
7	Real	<i>hT(i)</i>	Prescribed pressure head [L] at the surface (set equal to 0 if <i>KodBot</i> < 0).
7	Real	<i>tTop(i)</i>	Soil surface temperature [$^{\circ}\text{C}$] (is not specified if <i>lTemp</i> is equal to .false.).
7	Real	<i>tBot(i)</i>	Soil temperature at the bottom of the soil profile [$^{\circ}\text{C}$] (must not be specified if <i>lTemp</i> is equal to .false. , set equal to 0 if <i>kBotT</i> =0).
7	Real	<i>kTopCh(i)</i>	Code which refers to the field <i>ConcTab</i> for the value of the solute transport upper boundary condition. Sign of <i>kTopCh(i)</i> indicates whether a Dirichlet (positive) or Neumann (negative) boundary condition is to be applied at the soil surface. <i>ConcTab(abs(kTopCh(i)),j)</i> is the boundary condition for the soil surface for species <i>j</i> . Permissible values are $\pm 1, \pm 2, \pm 3, \dots, \pm n_{\text{SolConc}}$.
7	Real	<i>kBotCh(i)</i>	Code which refers to the field <i>ConcTab</i> for the value of the solute transport lower boundary condition. Sign of <i>kBotCh(i)</i> indicates whether a Dirichlet (positive) or Neumann (negative) boundary condition is to be applied at the bottom of the soil profile. <i>ConcTab(abs(kBotCh(i)),j)</i> is the boundary condition for the bottom of the soil profile for species <i>j</i> . Permissible values are $\pm 1, \pm 2, \pm 3, \dots, \pm n_{\text{SolConc}}$.

* Block J need not be supplied if both logical variables *TopInF* and *BotInF* (Block A) are set equal to **.false.**.

Table 12.11. Input file 'COMP.DAT'[Felmy,1990].

001080	H2O	0
011000	Na+	1
019000	K+	1
020000	Ca++	2
012000	Mg++	2
001000	H+	1
012080	MgOH+	1
000170	Cl-	-1
000160	SO4--	-2
000161	HSO4-	-1
000080	OH-	-1
000060	CO3--	-2
000061	HCO3-	-1
000062	CO2 (aq)	0
020060	CaCO3 (aq)	0
012060	MgCO3 (aq)	0
000050	B (OH) 3	0
000051	B (OH) 4-	-1
000052	B3O3 (OH) 4-	-1
000053	B4O5 (OH) 4--	-2
020051	CaB (OH) 4+	1
012051	MgB (OH) 4+	1
100060	CO2 (GAS)	
-1		

Table 12.12. Input file 'BINARYP.DAT' [Felmy,1990].

011000	000170	.0765	.2664	.000	.00127
011000	000160	.01958	1.113	.000	.00497
011000	000161	.0454	.398	.000	.0000
011000	000080	.0864	.253	.000	.0044
011000	000061	.0277	.0411	.000	.0000
011000	000060	.0399	1.389	.000	.00440
011000	000051	-.0427	.089	.000	.0114
011000	000052	-.056	-.910	.000	.0000
011000	000053	-.110	-.40	.000	.0000
019000	000170	.04835	.2122	.000	-.00084
019000	000160000	.0000
019000	000161	-.0003 04995	.7793 .1735	.000	.000
019000	000080	.1298	.320	.000	.0041
019000	000061	.0296	-.013	.000	-.00800
019000	000060	.1488	1.43	.000	-.00150
019000	000051	.0350	.14	.000	.0000
019000	000052	-.130	.00	.000	.0000
019000	000053	-.022	.00	.000	.0000
020000	000170	.3159	1.614	.000	-.00034
020000	000160	.20	3.1973	-54.24	.000
020000	000161	.2145	2.530	.000	.000
020000	000080	-.1747	-.2303	-5.72	.000
020000	000061000	.000
012000	000170	.35235 400	2.9770 1.6815	.000	.00519
012000	000160	.2210	3.343	-37.23	.025
012000	000161	.4746	1.729	.000	.000
012000	000061	-0.1 329	1.658 .6072	.000	.00
012080	000170			.000	.00
001000	000170	.1775	.2945	.000	.0008
001000	000160	.0298	.0000	.000	.0438
001000	000161	.2065	.5556	.000	.000
012051	000170	.1600	.0000	.000	.000
020051	000170	.1200	.0000	.000	.000
000000					

Table 12.13. Input file 'TERNARY.P.DAT' [Felmy, 19903.

```

011000 019000  -.012 000170  -.0018 000160  -.010 000061  -.0030 000060  .00300
011000 020000  .070 000170  -.007 000160  -.055
011000 012000  .070 000170  -.012 000160  -.015
011000 001000  .036 000170  -.004 000161  -.0129
019000 020000  .032 000170  -.025
019000 012000  .000 000170  -.022 000160  -.048
019000 001000  .005 000170  -.011 000160  .197 000161  -.0265
020000 012000  .007 000170  -.012 000160  .024
020000 001000  .092 000170  -.015
012000 012080  .000 000170  .028
012000 001000  .10 000170  -.011 000161  -.0178
000170 000160  .02 011000  .0014 020000  -.018 012000  -.0040
000170 000161  -.006 011000  -.006 001000  .0130
000170 000080  -.05 011000  -.006 019000  -.006 020000  -.0250
000170 000061  .0000  -.0150 012000  -.096
000170 000060  -.0200 0300 011000 011000  .0085 019000  .00400
000160 000161  .00 011000  -.00940 019000  -.0677 012000  -.0425
000160 000080  -.013 011000  -.009 019000  -.050
000160 000061  .01 011000  -.00500 012000  -.161
000160 000060  .02 011000  -.005 019000  -.00900
000080 000060  .100 011000  -.0170 019000  -.0100
000061 000060  -.0400 011000  .00200 019000  .0120
000051 000170  -.065 011000  -.0073
000051 000160  -.012
000052 000170  .12 011000  -.024
000052 000160  .10
000052 000061  -.10
000053 000170  .074 011000  .026
000053 000160  .12
000053 000061  -.087
000000

```

Table 12.14. Input file 'LAMBDA.DAT' [*Felmy,1990*].

```
000050 011000  -.097 000160  .046
000050 001000  .000 000170  -.0102
000050 019000  -.14
000050 000170  .091
000050 000160  .018
000050 000052  -.20
000062 011000  .100
000062 019000  .0510
00.0062 020000  .183
000062 012000  .183
000062 000170  -.0050
000062 000160  .097
000000
```

13. OUTPUT DATA

The program output consists of 11 output files which are organized into 2 groups:

T-level information
T_LEVEL.OUT
CO2_INF.OUT
RUN_INF.OUT
OBS_NODE.OUT

P-level information
NOD_INF.OUT
BALANCE.OUT
CONC.OUT
SOLID.OUT
EQUIL.OUT
CHEMBAL.OUT

In addition, some of the input data are printed to the file I_CHECK.OUT. All output files are directed to the same directory as the input files, which must be created by the user prior to the program execution (the directory is created automatically if the user interface is used). The various output files are described in detail in this section.

The file I_CHECK.OUT contains a complete description of the space discretization, the hydraulic characteristics and the transport properties of each soil material and selected input data for the user to be able to easily check them.

T-level information- This group of output files contains information which is printed at the end of each time step. Printing can be suppressed by setting the logical variable *ShortF* in input Block A equal to .true.; the information is then printed only at selected print times. Output files printed at the T-level are described in Tables 13.1 through 13.3. Output file OBS_NODE.OUT gives transient values of the pressure head, water content, CO₂ concentration and temperature, as obtained during the simulation at specified observation nodes.

P-level information- This information is printed only at prescribed print times. The following output files are printed at the P-level:

NOD_INF.OUT	Nodal values of the pressure head, water content, carbon dioxide concentration, temperature, hydraulic conductivity and capacity, velocity, root water uptake, and CO ₂ production (see Table 13.4).
BALANCE.OUT	This file gives the total amount of water and carbon dioxide inside each specified subregion, the inflow/outflow rates to/from that subregion, together with the mean pressure head (<i>hMean</i>), the mean temperature (<i>TMean</i>) and the mean CO ₂ concentration (<i>cMean</i>) over each subregion (see Table 13.5). Absolute and relative errors in the water and solute mass balances and absolute error in CO ₂ mass balance are also printed to this file.
CONC.OUT	Nodal values of the aqueous concentrations for calcium, magnesium, sodium, potassium, alkalinity, sulfate, chloride, and hypothetical tracer (see Table 13.6).
SOLID.OUT	Nodal values of the mineral phase concentrations for calcite, gypsum, dolomite, hydromagnesite, nesquehonite, and sepiolite and nodal values of the adsorbed concentrations for calcium, magnesium, sodium, and potassium (see Table 13.7).
EQUIL.OUT	This file contains the chemical information such as activities of calcium, bicarbonate and water, alkalinity, <i>pH</i> , <i>SAR</i> , electric conductivity of the solution, ionic strength, osmotic coefficient, osmotic pressure head, and ion activity products for calcite, gypsum and dolomite (see Table 13.8).
CHEMBAL.OUT	This file contains the information about the total amount of particular species (e.g. Ca, Mg, SO ₄ ,...) in solution, mineral phase and surface species form in the entire flow region, as well as the cumulative boundary fluxes and absolute mass error in particular species.

Table 13.1. T_LEVEL.OUT - pressure heads and fluxes on the boundaries and in the root zone.

<i>Time</i>	Time, t , at current time-level [T].
<i>rTop</i>	Potential surface flux [LT^{-1}] (infiltration/evaporation: -/+).
<i>rRoot</i>	Potential transpiration rate [LT^{-1}].
<i>vTop</i>	Actual surface flux [LT^{-1}] (infiltration/evaporation: -/+).
<i>vRoot</i>	Actual transpiration rate [LT^{-1}].
<i>vBot</i>	Actual flux at the bottom of the soil profile [LT^{-1}] (inflow/outflow: +/-).
<i>sum(rTop)</i>	Cumulative value of the potential surface flux [L] (infiltration/evaporation: -/+).
<i>sum(rRoot)</i>	Cumulative value of the potential transpiration rate [L].
<i>sum(vTop)</i>	Cumulative value of the actual surface flux [L] (infiltration/evaporation: -/+).
<i>sum(vRoot)</i>	Cumulative value of the actual transpiration rate [L].
<i>sum(vBot)</i>	Cumulative value of the actual flux across the bottom of the soil profile [L] (inflow/outflow: +/-).
<i>hTop</i>	Pressure head at the soil surface [L].
<i>hRoot</i>	Mean value of the pressure head over the region for which $Beta(n) > 0$ (i.e., within the root zone) [L].
<i>hBot</i>	Pressure head at the bottom of the soil profile [L].
<i>TLevel</i>	Time-level (current time-step number) [-].

Table 13.2. CO₂_INF.OUT - CO₂ concentrations and CO₂ fluxes on the boundaries and in the root zone.

<i>CvTop</i>	Actual CO ₂ flux at the soil surface [$L^3L^{-2}T^{-1}$] (inflow/outflow: -/+).
<i>CvBot</i>	Actual CO ₂ flux at the bottom of the soil profile [$L^3L^{-2}T^{-1}$] (inflow/outflow: +/-).
<i>sum(CvTop)</i>	Cumulative CO ₂ flux at the soil surface [L^3L^{-2}].
<i>sum(CvBot)</i>	Cumulative CO ₂ flux at the bottom of the soil profile [L^3L^{-2}].
<i>cTop</i>	CO ₂ concentration at the soil surface [L^3L^{-3}].
<i>cRoot</i>	Mean CO ₂ concentration in the root zone [L^3L^{-3}].
<i>cBot</i>	CO ₂ concentration at the bottom of the soil profile [L^3L^{-3}].
<i>vProd</i>	CO ₂ production by soil microorganisms and plant roots in the soil profile [$L^3L^{-2}T^{-1}$].
<i>sum(vProd)</i>	Cumulative CO ₂ production by soil microorganisms and plant roots in the soil profile [L^3L^{-2}].
<i>sum(Sink)</i>	Cumulative CO ₂ root uptake in the soil profile [L^3L^{-2}].

Table 13.3. RUN_INF.OUT - time and iteration information.

<i>TLevel</i>	Time-level (current time-step number).
<i>Time</i>	Time, t , at current time-level.
<i>dt</i>	Time step, Δt .
<i>Iter</i>	Number of iterations for solution of the water flow equation.
<i>IterCh</i>	Number of iterations between the solute transport and chemical modules.
<i>ItCum</i>	Cumulative number of iterations for water flow.
<i>KodTop</i>	Code of the upper boundary condition for water flow.
<i>KodBot</i>	Code of the lower boundary condition for water flow.
<i>lConverg</i>	Indication as to whether or not the numerical convergence for water flow was achieved at the current time level.
<i>Peclet</i>	Maximum local Peclet number.
<i>Cow-ant</i>	Maximum local Courant number.

Table 13.4. NOD_INF.OUT - Profile information.

<i>Node</i>	Number of nodal point n .
<i>Depth</i>	z -coordinate of node n .
<i>Head</i>	Nodal values of the pressure head [L].
<i>Moisture</i>	Nodal values of the moisture content [-].
<i>c o 2</i>	Nodal values of the CO ₂ concentration [L ³ L ⁻³].
<i>Temp</i>	Nodal values of the temperature [K].
<i>K</i>	Nodal values of the hydraulic conductivity [LT ⁻¹].
<i>C</i>	Nodal values of the hydraulic capacity [L ⁻¹].
<i>Flux</i>	Nodal values of the Darcian velocity [LT ⁻¹].
<i>Sink</i>	Nodal value of the root water uptake [T ⁻¹].
<i>Product</i>	Nodal values of the CO ₂ production [L ³ L ⁻³ T ⁻¹].

Table 13.5. BALANCE.OUT - mass balance variables.

<i>Area</i>	Length of the entire flow domain or of a specified subregion [L].
<i>W-volume</i>	Volume of water in the entire flow domain or in a specified subregion [L].
<i>In-Flow</i>	Inflow/Outflow to/from the entire flow domain or specified subregion [LT ⁻¹].
<i>hMean</i>	Mean pressure head in the entire flow domain or in a specified subregion [L].
<i>COVol</i>	Volume of CO ₂ in the entire flow domain or in a specified subregion [L ³ L ⁻²].
<i>COMean</i>	Mean CO ₂ concentration in the entire flow domain or in a specified subregion [L ³ L ⁻³].
<i>Cnc Vol</i>	Volume of tracer in the entire flow domain or in a specified subregion [ML ⁻²].
<i>cMean</i>	Mean tracer concentration in the entire flow domain or in a specified subregion [ML ⁻³].
<i>TMean</i>	Mean temperature concentration in the entire flow domain or in a specified subregion (°C).
<i>Top Flux</i>	Actual surface flux [LT ⁻¹] (infiltration/evaporation: -/+).
<i>Bot Flux</i>	Actual flux at the bottom of the soil profile [LT ⁻¹] (inflow/outflow: +/-).
<i>WatBalT</i>	Absolute error in the water mass balance for the entire flow domain [L].
<i>WatBalR</i>	Relative error in the water mass balance for the entire flow domain [%].
<i>CO2BalT</i>	Absolute error in the CO ₂ mass balance for the entire flow domain [L].
<i>CncBalT</i>	Absolute error in the tracer mass balance in the entire flow domain [ML ⁻²].
<i>CncBalR</i>	Relative error in the tracer mass balance in the entire flow domain [%].
<i>Crop Yield</i>	Relative crop yield, 100 Y/Y_M [%].

Table 13.6. CONC.OUT - solute concentration information.

<i>Node</i>	Number of nodal point <i>n</i> .
<i>Depth</i>	z-coordinate of node <i>n</i> .
<i>Ca</i>	Analytical concentration of calcium ($\text{mmol}_c\ell^{-1}$) at node <i>n</i> .
<i>Mg</i>	Analytical concentration of magnesium ($\text{mmol}_c\ell^{-1}$) at node <i>n</i> .
<i>Na</i>	Analytical concentration of sodium ($\text{mmol}_c\ell^{-1}$) at node <i>n</i> .
<i>K</i>	Analytical concentration of potassium ($\text{mmol}_c\ell^{-1}$) at node <i>n</i> .
<i>HC03</i>	Analytical concentration of alkalinity ($\text{mmol}_c\ell^{-1}$) at node <i>n</i> .
<i>so4</i>	Analytical concentration of sulfate ($\text{mmol}_c\ell^{-1}$) at node <i>n</i> .
<i>Cl</i>	Analytical concentration of chloride ($\text{mmol}_c\ell^{-1}$) at node <i>n</i> .
<i>Tracer</i>	Analytical concentration of hypothetical tracer [-] at node <i>n</i> .

Table 13.7. SOLID.OUT - precipitated and adsorbed concentrations.

<i>Node</i>	Number of nodal point <i>n</i> .
<i>Depth</i>	<i>z</i> -coordinate of node <i>n</i> .
<i>Calcite</i>	Mineral phase Ca concentration present as calcite at node <i>n</i> (mmol _c kg ⁻¹).
<i>Gypsum</i>	Mineral phase Ca concentration present as gypsum at node <i>n</i> (mmol _c kg ⁻¹).
<i>Dolomite</i>	Mineral phase Ca concentration present as dolomite at node <i>n</i> (mmol _c kg ⁻¹).
<i>Nesqeh.</i>	Mineral phase Mg concentration present as nesquehonite at node <i>n</i> (mmol _c kg ⁻¹).
<i>HydroMg.</i>	Mineral phase Mg concentration present as hydromagnesite at node <i>n</i> (mmol _c kg ⁻¹).
<i>Sepiol.</i>	Mineral phase Mg concentration present as sepiolite at node <i>n</i> (mmol _c kg ⁻¹).
<i>XCa</i>	Surface species concentration of calcium at node <i>n</i> (mmol _c kg ⁻¹).
<i>XMg</i>	Surface species concentration of magnesium at node <i>n</i> (mmol _c kg ⁻¹).
<i>XNa</i>	Surface species concentration of sodium at node <i>n</i> (mmol _c kg ⁻¹).
<i>XK</i>	Surface species concentration of potassium at node <i>n</i> (mmol _c kg ⁻¹).

Table 13.5. EQUIL.OUT - chemical information.

<i>Node</i>	Number of nodal point <i>n</i> .
<i>Depth</i>	z-coordinate of node <i>n</i> .
<i>aCa</i>	Activity of Ca ²⁺ [-].
<i>aHCO₃</i>	Activity of HCO ₃ ⁻ [-].
<i>aH₂O</i>	Activity of water [-].
<i>Alk</i>	Alkalinity (mmol _e kg ⁻¹).
<i>pH</i>	Negative logarithm of hydrogen activity, -log(H), [-].
<i>SAR</i>	Sodium adsorption ratio, defined as [Na/(Ca+Mg) ^{0.5}](mmol ^{0.5} l ^{-0.5}).
<i>EC</i>	Electric conductivity of the soil solution (dSm ⁻¹).
<i>U</i>	Ionic strength (mol kg ⁻¹).
<i>pIAP(c)</i>	Negative logarithm of the ion activity product for calcite, -log[(Ca ²⁺)(CO ₃ ²⁻)], [-].
<i>pIAP(g)</i>	Negative logarithm of the ion activity product for gypsum, -log[(Ca ²⁺)(SO ₄ ²⁻)(H ₂ O) ²], [-].
<i>pIAP(d)</i>	Negative logarithm of the ion activity product for dolomite, -log[(Ca ²⁺)(Mg ²⁺)(CO ₃ ²⁻) ²], [-].
<i>phi</i>	Osmotic coefficient [-].
<i>hphi</i>	Osmotic pressure head [L].

14. PROGRAM ORGANIZATION

The program consists of a main program and 59 subprograms. The subprograms are organized by means of 11 source tiles which are stored and compiled separately and then linked together with the main program to form an executable program. Below are a list and brief descriptions of the source files and the associated subprograms.

WATCHEM.FOR	(Main program unit)
INPUT.FOR	BasInf, MatIn, GenMat, TmIn, NodInf, RootIn, SinkIn, ChemIn, TempIn, CO2In, Profil
WATFLOW.FOR	WatFlow, Reset, Gauss, Shift, SetMat, Veloc, Fqh, W_Flux
TIME.FOR	TmCont, SetBC
MATERIAL.FOR	FK, FC, FQ, FH, FS
SINK.FOR	SetSnk, SetRG
OUTPUT.FOR	TLInf, ALInf, SubReg, NodOut, ObsNod, Balance, ChemOut
SOLUTE.FOR	Solute, Toler, Mat1
TEMPER.FOR	Temper
CARBON.FOR	Gas, Produc
CARBRATE.FOR	Equil, SChem, Chem, Xchang, CalRat, DolRat, TDep, D_H, Unit, Polyn, Ecal, Precip, Hydrog, Magnes
PITZER.FOR	PitzIn, Pitzer, Homix, Elects

Main program unit WATCHEM. FOR

This is the main program unit of UNSCIEM. This unit controls execution of the program and determines which optional subroutines are necessary for a particular application.

Source file INPUT.FOR

Subroutines included in this source file are designed to read data from different input blocks. The following table summarizes the input file and input block (described in Section 12) read by a particular subroutine.

Table 14.1. Input subroutines/files.

Subroutine	Input Block	Input File
BasInf	A. Basic information	
BasInf,MatIn	B. Water flow information	
TmIn	C. Time information	
RootIn	D. Root growth information	SELECTOR.IN
SinkIn	E. Root water uptake information	
TempIn	F. Heat transport information	
CO2In	G. CO ₂ transport and production information	
ChemIn	H. Solute transport and chemical information	
NodInf	I. Nodal information	PROFILE.DAT
AtmIn	J. Atmospheric information	ATMOSPH.IN
PitzIn	L. Pitzer information	COMP.DAT BINARYP.DAT TERNARYP.DAT LAMBDA.DAT

Subroutine **Profil** writes into the output file I_CHECK.OUT the information about the soil profile, such as residual and saturated water contents, saturated hydraulic conductivities, air-entry pressure heads, and spatial distribution of the root water uptake.

Subroutine **GenMat** generates a table of water contents, hydraulic conductivities, and specific water capacities from a set of hydraulic parameters for each soil type in the flow domain.

Source file WATFLOW.FOR

Subroutine **WatFlow** is the main subroutine for simulating water flow; this subroutine controls the entire iterative procedure for solving the Richards equation.

Subroutine **Reset** constructs the global matrix equation for water flow, including the right-hand side vector.

Subroutine **Gauss** solves the tridiagonal symmetric matrix equation for water flow by Gaussian elimination.

Subroutine **Shift** changes atmospheric or seepage face boundary conditions from Dirichlet type to Neumann type conditions, or vice versa, as needed.

Subroutine **SetMat** determines the nodal values of the hydraulic properties $K(h)$, $C(h)$ and $\theta_w(h)$ by interpolation between values in the hydraulic property tables.

Subroutine **Veloc** calculates nodal water fluxes based on a Darcy's law.

Function **Fqh** describes the groundwater level - discharge relationship, $q_w(h)$, defined by equation (10.1). This function is called only from subroutine SetBC.

Subroutine **W_Flux** calculates nodal water fluxes based on the mass balance equation.

Source file TIME.FOR

Subroutine **TmCont** adjusts the current value of the time increment Δt .

Subroutine **SetBC** updates time variable boundary conditions.

Source file OUTPUT.FOR

The subroutines included in this file are designed to print data to different output files. Table 14.2 summarizes which output files are generated by a particular subroutine.

Table 14.2. Output subroutines/files.

Subroutine	Output File
TLInf	T_LEVEL.OUT CO2_INF.OUT RUN_INF.OUT
NodOut	NOD_MF.OUT
ChemOut	CONC.OUT SOLID.OUT
SubReg	BALANCE.OUT
Balance	CHEMBAL.OUT
Equil	EQUIL.OUT
ObsNod	POINT.OUT

Source file SINK2. FOR

Subroutine **SetSnk** calculates the actual root water extraction rate as a function of water and salinity stress in the soil root zone.

Subroutine **SetRG** calculates the rooting depth based on the root growth model.

Source file MATERIAL. FOR

This file includes the functions FK, FC, FQ, FH, and FS which define the unsaturated hydraulic properties $K(h)$, $C(h)$, $\theta_w(h)$, $h(\theta_w)$, and $S_e(h)$ for each soil material.

Source file SOLUTE. FOR

Subroutine **Solute** is the main subroutine for simulating multicomponent solute transport; it computes the optimum weighing factors for all elements. it calculates the maximum local Peclet and Courant numbers and the maximum permissible time step, it constructs and solves the global

matrix equation for solute transport.

Subroutine **Toler** checks the convergence between the solute transport and chemical modules.

Subroutine **Mat1** transfers one matrix into another matrix.

Source file TEMPER. FOR

Subroutine **Temper** is the main subroutine for simulating heat transport; it constructs and solves the global matrix equation for heat transport.

Source file CARBON. FOR

Subroutine **Gas** is the main subroutine for simulating CO₂ transport; it constructs and solves the global matrix equation for CO₂ transport.

Subroutine **Produc** calculates the actual CO₂ production by plant roots and soil microorganisms as a function of water and salinity stress, temperature, and CO₂ concentration in the soil root zone.

Source file CARBONATE. FOR

Subroutine **Equil** prepares the variables for the equilibrium and kinetic carbonate chemistry.

Subroutine **SCHEM** is the governing routine for kinetic precipitation/dissolution.

Subroutine **CHEM** is the governing routine for equilibrium chemistry.

Subroutine **XCHANG** brings the solution into equilibrium with the exchangeable cations.

Subroutine **CalRat** calculates the rate of calcite precipitation or dissolution.

Subroutine **DolRat** calculates the rate of dolomite dissolution.

Subroutine **TDep** determines temperature dependent constants.

Subroutine **D_H** calculates activity coefficients using the Debye-Hückel equation.

Subroutine **Unit** converts units from $\text{mmol}\cdot\text{kg}^{-1}$ to $\text{mol}\cdot\text{kg}^{-1}$ or $\text{mol}\cdot\text{kg}^{-1}$ to $\text{mmol}\cdot\text{kg}^{-1}$.

Subroutine **Polyn** solves the 3rd order polynomial by Newton's method.

Subroutine **Ecal** determines electrical conductivity based on the method 3 of *McNeal et al.* [1970].

Subroutine **Precip** calculates precipitation-dissolution for system $(A)\cdot(B)**2$.

Subroutine **Hydrog** calculates hydrogen concentration based on the electric charge equation.

Subroutine **Magnes** calculates precipitation/dissolution of Mg mineral phases.

Source file PITTER.FOR

Subroutine **PitzIn** reads in the necessary Pitzer parameters for a non-ideal solution model. Adopted from *Felmy*[1990].

Subroutine **Pitzer** computes activity for electrolyte solutions based on Pitzer's equations. Adopted from *Felmy*[1990].

Subroutine **Homix** calculates higher order mixing terms for unsymmetrical electrolyte misings. Adopted from *Felmy*[1990].

Subroutine **Elects** calculates higher order electrostatic functions. Adopted from *Felmy* [1990].

15. REFERENCES

- Abriola, L. M., Modeling contaminant transport in the subsurface: An interdisciplinary challenge, *Reviews of Geophysics*, 25(2), 125-134, 1987.
- Anderson, J. M., Carbon dioxide evolution from two temperate, deciduous woods and soils, *J. Appl. Ecol.*, 10, 361-378, 1973.
- Armstrong, W., and T. J. Gaynard, The critical oxygen pressures for respiration in intact plant, *Physiol. Plant*, 37, 200-206, 1976.
- Baehr, A. L., Selective transport of hydrocarbons in the unsaturated zone due to aqueous and vapor phase partitioning, *Water Resour. Res.*, 23(10), 1926-1938, 1987.
- Bell, R. P., and J. H. B. George, Dissociation of thallus and Ca sulfate salts at different temperatures, *Trans. Faraday Soc.*, 49, 619-627, 1953.
- Bresler, E., Simultaneous transport of solute and water under transient unsaturated flow conditions, *Water Resour. Res.*, 9, 975-986, 1973.
- Bridge, B. J., and A. J. Rixon, Oxygen uptake and respiratory quotient of field soil cores in relation to their air filled pore space, *J. Soil Sci.*, 27, 279-286, 1976.
- Bryant, S. L., R. S. Schechter, and L. W. Lake, Interactions of precipitation/dissolution waves and ion exchange in flow through permeable media, *AIChE J.*, 32(5), 751-764, 1986.
- Busenberg, E., and L. N. Plummer, The kinetics of dissolution of dolomite in CO₂-H₂O systems at 1.5 to 65 C and 0 to 1 ATM P_{CO₂}, *Am. J. Sci.*, 282, 45-78, 1982.
- Buyanovsky, G. A., and G. I-I. Wagner, Annual cycles of carbon dioxide level in soil air, *Soil Sci. Soc. Am. J.*, 47, 1139-1145, 1983.
- Buyanovsky, G. A., G. H. Wagner, and C. J. Gentzer, Soil respiration in a winter wheat ecosystem, *Soil Sci. Soc. Am. J.*, 50, 338-344, 1986.
- Carey, R. W., and J. A. Berry, Effects of low temperature on respiration and uptake of rubidium ions by excised barley and corn roots, *Plant Physiol.*, 61, 858-860, 1978.
- Cederberg, G. A., R. L. Street, and J. O. Leckie, A groundwater mass transport and equilibrium chemistry model for multicomponent systems, *Water Resour. Res.*, 21(8), 1095-1104, 1985.
- Celia, M. A., E. T. Bououtas, and R. L. Zarba, A general mass-conservative numerical solution for the unsaturated flow equation, *Water Resour. Res.*, 26(7), 1483-1496, 1990.
- Chung S.-K., and R. Horton, Soil heat and water flow with a partial surface mulch, *Water Resour. Res.*, 23(12), 2175-2186, 1987.
- Davis, L. A., and S. P. Neuman, Documentation and user's guide: UNSAT2 - Variably saturated flow model, *Final Rep.*, WWL/TM-1 791-1, Water, Waste & Land, Inc., Ft. Collins, Colorado, 1983.

- de Jong, E. and H. Schappert, Calculation of soil respiration and activity from CO₂ profiles in the soil, *Soil Sci.*, 113(5), 1972.
- de Marsily, G., *Quantitative Hydrogeology*, Academic Press, 1986.
- de Vries, D. A., The thermal properties of soils, In: *Physics of Plant Environment*, edited by R. W. van Wijk, pp. 21 O-235, North Holland, Amsterdam, 1963.
- Dudley, L. M., R. J. Wagenet, and J. J. Jurinak, Description of soil chemistry during transient solute transport, *Water Resour. Res.*, 17(5), 1498-1504, 1981.
- Edwards, N. T., and P. Sollins, Continuous measurement of carbon dioxide evolution from partitioned forest floor components, *Ecology*, 54, 406-412, 1973.
- Ekpete, D. M., and A. H. Cornfield, Effect of varying static and changing moisture levels during incubation on the mineralization of carbon in soil, *J. Agric. Sci.*, 64, 205-209, 1965.
- Feddes, R. A., E. Bresler, and S. P. Neuman, Field test of a modified numerical model for water uptake by root systems, *Water Resour. Res.*, 10(6), 1199-1206, 1974.
- Feddes, R. A., P. J. Kowalik, and H. Zaradny, *Simulation of field water use and crop yield*, John Wiley & Sons, New York, 188 p., 1978.
- Felmy, A. R., and J. H. Weare, The prediction of borate mineral equilibria in natural waters: Application to Searles Lake, California, *Geochim. Cosmochim. Acta*, 50, 2771-2783, 1986.
- Felmy, A. R., *GMIN: A computerized chemical equilibrium model using a constrained minimization of the Gibbs free energy*, Pacific Northwest Lab., Richland, Washington, 1990.
- Förster, R., A multicomponent transport model, *Geoderma*, 35, 261-278, 1986.
- Förster, R., and H. Gerke, Integration von Modellen des Wasser- und Stofftransports sowie physikochemischer Wechselwirkungen zur Analyse von Agrar-Ökosystemen, *Verhandlungen der Gesellschaft für Ökologie, Band XVIII*, Essen, 1988.
- Freijer, J. I., and P. A. Leffelaar, Adapted Fick's law applied to soil respiration, *Water Resour. Res.*, 32, 791-800, 1996.
- Gallagher, J. N., and P. V. Biscoe, Field studies of cereal leaf growth, *J. of Expt. Bot.*, 10, 645-655, 1979.
- Gilmore, E. and J. S. Rogers, Heat units as a method of measuring maturity in corn, *Agron. J.*, 50, 611-615, 1958.
- Glinski, J., and W. Stepniewski, *Soil aeration and its role for plants*, CRC Press, Boca Raton, Florida, 1985.
- Gureghian, A. B., A two-dimensional finite-element solution for the simultaneous transport of water and multi solutes through a nonhomogeneous aquifer under transient saturated-unsaturated flow conditions, *Sci. Total Environ.*, 21, 329-337, 1981.
- Hanks, R. J., and R. W. Hill, *Modeling crop responses to irrigation in relation to soils, climate and salinity*, Dept. of Soil Sci. and Biometeorology, Utah State Univ., Utah, 1980.

- Hansen, S., and H. C. Aslyng, *Nitrogen balance in crop production: Simulation model NITCROS*, Hydrotech. Lab., The Royal Veter. and Agric. Univ., Copenhagen, 1984.
- Harned, H. S., and R. Davis, Jr., The ionization constant of carbonic acid and the solubility of carbon dioxide in water and aqueous salt solutions from 0 to 50 C, *J. Am. Chem. Soc.*, 65, 2030-2037, 1943.
- Harvie, Ch. E., N. Moller, and J. H. Weare, The prediction of mineral solubilities in natural waters: The Na-K-Mg-Ca-H-Cl-SO₄-OH-HCO₃⁻-CO₂-H₂O- system to high ionic strengths at 25°C, *Geochim. Cosmochim. Acta*, 48, 723-751, 1984.
- Hillel, D., and C. H. M. van Bavel, Simulation of profile water storage as related to soil hydrologic properties, *Soil Sci. Soc. Am. J.*, 40, 807-815, 1976.
- Holt, J. A., M. J. Hodgen, and D. Lamb, Soil respiration in the seasonally dry tropics near Townsville, North Queensland, *Austr. J. Soil Res.*, 28, 737-745, 1990.
- Hopmans, J. W., and J. N. M. Stricker, Stochastic analysis of soil water regime in a watershed, *J. Hydrol.*, 105, 57-84, 1989.
- Howard, P. J. A., and D. M. Howard, Respiration of decomposing litter in relation to temperature and moisture. Microbial decomposition of tree and shrub leaf litter, *Oikos*, 33, 457-465, 1979.
- Huyakorn, P. S. and K. Nilkuha, Solution of transient transport equation using an upstream finite element scheme, *Appl. Math. Modeling*, 3, 7-17, 1979.
- Huyakorn, P. S., and G. F. Pinder, *Computational Methods in Subsurface Flow*, Academic Press, London, United Kingdom, 1983.
- Huyakorn, P. S., J. B. Kool, and Y. S. Wu, VAM2D- Variably saturated analysis model in two dimensions, Version 5.2 with hysteresis and chained decay transport, Documentation and user's guide, *NUREG/CR-5352*, Rev. 1, U.S. Nuclear Regulatory Commission, Washington, DC, 1991.
- Inskip, W. P., and P. R. Bloom, An evaluation of rate equations for calcite precipitation kinetics at $p\text{CO}_2$ less than 0.01 atm and pH greater than 8, *Geochim. Cosmochim. Acta*, 49, 2165-2180, 1985.
- Inskip, W. P., and P. R. Bloom, Kinetics of calcite precipitation in the presence of water-soluble organic ligands, *Soil Sci. Soc. Am. J.*, 50, 1167-1172, 1986.
- Jacobson, R., *Controls on the quality of some carbonate ground waters: dissociation constant of calcite and CaHCO_3^+ from 0 to 50°C*, Ph. D. Thesis, Pennsylvania State Univ, 13 lp., 1973.
- Jennings, A. A., D. J. Kirkner, and T. L. Theis, Multicomponent equilibrium chemistry in groundwater quality models, *Water Resour. Res.*, 18(4), 1089-1096, 1982.
- Jury, W. A., W. F. Spencer, and W. J. Farmer, Behavior assessment model for trace organics in soil, I. Model description, *J. Environ. Qual.*, 12, 558-564, 1983.

- Jury, W. A., D. Russo, G. Streile, and H. E. Abd, Evaluation of volatilization by organic chemicals residing below the soil surface, *Water Resour. Res.*, 26(1), 13-20, 1990.
- Kirkham, D., and W. L. Powers, *Advanced soil physics*, John Wiley & Sons, New York, 1972.
- Kirkner, D. J., A. A. Jennings, and T. L. Theis, Multisolute mass transport with chemical interaction kinetics, *J. Hydrol.*, 76, 107-117, 1985.
- Kirkner, D. J., and H. Reeves, Multicomponent mass transport with homogeneous and heterogeneous chemical reactions: Effect of the chemistry on the choice of numerical algorithm. 1. Theory, *Water Resour. Res.*, 24(10), 1719-1729, 1988.
- Kucera, C. L., and D. R. Kirkham, Soil respiration studies in tallgrass prairie in Missouri, *Ecology*, 52, 912-915, 1971.
- Liu, Chen Wuing, and T. N. Narasimhan, Redox-controlled multiple-species reactive chemical transport. 1. Model development, *Water Resour. Res.*, 25(5), 869-882, 1989a.
- Liu, Chen Wuing, and T. N. Narasimhan, Redox-controlled multiple-species reactive chemical transport. 2. Verification and application, *Water Resour. Res.*, 25(5), 883-910, 1989b.
- Logan, S. H., and P. B. Boyland, Calculating heat units via a sine function, *J. Amer. Soc. Hort. Sci.*, 108, 977-980, 1983.
- Luckner, L., M. Th. van Genuchten, and D. R. Nielsen, A consistent set of parametric models for the two-phase flow of immiscible fluids in the subsurface. *Water Resour. Res.*, 25(10), 2187-2193, 1989.
- Lundegard, H., Carbon dioxide evolution of soil and crop growth, *Soil Sci.*, 23, 417-454, 1927.
- Luxmoore, R. J., L. H. Stolzy, and J. Letey, Oxygen diffusion in the soil plant system. I. A model, *Agron. J.*, 62, 317-321, 1970.
- Maas, E. V., Chapter 13, Crop salt tolerance, in: *Agric. Salinity Assessment and Management, ASCE Manual & Reports on Engineering No. 71*, edited by K. K. Tanji, ASCE, N.Y., pp. 262-304, 1990.
- Mangold, D. C. and Chin-Fu Tsang, A summary of subsurface hydrological and hydrochemical models, *Reviews of Geophysics*, 29(1), 1991.
- Massmann, J., and D. F. Farrier, Effects of atmospheric pressure on gas transport in the vadose zone, *Water Resour. Res.*, 28(3), 777-791, 1992.
- McNeal, B.L, Prediction of the effect of mixed-salt solutions on soil hydraulic conductivity, *Soil Sci. Soc. Amer. Proc.*, 32, 190-193, 1968.
- McNeal, B. L., J. D. Oster, and J. T. Hatcher, Calculation of electrical conductivity from solution composition data as an aid to in-situ estimation of soil salinity, *Soil Sci.*, 110, 405-414, 1970.
- McNeal, B.L, Soil salts and their effects on water movement, In: *Drainage for Agriculture*, Edited by J. van Schilfgaard, Agronomy No 17, Am.Soc.Agr., Madison, Wi. 1974.

- Miller, R. D., and D. D. Johnson, The effect of soil moisture tension on carbon dioxide evolution, nitrification, and nitrogen mineralization, *Soil Sci. Soc. Am. Proc.*, 28, 644-647, 1964.
- Millington, R. J., and J. M. Quirk, Permeability of porous solids, *Trans. Faraday Soc.*, 57, 1200-1207, 1961.
- Mls, J, Formulation and solution of fundamental problems of vertical infiltration, *Vodohosp. Čas.*, 30, 304-313 (in Czech), 1982.
- Molz, F. J., Models of water transport in the soil-plant system: a review, *Water Resow. Res.*, 17, 1245-1260, 1981.
- Monteith, J. L., G. Szeicz, and E. A. Paul, Crop photosynthesis and the flux of carbon dioxide below the canopy, *J. Appl. Ecol.*, 6, 321-337, 1964.
- Mualem, Y., A new model for predicting the hydraulic conductivity of unsaturated porous media, *Water Resow. Res.*, 12(3), 5 13-522, 1976.
- Narasimhan, T. N., A. F. White, and T. Tokunaga, Groundwater contamination from an inactive uranium mill tailings pile, 2. Application of a dynamic mixing model, *Water Resow. Res.*, 22(13), 1820-1834, 1986.
- Neuman, S. P., A. Feddes, and E. Bresler, Finite element simulation of flow in saturated-unsaturated soils considering water uptake by plants, *Third Annual Report, Project No. Al 0-SWC- 77*, Hydraulic Engineering Lab., Technion, Haifa, Izrael, 1974.
- Nielsen, D. R., M. Th. van Genuchten, and J. W. Biggar, Water flow and solute transport processes in the unsaturated zone, *Water Resour. Res.*, 22(9), 89S-108S, 1986.
- Patwardhan, A. S., J. L. Nieber, and I. D. Moore, Oxygen, carbon dioxide. and water transfer in soils: mechanism and crop response, *Transaction of ASEA*, 31(5), 1383-1395, 1988.
- Perrochet, P., and D. Berod. 1993. Stability of the standard Crank-Nicolson-Galerkin scheme applied to the diffusion-convection equation: Some new insights, *Water Resow. Res.*, 29(9), 329 1-3297.
- Pinder, G. F., and W. G. Gray, *Finite Element Simulation in Surface and Subsurface Hydrology*, Academic Press, New York, N.Y., 1977.
- Pirasteh, B., and J. R. Welsh, Effect of temperature on the heading date of wheat cultivars under a lengthening photoperiod, *Crop Sci.*, 20, 453-456, 1980.
- Pitzer, K. S., Thermodynamics of electrolytes I: Theoretical basis and general equations, *J. Phys. Chem.*, 77, 268-277, 1973.
- Pitzer, K. S., *Activity Coefficients in Electrolyte Solutions*, Chap. 7, CRC Press, Boca Raton, FL., 1979.
- Plummer, L. N., T. M. Wigley, and D. L. Parkhurst, The kinetics of calcite dissolution in CO₂ systems at 5° to 60°C and 0.0 to 1.0 atm CO₂, *Am. J. Sci.*, 278, 179-2 16, 1978.

- Plummer, L. N., and E. Busenberg, The solubilities of calcite, aragonite and vaterite in CO₂-H₂O solutions between 0 and 90°C, and an evaluation of the aqueous model for the system CaCO₃-CO₂-H₂O, *Geochim. Cosmochim. Acta*, 46, 1011-1040, 1982.
- Raats, P. A. C., Steady flows of water and salt in uniform soil profiles with plant roots, *Soil Sci. Soc. Am. Proc.*, 38, 717-722, 1974.
- Rawls, W. J., D. L. Brakensiek, and K. E. Saxton, Estimation of soil water properties, *Trans. ASAE*, 25, 1316-1320, 1982.
- Reardon, E. J., *Thermodynamic Properties of Some Sulfate, Carbonate and Bicarbonate Ion Pairs*, Ph.D. Thesis, Pennsylvania State Univ, 85p., 1974.
- Reardon, E. J., and D. Langmuir, Thermodynamic properties of the ion pairs MgCO₃⁰ and CaCO₃⁰ from 10 to 50°C, *Am. J. Sci.*, 274, 599-612, 1974.
- Reardon, E. J., and D. Langmuir, Activity coefficients of MgCO₃⁰ and CaSO₄⁰ ion pairs as a function of ionic strength, *Geochim. Cosmochim. Acta*, 40, 549-554, 1976.
- Rhoades, J. D., and D. L. Suarez, Reducing water quality degradation through minimized leaching management, *Agric. Water Management*, 1(2), 127-142, 1977.
- Richards, L. A., Water conducting and retaining properties of soils in relation to irrigation, *Proc., Inter. Symp. on Desert Res.*, Jerusalem, 1952.
- Rixon, A. J., Oxygen uptake and nitrification at various moisture levels by soils and mats from irrigated pastures, *J. Soil. Sci.*, 19, 56-66, 1968.
- Robbins, C. W., R. J. Wagenet, and J. J. Jurinak, A combined salt transport-chemical equilibrium model for calcareous and gypsiferous soils, *Soil Sci. Soc. Am. J.*, 44, 1191-1194, 1980a.
- Robbins, C. W., R. J. Wagenet, and J. J. Jurinak, Calculating cation exchange in a salt transport model, *Soil Sci. Soc. Am. J.*, 44, 1195-1200, 1980b.
- Robinson, R. A., and R. H. Stokes, *Electrolyte Solutions*, Butterworths. London, 571p., 1965.
- Ross, D. J., and A. Cairns, Influence of temperature on biochemical processes in some soils from tussock grasslands, *N.Z. J. Sci.*, 21, 581-589, 1978.
- Rubin, J., Solute transport with multisegment, equilibrium controlled reactions: A feed forward simulation method, *Water Resour. Res.*, 26, 2029-2055, 1990.
- Russo, D.**, Simulation of leaching of a gypsiferous-sodic desert soil, *Water Resour. Res.*, 22(8), 1341-1349, 1986.
- Shainberg, I., and G. J. Levy, Physico-chemical effects of salts upon infiltration and water movement in soils, In: *Interacting Processes in Soil Science*, edited by R. J. Wagenet, P. Baveye, B. A. Stewart, Lewis Publishers, CRC Press, Boca Raton, Florida, 1992.

- Šimůnek, J., Numerical simulation of the transport processes in soil, *Vodohosp. Čas.*, 39, 20-34 (in Czech), 1991.
- Simbnek, J., T. Vogel and M. Th. van Genuchten, The SWMS_2D Code for Simulating Water Flow and Solute Transport in Two-Dimensional Variably Saturated Media, Version 1.1., *Research Report No. 126*, U. S. Salinity Laboratory, USDA, ARS, Riverside, California, 1992.
- Šimůnek, J., and D. L. Suarez, Modeling of carbon dioxide transport and production in soil: 1. Model development, *Water Resour. Res.*, 29(2), 487-497, 1993a.
- Simbnek, J., and D. L. Suarez, The UNSATCHEM-2D code for simulating two-dimensional variably saturated water flow, heat transport, carbon dioxide transport, and solute transport with major ion equilibrium and kinetic chemistry, Version 1.1, *Research Report No. 128*, U.S. Salinity Laboratory, USDA, ARS, Riverside, California, 1993b.
- Šimůnek, J., and D. L. Suarez, The SOILCO2 code for simulating one-dimensional carbon dioxide production and transport in variably saturated porous media, Version 1.1, *Research Report No. 127*, U.S. Salinity Laboratory, USDA, ARS, Riverside, California, 1993c.
- Simbnek, J., and D. L. Suarez, Major ion chemistry model for variably saturated porous media, *Water Resour. Res.*, 30(4), 1115-1133, 1994.
- Simbnek, J., and M. Th. van Genuchten, The CHAIN_2D code for simulating two-dimensional movement of water flow, heat, and multiple solutes in variably-saturated porous media, Version 1.1, *Research Report No 136*, U.S. Salinity laboratory, USDA, ARS, Riverside, California, 1994.
- Singh, J. S., and S. R. Gupta, Plant decomposition and soil respiration in terrestrial ecosystems, *The Botanical Review*, 43, 449-528, 1977.
- Šír, M., T. Vogel, and M. Císlerová, Analytical expression of the retention curve and hydraulic conductivity for porous material, *Vodohosp. Čas.*, 33(1), 74-85 (in Czech), 1985.
- Skaggs, R. W., E. J. Monke, and L. F. Huggins, An approximate method for determining the hydraulic conductivity function of an unsaturated soil, *Techn. Rep. No. II*, Water Resour. Res. Center, Purdue University, Lafayette, Indiana, 1970.
- Sleep, B. E. and J. F. Sykes, Modeling the transport of volatile organics in variably saturated media, *Water Resour. Res.*, 22(1), 81-92, 1989.
- Sophocleous, M., Analysis of water and heat flow in unsaturated-saturated porous media, *Water Resour. Res.*, 15(5), 1195-1206, 1979.
- Solomon, D. K., and T. E. Cerling, The annual carbon dioxide cycle in a Montane soil: observation, modeling, and implication for weathering, *Water Resour. Res.*, 23(12), 2257-2265, 1987.
- Stewart, J. I., and Hagan, R. M., Function to predict effects of crop water deficits, *J. Irr. Drain. Div., ASCE*, 99(LR4), 421-439, 1973.

- Stewart, J. I., R. M. Hagan, and W. O. Pruitt, Functions to predict optimal irrigation programs, *J. Irr. Drain. Div., ASCE*, 100(IR2), 179-199, 1974.
- Stewart, J. I., R. D. Misra, and W. O. Pruitt, Irrigation of corn and grain sorghum with a deficient water supply, *Trans. ASCE*, 18(2), 270-280, 1975.
- Stewart, J. I., R. E. Danielson, R. J. Hanks, E. B. Jackson, R. M. Hagan, W. O. Pruitt, W. T. Franklin, and J. P. Riley, *Optimizing crop production through control of water and salinity levels in the soil*, Utah Water Res. Lab. PR 15 1-1, Logan, Utah, 191 pp., 1977.
- Stokes, R. H., Thermodynamics of solutions, In: R. M. Pitkowitz, *Activity Coefficients in Electrolyte Solutions*, CRC Press, Inc., Boca Raton, Florida, 1979.
- Stumm, W., and J. J. Morgan, *Aquatic Chemistry: An Introduction Emphasizing Chemical Equilibria in Natural Waters*, John Wiley & Sons, New York, 1981.
- Suarez, D. L., Magnesium, carbonate, and silica interactions in soils, U.S. *Salinity Laboratory Annual Report*, USDA, 120 pp., 1977a.
- Suarez, D. L., Ion activity products of calcium carbonate in waters below the root zone, *Soil Sci. Soc. Am. J.*, 41, 310-315, 1977b.
- Suarez, D. L., Relation between pH_c and sodium adsorption ratio (SAR) and an alternative method of estimating SAR of soil or drainage waters, *Soil Sci. Soc. Am. J.*, 45, 469-475, 1981.
- Suarez, D. L., and J. D. Rhoades, The apparent solubility of calcium carbonate in soils, *Soil Sci. Soc. Am. J.*, 46, 716-722, 1982.
- Suarez, D. L., J. D. Rhoades, R. Lavado, and C. M. Grieve, Effect of pH on saturated hydraulic conductivity and soil dispersion, *Soil Sci. Soc. Am. J.*, 48, 50-55, 1984.
- Suarez, D. L., Prediction of major ion concentrations in arid land soils using equilibrium and kinetic theories, In: Donn G. DeCoursey, ARS Modeling Symposium, *USDA-ARS-30*, 170-175, Pingree Park, Co, 1985.
- Suarez, L. D., and J. Šimůnek, Modeling of carbon dioxide transport and production in soil: 2. Parameter selection, sensitivity analysis and comparison of model predictions to field data, *Water Resour. Res.*, 29(2), 499-513, 1993.
- Suarez, L. D., and J. Šimůnek, UNSATCHEM: Unsaturated water and solute transport model with equilibrium and kinetic chemistry, *Soil Sci. Soc. Am. J.*, (submitted), 1997.
- Thorstenson, D. C., and D. W. Pollock, Gas transport in unsaturated zones: Multicomponent systems and the adequacy of Fick's laws, *Water Resour. Res.*, 25(3), 477-507, 1989.
- Truesdell, A. H., and B. F. Jones, WATEQ, a computer program for calculating chemical equilibria of natural waters, *J. Res. U. S. Geol. Surv.*, 2(2), 233-248, 1974.
- Valocchi, A. J., R. L. Street, and P. V. Roberts, Transport of ion-exchanging solutes in groundwater: Chromatographic theory and field simulation, *Water Resour. Res.*, 17(5), 1517-1527, 1981.

- van Bavel, C. H. M., A soil aeration theory based on diffusion, *Soil Sci.*, 72, 33-46, 1951.
- van Genuchten, M. Th., On the accuracy and efficiency of several numerical schemes for solving the convective-dispersive equation, In: *Finite Elements in Water Resources*, edited by W. G. Gray et al., Pentech Press, London, pp. 1.71-1.90, 1976.
- van Genuchten, M. Th., Calculating the unsaturated hydraulic conductivity with a new closed-form analytical model, *Water Resour. Program*, 78-WR-08, Princeton University, N.J., 1978.
- van Genuchten, M. Th., A closed-form equation for predicting the hydraulic conductivity of unsaturated soils, *Soil Sci. Soc. Am. J.*, 44(5), 892-898, 1980.
- van Genuchten, M. Th., A numerical model for water and solute movement in and below the root zone, *Unpub. Research. Report*, U. S. Salinity Laboratory, USDA, ARS, Riverside, California, 1987.
- Vogel, T, SWMI - Numerical model of one-dimensional flow in a variably saturated porous medium, *PhD thesis*, CVUT, Prague (in Czech), 1988.
- Vogel, T, SWMII - Numerical model of two-dimensional flow in a variably saturated porous medium, *Research Rep. No. 87*, Dept. of Hydraulics and Catchment Hydrology, Agricultural Univ., Wageningen, The Netherlands, 1987.
- Vogel, T., and M. Císlerová, On the reliability of unsaturated hydraulic conductivity calculated from the moisture retention curve, *Transport in Porous Media*, 3, 1-15, 1988.
- Wagenet R. J., and J. L. Hutson, LEACHM: Leaching Estimation And Chemistry Model, A process-based model of water and solute movement, transformations, plant uptake and chemical reactions in the unsaturated zone, *Continuum 2*, Dept. of Agronomy, Cornell University, Ithaca, N.Y., 1987.
- Walsh, M. P., S. L. Bryant, R. S. Schechter, and L. W. Lake, Precipitation and dissolution of solids attending flow through porous media, *AIChE Jour.*, 30(2), 317-328, 1984.
- Westall, J. C., J. L. Zachary, and F. M. M. Morel, MINEQL: A computer program for the calculation of chemical equilibrium composition of aqueous systems, *Tech. Note 18*, 91pp., Dep. of Civ. Eng., Mass. Inst. of Technol., Cambridge, 1976.
- White, N., and L. W. Zelazny, Charge properties in soil colloids, In: *Soil Physical Chemistry*, edited by D. L. Sparks, CRC Press, Boca Raton, Florida, 1986.
- Williams, S. T., M. Shameemullah, E. T. Watson, and C. I. Mayfield, Studies on the ecology of actinomycetes in soil. IV. The influence of moisture tension on growth and survival, *Soil Biol. Biochem.*, 4, 215-225, 1972.
- Wilson, J. M., and D. M. Griffin, Water potential and the respiration of microorganisms in the soils, *Soil Biol. Biochem.*, 7, 199-204, 1975.
- Witkamp, M. and M. L. Frank, Evolution of CO₂ from litter, humus, and subsoil of a pine stand, *Pedobiologia*, 9, 358-366, 1969.

- Yeh, G. T., and D. D. Huff, FEMA: A finite element model of material transport through aquifers, *Rep. ORNL-6063*, Oak Ridge Natl. Lab., Oak Ridge, Tennessee, 1985.
- Yeh, G. T., and V. S. Tripathi, A critical evaluation of recent developments in hydrogeochemical transport models of reactive multichemical components, *Water Resow. Res.*, 25(1), 93-108, 1989.
- Yeh, G. T., and V. S. Tripathi, HYDROGEOCHEM: A coupled model of HYDROlogic transport and GEOCHEMical equilibria in reactive multicomponent systems, *Environs Sci. Div., Publ. No. 3170.*, Oak Ridge National Lab., Oak Ridge, Tennessee, 1990.
- Yeh, G. T., and V. S. Tripathi, A model for simulating transport of reactive multispecies components: Model development and demonstration, *Water Resow. Res.*, 27(12), 3075-3094, 1991.

PART B

Interactive Graphics-Based User Interface

UNSATCH

Version 1 .0

by

J. Šimůnek, M. Šejna, M. Th. van Genuchten, and D. L. Suarez

Even with well-documented numerical computer models available, one major problem often preventing the use of such codes is the extensive work required for data preparation, finite element grid design, and graphical presentation of the output results. To avoid or simplify the preparation and management of relatively complex input data files and to graphically display final simulation results, we developed an interactive graphics-based user-friendly interface UNSATCH for the MS Windows 3.x, Windows 95, and Windows NT environments. The graphics interface is connected directly to the UNSCHEM FORTRAN code. The complete computer software package UNSATCHEM includes three modules and one dynamic linked library (DLL) (Table B.1).

In addition to information given in this chapter, extensive context-sensitive on-line help is made part of every module of the interface. By pushing the F1 button, or clicking on the Help button while working in any window, the user obtains information about the window content. In addition, context-sensitive help is available in every module using the "SHIFT+F1" help button. In this mode, the mouse cursor changes to a help cursor (a combination arrow + question mark), and the user proceeds to click on the object for which he needs help (i.e, a menu item, toolbar button, or other features). At that point, a help tile will be displayed giving information about the item on which the user clicked. Except for the UNSCHEM FORTRAN application itself, all modules are written in C++.

The interactive graphic-based user interface UNSATCH has many features similar to the interface **HYDRUS1D** [Šimůnek *et al.*, 1997] and thus there is repetition in both manuals, as well as in the context-sensitive help files.

Table B.1. Main modules of the UNSATCHEM software package.

UNSATCH	main program unit, input parameters, output graphics
POSITION	project manager (DLL)
PROFILE	transport domain geometry, finite element mesh generator, boundary and initial conditions, material distribution
UNSCHEM	FORTRAN application (UNSCHEM version 2.0)

B. *Brief Description of Selected Modules*

B. 1. *Module UNSATCH*

UNSATCH (Fig. B.1) is the main program unit defining the overall computational environment of the system. This module controls execution of the program and determines which other optional modules are necessary for a particular application. The module contains a project manager and both pre-processing and post-processing units. The pre-processing unit includes specification of all necessary parameters to successfully run the UNSCHEM FORTRAN code, and a small catalog of soil hydraulic properties. Table B.2 lists all commands accessible through the menu, whereas Table B.3 gives a brief discussion of the action taken with the particular commands. More detailed descriptions are available through the on-line help. The post-processing unit consists of simple x-y graphics for graphical presentation of soil hydraulic properties, as well as such output as transient values of a particular variable at selected observation points in the domain, and actual or cumulative water, carbon dioxide and solute fluxes across boundaries. Table B.4 gives an overview of the different graph options made available through the interface. The UNSATCH and PROFILE modules mutually communicate through the file UNSATCH.DAT, a description of which is given in Table B.5.

The work for a new project should begin by opening the Project Manager (see Section B.2), and giving a name and brief description to this new project. Then select the Main Processes command from the Main Information Menu. From this point on, the program will navigate the user through the entire process of entering input files. The user may either select particular commands from a menu, or allow the interface to lead him through the process of entering input data by selecting the Next buttons. Alternatively, clicking the Previous button will return the user to the previous window.

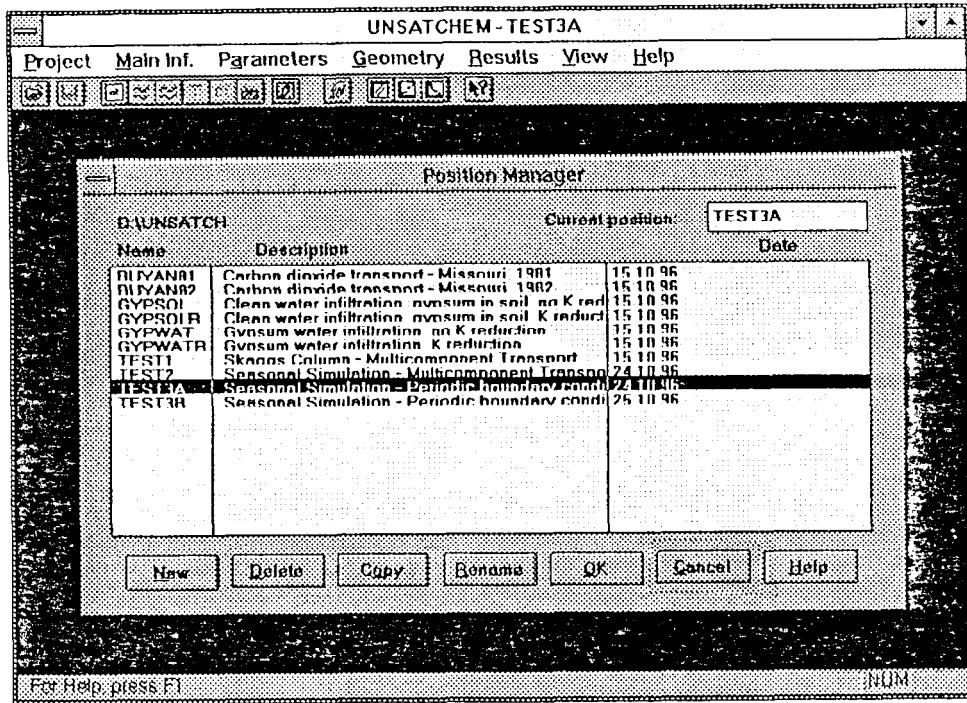


Fig. B. 1. The main window of the UNSATCI-I module, including the project manager.

Table B.2. Menu commands in the main module UNSATCH.

Group	Menu	Submenu	Sub-Submenu
A	Project	Project Manager Save Data Exit	
B	Main Information	Main Processes Main Geometry Information Main Time Information Print Information	
C	Parameters	Water Flow Parameters Solute Transport Parameters Heat Transport Parameters Carbon Dioxide Transport Root Water Uptake Root Growth Variable Boundary Conditions	Iteration Criteria Water Flow Parameters Boundary Conditions Constant Boundary Fluxes Deep Drainage BC General Information Chemical Parameters Solute Transport Parameters Solution Compositions Boundary Conditions Heat Transport Parameters Boundary Conditions CO ₂ Transport Parameters Soil CO ₂ Production Parameters Root CO ₂ Production Parameters Root Growth Model Type Root Growth Parameters
D	Geometry	Profile Information Profile Summary Execute LJNSCHEM	
E	Results	Observation Points Profile Informations T_Level Information Run Time Information Soil Hydraulic Properties Mass Balance Information Chemical Mass Balance Information	Basic Information Solution Concentrations Solid Concentrations Chemical Information Water Flow Carbon Dioxide Transport
F	View	Toolbar Status Bar	

Table B.2. (continued).

Group	Menu	Submenu	Sub-Submenu
G	Help	Index Using Help About	

Table B.3. Description of all menu commands in the main module UNSATCH.

Group	Command	Brief description of the command
A	Project Manager	Calls the project manager to manage data of existing projects; helps to locate, open, copy, delete or rename the desired projects and their data.
	Save Data	Saves the input data of an actual project specified in the main program module if the data were either newly created or changed during an application run. At the same time this command deletes all existing output files of a selected project since the output data are no longer consistent with the changed input data. A warning is issued to the user before the data are saved.
	Exit	Closes the project and leaves the program. This command informs the user before exiting the application whether or not the input data of an actual project were changed during the application run. If changes did occur, the user is given the option to save data before exiting the application.
B	Main Processes	Selects the title which is printed into output files, and specifies the processes to be simulated, i.e., water flow, carbon dioxide production and transport, multicomponent solute transport, heat transport, root growth, and/or root water uptake.
	Main Geometry Information	Selects the length unit, specifies the depth and inclination of the soil profile to be analyzed, and determines the number of materials to be used.
	Main Time Information	Selects time units, and gives the time discretization information.
	Print Information	Specifies print options.
C	Iteration Criteria	Specifies iteration criteria for the solution precision, and parameters for the time step control.
	Water Flow Parameters	Specifies parameters in the soil hydraulic model.
	Boundary Conditions	Specifies the types of upper and lower boundary conditions.
	Constant Boundary Fluxes	Specifies constant boundary fluxes and constant root water uptake when no time-variable boundary conditions are given.
	Deep Drainage BC	Specifies parameters for the deep drainage boundary condition.

Table B.3. (continued).

Group	Command	Brief description of the command
	General ST Information	Selects the time and spatial weighting schemes for numerical solution of the solute transport equation; specifies the number of solution, surface species, and mineral phases combinations to be considered.
	Chemical Parameters	Selects kinetic or equilibrium model for calcite precipitation/dissolution, specifies critical ionic strength and max. number of iterations.
	Solute Transport Parameters	Specifies solute transport parameters.
	Solution Compositions	Specifies different solution, adsorbed and mineral phases compositions.
	ST Boundary Conditions	Specifies the upper and lower boundary conditions for solute transport.
	Heat Transport Parameters	Specifies heat transport parameters.
	Heat Transport Boundary Cond.	Specifies the upper and lower boundary conditions for heat flow.
	CO, Transport Parameters	Specifies carbon dioxide transport parameters including boundary conditions.
	Soil CO, Production Parameters	Specifies soil (microbial) CO, production parameters.
	Root CO, Production Parameters	Specifies root CO, production parameters.
	Root Water Uptake	Specifies parameters in the root water uptake water stress and salinity response models.
	Root Growth Model Type	Selects the root growth model and model for the root spatial distribution.
	Root Growth Parameters	Specifies parameters in the Verhulst-Pearl logistic growth function or degree day concept used to describe root growth during the growing season.
	Variable Boundary Condition	Specifies time-dependent boundary conditions for all transport processes.
D	Profile Information	Calls external module PROFILE, for users to discretize the soil profile and to specify the vertical distribution of relevant parameters.
	Profile Summary	Summarizes in tabular form the spatial discretization and spatial distribution of soil properties, initial conditions, and other variables. This command allows the user to summarize and modify the parameter setup in the external module PROFILE.
	Execute UNSCHEM	Executes a UNSCHEM version 2.0 FORTRAN application.
E	Observation Points	Graphical presentation of changes in water content, pressure head, carbon dioxide, and/or temperature at specified observation nodes.
	Basic Informations	Graphical presentation of pressure head, water content, velocity, root water uptake, temperature, and carbon dioxide concentration profiles at different times.
	Solution Concentrations	Graphical presentation of major ion concentrations: Ca, Mg, Na, K, alkalinity, SO ₄ , Cl, and tracer.
	Solid Concentrations	Graphical presentation of surface species and mineral phase concentrations: Ca, Mg, Na, K, calcite, gypsum, dolomite, nesquehonite, hydromagnesite, scpiolite.
	Chemical Information	Graphical presentation of major chemical information (pH , SAR, (H_2O^0) , (Ca^{2+}) , (HCO_3^-) , $pIAP^c$, $pIAP^p$, $pIAP^i$, EC , . . .).
	Water Flow Boundary Inform	Graphical presentation of actual and cumulative boundary water fluxes, and surface, root zone, and bottom pressure heads.

Table B.3. (continued).

Group	Command	Brief description of the command
E	Carbon Dioxide Transport	Graphical presentation of actual and cumulative boundary CO, fluxes, and surface, root zone, and bottom boundary CO ₂ concentrations.
	Soil Hydraulic Properties	Graphical presentation of the soil hydraulic properties.
	Run Time Information	Graphical presentation of information about the number of iterations, time step, and Peclet and Courant numbers.
	Mass Balance Information	Displays mass balance information and mean profile properties.
	Chemical Mass Balance Inform.	Displays mass balance information for chemical species.
F	Toolbar	Shows or hides the toolbar.
	Status Bar	Shows or hides the status bar.
G	Index	Offers an index of topics for which help is available.
	Using Help	Provides general instructions on using help.
	About	Displays the version and authors of the UNSATCHEM application.

Table B.4. Graph options in the UNSATCHEM interface.

Command	Horizontal Axis	Vertical Axis
Observation Points	Time	Pressure Head Water Content Temperature CO, Concentration
Basic Profile Information	Pressure Head Water Content CO, Concentration Temperature Hydraulic Conductivity Soil Water Capacity Water Flux Root Water Uptake CO, Production	Depth
Solution Concentrations	Calcium Magnesium Sodium Potassium Alkalinity Sulfate Chloride Tracer	Depth

Table B.4. (continued)

Command	Horizontal Axis	Vertical Axis
Solid Concentrations	Calcite Gypsum Dolomite Nesquehonite Hydromagnesite Sepiolite Adsorbed Calcium Adsorbed Magnesium Adsorbed Sodium Adsorbed Potassium	Depth
Chemical Information	Calcium Activity Bicarbonate Activity Water Activity Alkalinity PH SAR Electric Conductivity Ionic Strength pIAP Calcite pIAP Gypsum pIAP Dolomite Osmotic Coefficient Osmotic Pressure Head	Depth
T_Level Information - Water Flow	Time	Potential Surface Flux Potential Root Water Uptake Rate Actual Surface Flux Actual Root Water Uptake Rate Bottom Flux Cumulative Potential Surface Flux Cumulative Potential Root Water Uptake Rate Cumulative Actual Surface Flux Cumulative Actual Root Water Uptake Rate Cumulative Bottom Flux Surface Pressure Head Average Root Zone Pressure Head Bottom Pressure Head

Table B.4. (continued)

Command	Horizontal Axis	Vertical Axis
- CO, Transport	Time	Surface CO ₂ Flux Bottom CO, Flux Cumulative Surface CO, Flux Cumulative Bottom CO, Flux Surface CO, Concentration Average Root Zone CO, Concentration Bottom CO, Concentration CO, Production Cumulative CO, Production Cumulative CO, Root Uptake
Soil Hydraulic Properties	Pressure Head Log Pressure Head	Water Content Soil Water Capacity Hydraulic Conductivity Log Hydraulic Conductivity Effective Water Content
Run-Time Information	Time Level Time	Time Step Number of Iterations Cumulative Number of Iterations Peclet Number Courant Number Number of Solute Iterations

Table B.5. Information in the UNSATCH.DAT file.

Group	Variable	Type	Description
Main	WaterFlow	Integer	Variable which specifies whether or not transient water flow is to be calculated.
	SoluteTransport	Integer	Variable which specifies whether or not solute transport is to be calculated.
	HeatTransport	Integer	Variable which specifies whether or not heat transport is to be calculated.
	CO2Transport	Integer	Variable which specifies whether or not carbon dioxide transport is to be calculated.
	RootWaterUptake	Integer	Variable which specifies whether or not root water uptake is to be calculated.
	RootGrowth	Integer	Variable which specifies whether or not root water growth is to be calculated.
	MaterialNumbers	Integer	Number of materials considered.
	SubregionNumbers	Integer	Number of subregions considered for mass balance calculation.
	SpaceUnit	String	Space units.
	TimeUnit	String	Time units.
	PrintTimes	Integer	Number of print-times.
	SolutionConcNumber	Integer	Number of solution combinations considered in the application.
	AdsorbedConcNumber	Integer	Number of surface species combinations considered in the application.
	SolidConcNumber	Integer	Number of mineral phase combinations considered in the application.
Profile	NumberOfNodes	Integer	Number of nodes used to discretize the soil profile.
	ProfileDepth	Float	Depth of the soil profile.
	ObservationNodes	Integer	Number of observation nodes.
	GridVisible	Integer	Variable which specifies whether or not the grid is to be visible.
	SnapToGrid	Integer	Variable which specifies whether or not the mouse should move in steps defined by the grid.
	ProfileWidth	Integer	Number of pixels for graphical display of the soil profile.
	LeftMargin	Integer	Number of pixels for graphical display of the nodal discretization.
	GridOrgX	Real	X-coordinate of the grid origin.
	GridOrgY	Real	Y-coordinate of the grid origin.
	GridDX	Real	Step in the x direction between grid nodes.
	GridDY	Real	Step in the y direction between grid nodes.

B.2. Module *POSITION*

A project manager, **POSITION** (DLL) (Fig. B.1), is used to manage data of existing projects, and to help locating, opening, copying, deleting and/or renaming desired projects or their input or output data. A “project” represents any particular problem to be solved by UNSATCHEM. The project name (8 letters), as well as a brief description of the project helps to locate a particular problem. Input and output data for each project are placed in a subdirectory with the same name as the project.

B.3. Module *PROFILE*

B.3.1. *Soil Profile Discretization*

The module **PROFILE** (Fig. B.2) is used, among other things, to discretize a one-dimensional soil profile into discrete nodes. Nodes are generated by dividing the soil profile into small elements. If no previous nodes exist, the program automatically generates a default equidistant point distribution. The location of nodes can be edited by the user to optimize the thickness of the different elements. There are two ways of specifying appropriate distributions of the nodes, i.e., by (1) editing the number of points, and (2) specifying fixed points and nodal densities. The nodal density determines the relative length of the elements, and can be specified only at fixed points. Fixed points can be inserted or deleted anywhere in the soil profile. The user can edit the nodal density at a fixed point in order to locally refine the nodal distribution around this point. Careful placement of the nodes is important since the nodal distribution determines in a very substantial manner the ultimate quality and speed of the calculations.

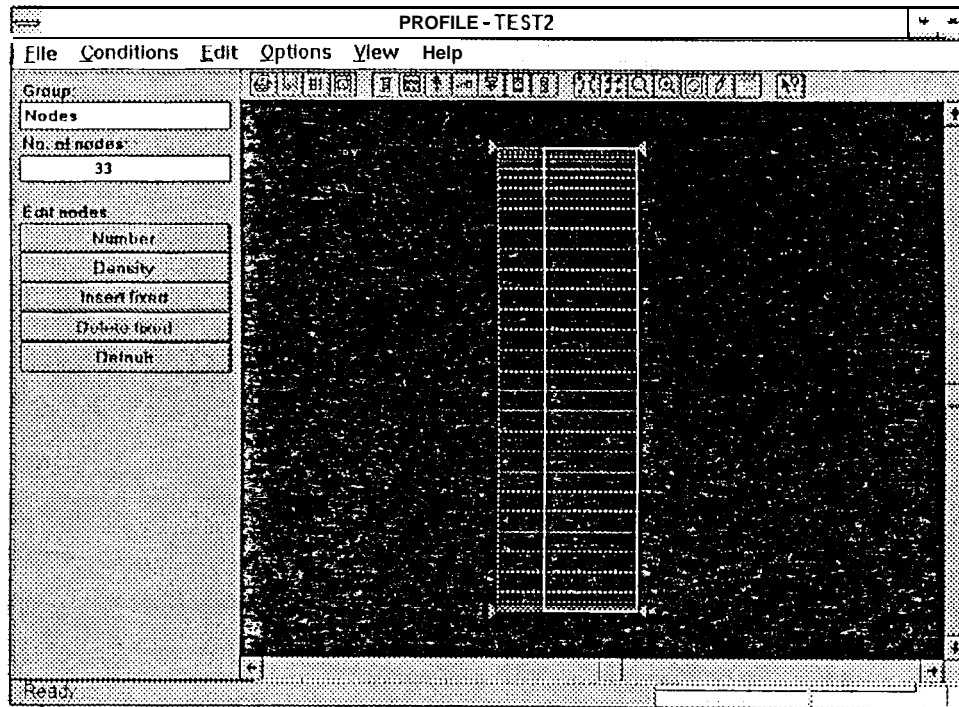


Fig. B.2. The main window of the PROFILE module; when used for soil profile discretization.

B.3.2. Specification of Soil Properties within the Soil Profile

The PROFILE module (Fig. B.3.) helps a user to define also the spatial distribution of parameters characterizing the flow domain (e.g., spatial distribution of soil materials, hydraulic scaling factors, root-water uptake parameters) and/or observation nodes. All parameters in this module are specified in a graphical environment with the help of a mouse.

Specification of parameters characterizing the flow domain (initial conditions, material distribution) is relatively straightforward. The users must first select that part of the transport domain to which they want to assign a particular value of the selected variable. It is possible to select the entire transport domain, part of it, or **only** individual nodes. A particular part of the

Table B.6. Definition of terms used in module PROFILE.

Nodal Point	Nodal points are nodes which discretize the soil profile and which are marked by green crosses. These nodes are ordered from the top (node number 1) to the bottom (node <i>NumNP</i>).
Elements	Elements are layers discretizing the soil profile. They connect the generated nodal points.
Fixed Points	Fixed points are points in the soil profile marked by purple stars. These points may be used to adjust the local discretization density of nodal points. By default, fixed points are placed at the top and bottom of the soil profile, but they can be inserted or deleted also at any other point in the soil profile.
Nodal Density	The nodal density is a real number in the range $\langle 0.01, 100 \rangle$ specifying the local density of nodal points. The density can be specified only at fixed points. The program distinguishes between top and bottom density. The top (bottom) density at a fixed point specifies the relative thickness of the elements above (or below) this point. If the top and bottom densities are equal then the nodal density is continuous throughout the profile, i.e., both elements have the same thickness. If the top and bottom density values are different then the element thicknesses will be different as well. For example: if $DT = 3.$, $DB = 2.$ then $LT/LB = 1.5$, where DT and DB are the top and bottom densities at a fixed point, respectively, and LT and LB are the thicknesses of elements above and below that fixed point, respectively.

transport domain can be selected as follows: the user must first click the Edit Condition button, and then move the mouse to a selected position. The beginning and end of the selection operation is framed by clicking the left button. The selected area is the vertical defined by the two mouse positions when the left button was clicked. When the selection is completed, the window Condition Specification pops up and the user must specify the value of a particular variable. That value will then be assigned to the selected area. When specifying the initial condition, the user has the option of assigning either a constant value to a selected domain, or specifying different values to the top and bottom of the selected region, in which case the program will linearly interpolate the variable within the selected region. Variables are always assigned to nodal points, not to elements.

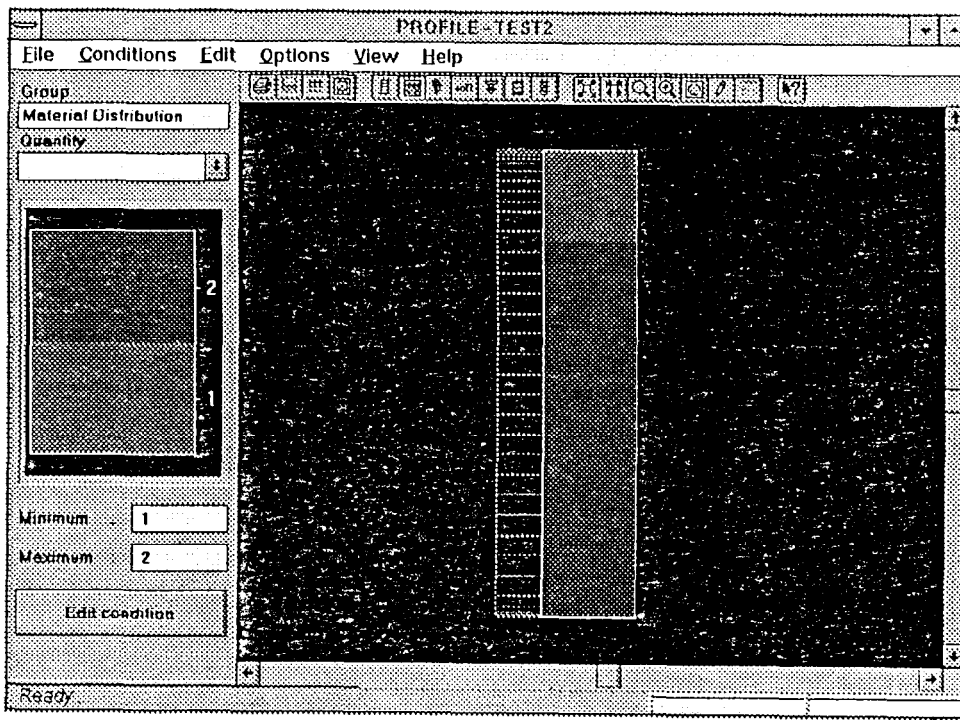


Fig. B.3. Main window of the PROFILE module; when used for specification of soil properties.